Abstract

A time-resolved holographic interferometer specially suited for high-speed visualization of the gas flow in shock tube experiments has been developed. Holographic interferometry, which is based on the recording of two coincident holograms at different times so that one of them acts as a reference field, can accurately reveal the density distribution in a gas. The device described here fills the need for a practical method to record short sequences of holographic interferograms documenting the evolution of shock wave reflections that are not self-similar in time.

Multiple hologram recording was implemented on an existing holographic interferometric system through the technique of spatial frequency multiplexing, in which the holograms are overlaid but the reference beam is angled differently for each exposure. Because the object beam is not involved in the multiplexing process, the imaging optics of the original system could be left unmodified. The upgrade only entailed the introduction of an angular sweeping system in the reference beam path.

The beam multiplexing assembly was initially based on a spinning mirror design, which produced fairly satisfactory recordings of non-interferometric holographic sequences but was incapable of accurately overlaying a second set of exposures establishing the reference field for each image. The mechanical sweeping system had other drawbacks as well, among them the tendency to create extraneous fringes in the holographic images because of the unavoidable angular motion of the reference beam over the duration of a laser pulse.

A solid-state multiplexing system was then devised in which the reference beam was split into several branches, each aimed at the film from a different direction and

individually shuttered by a ferroelectric liquid crystal light valve. Beam sweeping was achieved by opening the shutters in sequence as the laser was pulsed, but it was also possible to record the reference exposure on all images simultaneously with a single laser pulse by having all shutters open at the same time. A prototype three-image system was constructed and successfully tested by recording interferometric sequences of a shock wave reflecting off a model at framing intervals down to 100 μs.

Examiners:

Dr. J. M. Dewey, Supervisor (Department of Physics)

Dr. R. M. Clements, Departmental Member (Department of Physics)

Dr. G. B. Friedmann, Departmental Member (Department of Physics)

Dr. R. N. O'Brien, Outside Member (Department of Chemistry)

Dr. P. van den Driessche, Outside Member (Department of Mathematics)

Dr. D. K. Walker, Additional Member (Department of Physics)

Dr. T. R. Hsu, External Examiner (University of Manitoba, Dept. of Mech. Eng.)

Table of Contents

List of Figures

Acknowledgements

I wish to express my heartfelt thanks to Dr. John Dewey, with whom I first discussed this project and who guided and supervised me in its development. I am also indebted to my colleagues at the Shock Studies Laboratory, particularly Alex van Netten, for their help and advice and for sportingly putting up with my sometimes unorthodox research habits. David Smith and Peter Ward of the University of Victoria Physics machine shop, David Searle of the University of Victoria Chemistry glass shop, Jes Jessen of the Dominion Astrophysical Observatory optical shop, and Luke Roosma of Displaytech, Inc. provided invaluable technical assistance.

The financial support of the University of Victoria in the form of a Graduate Fellowship is gratefully acknowledged. All of the equipment used in this project, and the travel to international meetings which allowed fruitful discussion of the concepts with a critical audience, were financed by an operating grant from the Natural Sciences and Engineering Research Council of Canada.

I could not have persisted in this long task had it not been for the unfailing affection and support of my wonderful family, near and far. In a special way I am thankful to Bonny, now my wife, who was always close to me throughout this endeavour. My love and gratitude to all of them.

to Nino Racca

Chapter 1

Introduction

A variety of optical methods are used in the study of high-speed compressible flows and shock waves to gather information as detailed as possible about the local properties of a flow field. The capability to visualize and record with very short exposure times the propagation of a disturbance through a gaseous mass is particularly important under the nonsteady conditions associated with explosive flows. In the areas of shock tube and blast wave research, high-speed photography has been teamed with visualization methods such as shadowgraphy, schlieren, conventional interferometry and, latest in development, holographic interferometry. An extensive review of these applications appears in a recent monograph (Dewey, 1989). The above techniques, each one of which will be discussed at least briefly in later chapters, rely on the change in the refractive index of a gas caused by a shock wave to visualize the shock fronts or the density distribution behind them. The study of large scale blast waves must generally use visualization techniques based on the refraction of ambient light. Interferometric methods are particularly suited to the controlled environment of shock tubes, which allows precise illumination of a well defined test section with monochromatic light.

Interferometry reveals at every location in the test field the refractive index change relative to some reference point. In conventional (Mach-Zehnder) interferometry the optical length of a path passing through the test volume is compared at

every point with the optical length of a reference path, with differences appearing as fringes in the field of view. The method is therefore affected by any discrepancy between the two paths introduced by imperfections in the optical components, and consequently requires premium quality optics throughout the system. As will be seen later, holographic interferometry does away with this problem by comparing two wavefronts following a single path at different times, and may therefore be implemented with relative ease on optical systems of less than optimal quality

The potential usefulness of holographic interferometry in aerodynamics research was illustrated in the early paper by Heflinger et al. (1966). The popularity of this technique for shock tube research has been steadily increasing since the initial work of researchers such as Wortberg (1973), especially in the wake of the excellent recordings presented by Takayama (1983). The optical equipment associated with the shock tube in the University of Victoria Shock Studies Laboratory was recently converted to a holographic system (van Netten, 1988) to expand ongoing studies on the reflection of weak shock waves traditionally conducted by shadowgraph and schlieren methods (Walker et al., 1982) and particle flow tracing (Dewey et al., 1975).

The study by optical methods of shock tube phenomena that are not self-similar in time, such as the reflection of a shock from a double or curved wedge, requires the recording of a series of images separated by time intervals of the order of a few tens of microseconds. Holographic interferometric studies of such events are customarily conducted by recording a single interferogram during an experiment and building a temporal sequence by progressively delaying the laser pulse over a series of similar experiments (Takayama, 1983). This approach is inconvenient, requiring the shock tube to be fired repeatedly, and potentially inaccurate if the experimental conditions cannot be kept absolutely constant. Moreover, it would be inapplicable to cases where a model is mechanically affected by the shock in a non repeatable manner. A need therefore exists for a time-resolved holographic inter-

ferometric system capable of recording several images during a single experiment, and the present work was undertaken to attempt to fill that need.

In an endeavour to alter as little as possible the existing optical layout, which allowed the use of shadowgraphy, schlieren, particle tracer photography and holographic interferometry, spatial frequency multiplexing was chosen as the method to record multiple holograms. This technique required only the reference beam—that is, the non-image-carrying beam used in hologram recording—to be angled differently for each image in a sequence. The path of the image forming beam was not modified in any way from the layout used in the original holographic system or in the previous non-holographic configurations, and full backward compatibility was therefore retained. A first implementation of the multiplexing scheme based on a mechanical beam deflection system (Racca and Dewey, 1989a) gave some promising results when recording non-interferometric series of holograms, but failed to produce reliable interferometric sequences because of problems with the accurate overlaying of the required two exposures per image. This difficulty and other shortcomings of the method, particularly the appearance of spurious fringes due to the minute motion of the beam during exposures (Racca and Dewey, 1989a, 1989b) shifted the research emphasis toward a non-mechanical system.

Previous implementations of spatial frequency multiplexing by solid state means (Hinsch and Bader, 1974, Lauterborn and Ebeling, 1977, Yamamoto, 1989) were based on the principle of redirecting the entire energy of the reference beam along one of several paths converging at the film. These systems used acousto-optical or high-voltage electro-optical devices (see Chapter 7) as the active component, and were not reported to have been applied to interferometric work. Yamamoto (1989) also presented a system using two twin-pulse lasers to record spatial frequency multiplexed sequences of two holographic interferograms. Unwieldy as they may be, multiple lasers using either separate lasing elements or different portions of the same lasing medium have been employed to record sequences of holographic inter-

ferograms in specialized applications since fairly early times (Thomas et al., 1972).

In the work presented here, it was chosen to explore the capabilities as beam switchers of newly emerging low-voltage electro-optical light modulators based on ferroelectric liquid crystals, and to pursue a novel approach to beam selection. The reference beam was split into several coexisting branches, each aimed at the film from a different direction and individually shuttered by a liquid crystal light valve. Multiplexing of the beam was achieved by opening only one shutter at a time in sequence. If desired, however, more than one beam could be allowed to reach the film, and this capability was used to record the empty field exposure for interferometry on all images at once. Using this scheme, which offers several advantages that will be analysed later, a three-image prototype has been built which satisfactorily records interferometric sequences of shock tube experiments.

Chapter 2 of this dissertation presents a brief background on shock waves and the methods used to generate and visualize them in the laboratory, not including holographic interferometry. Chapter 3 gives a theoretical introduction to holography and then focuses on the kind of holographic interferometry commonly used in shock tube research, including an overview of the original holographic system used as the basis for this work. The concept of time-resolved holography and the possible approaches to it are discussed in Chapter 4, with an emphasis on spatial frequency multiplexing. The subsequent two chapters discuss its implementation by mechanical scanning, including in Chapter 6 a mathematical analysis of the formation of spurious fringes due to beam motion. The solid state approach to beam multiplexing is treated in Chapter 7, which goes from a broad evaluation of the available technologies and scanning strategies to a detailed discussion of the present method and its results, possibilities and limitations. Chapter 8 gives a closing view of the work performed and its foreseen applications and extensions.

Chapter 2

Shock waves

2.1 Nature of shock waves

A moving shock wave is formed when a compressional disturbance of finite amplitude propagates through a gas. Such a disturbance may be produced by phenomena such as the detonation of an explosive, the bursting of a balloon, or the motion of a supersonic aircraft. In a supersonic flow tunnel, a stationary shock wave is formed where a vector component of the flow makes a transition from a supersonic to a subsonic regime. Shock waves are characterized by a non-linear pressure profile with a sharp leading edge, known as the shock front, across which there is a virtually instantaneous change in the thermodynamic properties of the medium. The thickness of a shock front is about 10 to 20 mean free paths, which for a gas initially at standard atmospheric conditions amounts to about 10^{-5} cm. As a moving shock wave expands it weakens and eventually degenerates into a sound wave, which no longer significantly affects the properties of the medium through which it travels.

Interferometric methods and other experimental techniques such as tracer motion analysis can quantitatively reveal changes in the density of a gas throughout regions where it varies smoothly, but cannot always do so across a near-discontinuity such as a shock. The ratio of the thermodynamic properties of the medium on the two sides of a shock, however, can be derived analytically from the basic conser-

vation laws. The resulting relations are fundamental to the experimental study of shock waves.

2.2 The Rankine-Hugoniot equations

Starting from the continuity, momentum and energy equations for a compressible, inviscid and calorically perfect fluid, Rankine (1870) and Hugoniot (1887) derived the relations between the gas properties on the two sides of a *normal* shock– a shock that changes the properties of the flow in one co-ordinate direction only. Depending on the parameter in terms of which the ratios are expressed, these equations may take different but equivalent forms. The appellation of *Rankine-Hugoniot equations* is often given to the equations expressing the ratios across the shock as a function of the upstream Mach number, measured in a frame of reference where the shock is at rest. To maintain generality, the subscripts α and β will be used in this section to denote the conditions ahead of and behind a shock. Numeric subscripts will be reserved for the conditions in specific regions of a flow field.

The upstream Mach number M_α is defined as the ratio of the flow speed u_α to the local speed of sound a_α ahead of the shock wave (for an ideal gas, $a_\alpha = \sqrt{\gamma R T_\alpha}$, where R is the universal gas constant). The Rankine-Hugoniot equations for pressure, density, temperature and Mach number are:

$$\frac{p_\beta}{p_\alpha} = 1 + \frac{2\gamma}{\gamma+1}\left(M_\alpha^2 - 1\right), \tag{2.1}$$

$$\frac{\rho_\beta}{\rho_\alpha} = \frac{(\gamma+1)M_\alpha^2}{2+(\gamma-1)M_\alpha^2}, \tag{2.2}$$

$$\frac{T_\beta}{T_\alpha} = \left[1 + \frac{2\gamma}{\gamma+1}\left(M_\alpha^2 - 1\right)\right]\left[\frac{2+(\gamma-1)M_\alpha^2}{(\gamma+1)M_\alpha^2}\right], \tag{2.3}$$

$$\frac{M_\beta^2}{M_\alpha^2} = \frac{1+(\gamma-1)/2}{\gamma M_\alpha^2 - (\gamma-1)/2}, \tag{2.4}$$

where $\gamma \equiv c_p/c_v$ is the ratio of specific heats for the gas. A direct consequence of the continuity equation is that the ratio of flow velocity across a normal shock is the reciprocal of expression 2.2.

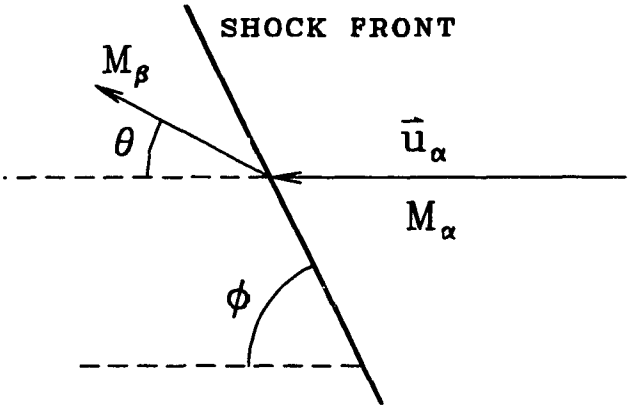

Figure 2.1: The geometry of the flow through an oblique shock in the frame of reference in which the shock is at rest.

A normal shock is a special case of the family of *oblique* shock waves that occur in supersonic flows. Seen in a reference frame where it is at rest, an oblique shock forms an angle ϕ with respect to the flow velocity vector $\vec{u}_\alpha$ upstream of it (Fig. 2.1). For a normal shock, ϕ is equal to $\pi/2$. An analysis of the continuity, momentum and energy equations for the components of flow tangential and normal to the shock front (Anderson, 1982) reveals that the tangential component is preserved across an oblique shock, and the normal component completely determines the downstream flow properties. The Rankine-Hugoniot equations can therefore be applied to oblique shocks simply by replacing M_α in expressions 2.1 to 2.3 with its component normal to the shock, $M_{\alpha_n} = M_\alpha \sin\phi$. In equation 2.4, the downstream Mach number M_β is also replaced by its normal component $M_{\beta_n} = M_\beta \sin(\phi - \theta)$. The reciprocal of expression 2.2 in its new form gives the ratio of the normal component of flow velocity across the shock. From this ratio and the fact that the tangential component of velocity is preserved, the following relation for the angle of flow deflection θ can be derived:

$$\tan\theta = 2\frac{M_\alpha^2 \sin^2\phi - 1}{M_\alpha^2(\gamma + \cos 2\phi) + 2}\cot\phi. \tag{2.5}$$

For a given Mach number, there is a maximum deflection angle $\theta_{\max}$ for which equation 2.5 has a solution. If the flow geometry is such that $\theta > \theta_{\max}$ then no solution exists for a straight oblique shock. For $\theta < \theta_{\max}$ there are two values for the shock angle that will satisfy the equation, the larger being called the strong shock solution and the smaller the weak shock solution. The weak shock solution is the one that usually occurs in nature.

2.3 Oblique shock wave reflection

Consider an incident shock wave i of Mach number M_i striking a rigid wedge of angle θ_w as shown in Figure 2.2(a). This shock wave induces a net flow in the gas with a component toward the surface of the wedge. In order to satisfy the boundary condition that requires the flow adjacent to a rigid surface to be parallel to it, a reflected shock r must develop which has the correct strength and geometry to bring the flow to the proper orientation. This shock configuration, in which the reflection point lies at the surface of the wedge, is known as *regular reflection.* To analyse the deflection angles, the shocks are considered straight in proximity of the reflection point G and the flow is assumed to be self-similar (von Neumann, 1943), that is, to become pseudo-stationary in a co-ordinate system $(x/t, y/t)$ fixed to point G (Jones et al., 1951). In this frame of reference (Fig. 2.2(b)) there is a steady flow of Mach number $M_0 = M_i \sec\theta_w$, directed down the wedge surface, which encounters a stationary oblique shock i at an angle $\phi_1 = \pi/2 - \theta_w$ and is deflected by an angle θ_1 determined by equation 2.5. The properties of the flow in region 1, including its Mach number M_1, are given by the Rankine-Hugoniot equations for oblique shocks. The flow then encounters the reflected shock r and is deflected by θ_2. Clearly θ_2 must equal θ_1 in order to bring the flow to be once again parallel to the wedge surface. This determines the shock angle ϕ_2 through equation 2.5 and hence completely defines the shock geometry and ultimately the properties of the flow in region 2. In regular reflection, therefore, there are three

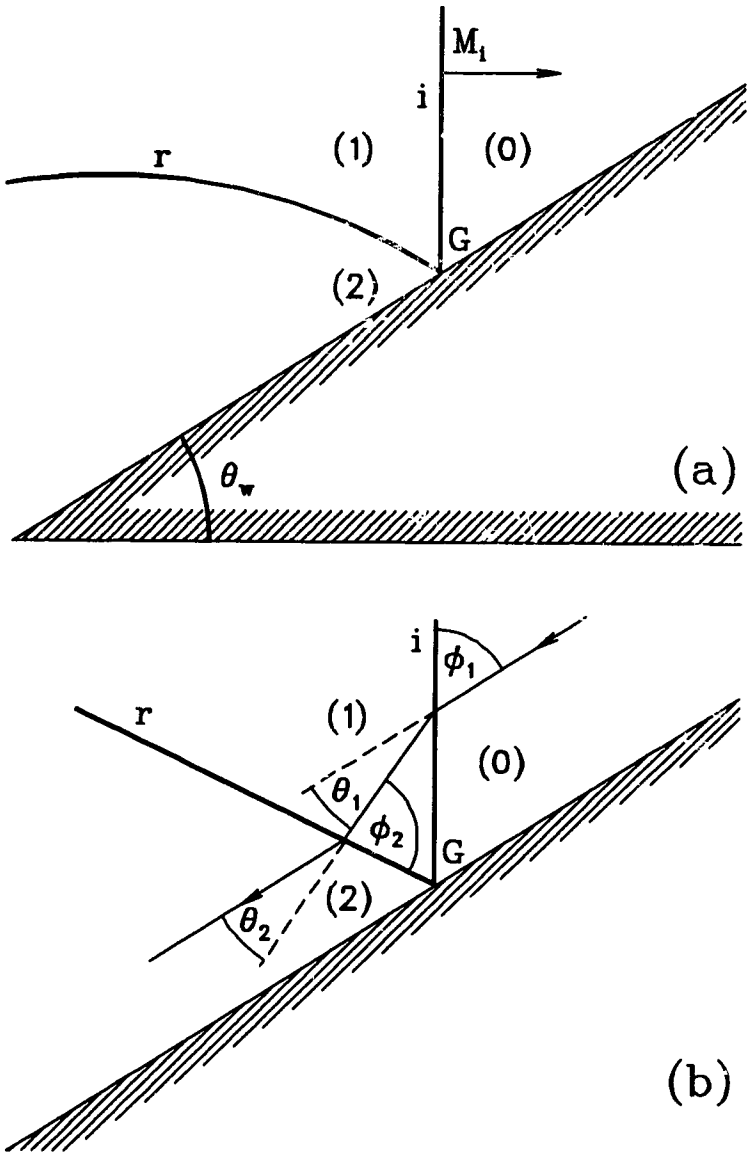

Figure 2.2: Regular reflection of a plane shock off a plane wedge of angle θ_w: (a) lab frame and (b) pseudo-stationary frame of reference.

distinct regions having different thermodynamic properties.

The above situation fails if the deflection angle θ_2 exceeds the maximum deflection angle $\theta_{\max}$ for which equation 2.5 has a solution at Mach number M_1. This happens when the shock strikes a wedge of sufficiently small angle θ_w. In that case regular reflection cannot occur and a new configuration called *Mach reflection* is formed (Fig. 2.3(a)), in which a shock m known as the Mach stem connects the wedge surface to a triple point T where the incident shock i and the reflected shock r meet. Considering the shocks straight near the triple point and assuming self-similarity as before, the flow is made pseudo-stationary by going to a co-ordinate system $(x/t, y/t)$ attached to point T. In this frame of reference (Fig. 2.3(b)) there is an incident flow of Mach number $M_0 = M_i \sec(\theta_w + \chi)$, a portion of which is deflected by the stationary oblique shocks i and r through angles θ_1 and θ_2 in succession. The portion of the incident flow encountering the stationary Mach stem m is deflected through an angle θ_3. Near the triple point the boundary condition is that $\theta_3 = \theta_1 - \theta_2$, which implies that the flows in regions 2 and 3 are parallel but not necessarily of the same speed. A contact surface or slipstream s separates the two regions. Across this boundary there is no change in pressure but there are changes in density, temperature and entropy. Mach reflection therefore forms four regions of distinct thermodynamic properties.

A shock configuration that is truly self-similar expands in time according to a purely linear law, as if it was being photographically enlarged. The experimental study of such phenomena only requires that the properties of the flow field be measured at one instant in time. Shock reflection off a single wedge, whether regular or Mach, generally satisfies this condition at least in the proximity of the reflection point or triple point. There are types of shock wave phenomena, however, where the flow field is not self-similar. As an example, if an incident shock travels along a wedge whose angle changes, either abruptly or gradually, the reflection geometry is continuously affected by a 'memory effect' of its past history that does

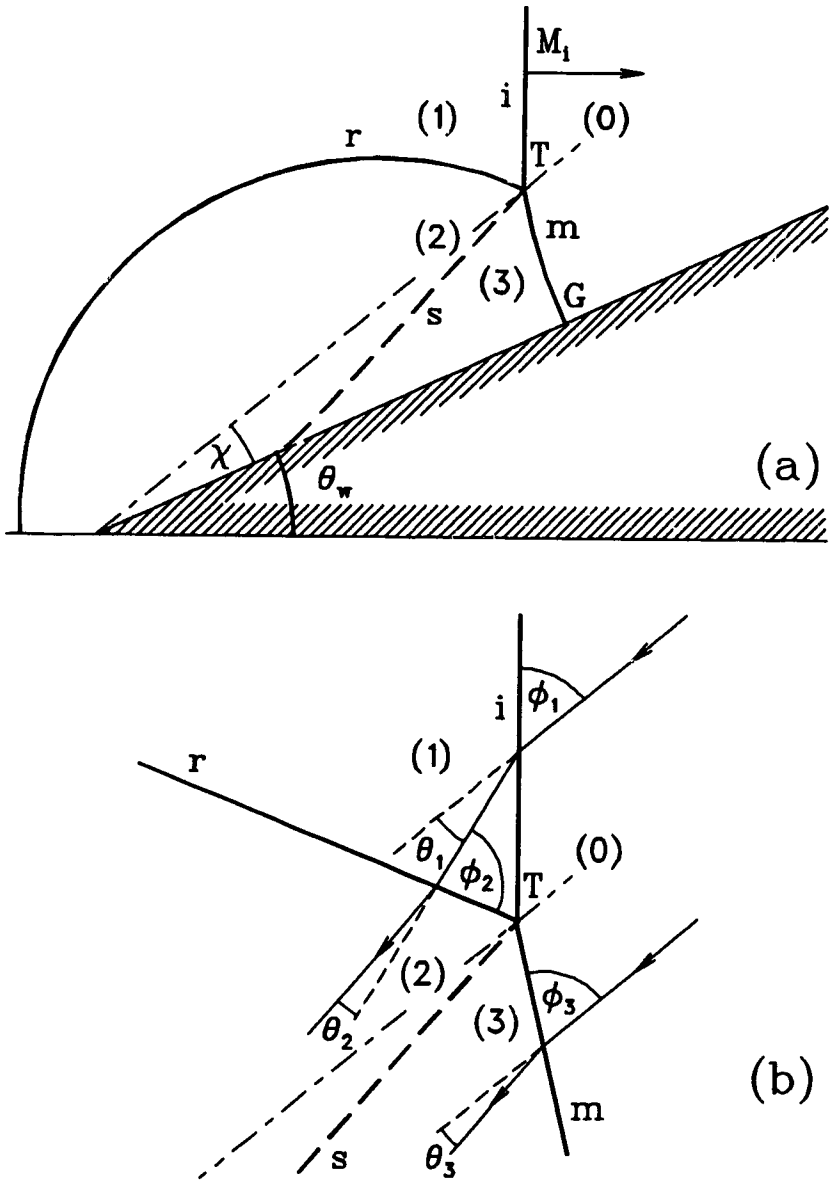

Figure 2.3: Mach reflection of a plane shock off a plane wedge of angle θ_w: (a) lab frame and (b) pseudo-stationary frame of reference.

not become pseudo-stationary in a time-dependent reference frame $(x/t, y/t)$.

2.4 Description of the shock tube

The flows to be studied were generated in a shock tube (Whitten, 1969) with internal cross-sectional dimensions of 7.65 cm width by 25.4 cm height. The shock tube consisted of a compression chamber 1.04 m long that could be filled with air pressurized up to 6 atmospheres, and an expansion chamber 7.01 m long open to atmosphere. The air in the compression chamber was confined by an acetate diaphragm which could be burst by a needle driven by a solenoid. The breaking of the diaphragm caused a shock wave to propagate down the expansion section, and by the time it reached the test area in the far end of the tube the shock front was planar for all practical purposes. Two pressure transducers along the expansion chamber allowed the shock velocity to be measured and also supplied a synchronization signal to the laser system used to photographically record the phenomenon.

The observation section near the end of the shock tube consisted of two thick optical-quality windows mounted flush with the inner surfaces of the tube sides. These windows allowed visibility of the full height of the tube cross section for a length of about 30 cm. A model off which the incident shock would reflect, generally a single- or multiple-sloped stainless steel wedge bolted to the shock tube floor, could be mounted between the windows. The model was uniform in shape across the width of the shock tube. For all practical purposes, the flow field in the test section could be considered purely two-dimensional in a plane parallel to the windows.

2.5 Visualization methods

2.5.1 Shadow and schlieren photography

The study of shock waves and their interactions requires that the geometry of the shock fronts be known as a reflection evolves. The optical techniques of shadowgraphy and schlieren photography visualize the shocks as sharp lines on a contrasting background, revealing their shape over the entire field of view. Strong vortices and contact surfaces between regions of the gas having different densities are also identified by these methods.

The simplest form of shock visualization is the direct contact shadowgraph, in which a photographic film is directly illuminated by a beam of parallel light that traverses the phenomenon. For two-dimensional flow fields, the illumination is perpendicular to the plane of the flow. The light source gives a pulse short enough to freeze shock motion. Because the light rays are deflected by the strong refractive index gradient at the shock fronts, the amount of light falling on the film is reduced in the region directly corresponding to a shock and increased in an adjacent region. Shock fronts appear therefore on the photographic record as thin double images opposite in exposure. It may be shown (see Goldstein, 1970) that the change in intensity at a point on the image plane relative to the intensity at the corresponding point of the test section is proportional to the *second* partial derivative of refractive index with respect to distance in the plane perpendicular to the axis of illumination.

Schlieren is similar in principle to shadowgraphy in that it is based on the deflection of originally parallel light rays due to refractive index gradients. In a schlieren system, however, the light having traversed the phenomenon is brought to a focal point before being imaged onto the film. A knife edge precisely positioned at the focal point cuts off any light ray that has been deviated from its normal path in such a way as to be intercepted. Because these deflected light rays are completely

removed from the image, schlieren photography visualizes refractive index changes with greater contrast than shadowgraphy. The change in intensity at a point on the image plane relative to the intensity at the corresponding point of the test section is proportional to the *first* partial derivative of refractive index with respect to distance in the direction perpendicular to the axis of illumination and the knife edge (see Goldstein, 1970). For certain applications it is advantageous to be able to control the directional sensitivity of the system by the orientation of the knife edge. If a uniform sensitivity is required in the plane perpendicular to the axis of illumination, a narrow circular aperture centered at the focal point is used in place of the knife edge.

2.5.2 Interferometry

Whereas the previously mentioned methods are only suitable for the visualization of shock fronts and other areas of large gradients in the refractive index of the gas, interferometry gives a much greater amount of information about the refractive index, and ultimately the density, of the gas at every location in the test field. This technique depends on the change in optical path length through the medium as a function of refractive index, rather than on the deflection of light rays. In fact, refraction effects are expected to be negligible in order for an interferogram to be accurate.

Until the advent of holography, the Mach-Zehnder interferometer was the most common type of interferometric system used for shock studies (Hall, 1954). This device uses a single plane wavefront of monochromatic light which is split into two beams by a beam splitter. The two beams are reflected by mirrors along separate paths, or arms, and eventually recombined by a second beam splitter into a single beam that is imaged onto the film. By accurate adjustment of the optical components, it is possible to make the optical path length along the two arms exactly identical over the entire area of the beam, in which case the output

beam will be uniformly bright since the two beams will interfere constructively everywhere. If one of the arms passes through the observation section containing the phenomenon, then any change in refractive index occurring in this section since the interferometer was aligned will cause the formation of interference fringes on the uniform background of the output beam. As it will be seen later, these fringes describe contours of constant refractive index and can be used to obtain a density map of the gas. Alternatively, by slightly tilting one of the beam splitters a pattern of uniform, straight background fringes may be overlaid on the output beam when the field is undisturbed. In the presence of a disturbance these fringes will shift locally, the amount of shift being proportional to the change in refractive index.

Because of the requirement that the optical path length along the two arms be equal everywhere, the Mach-Zehnder interferometer is relatively difficult to align and requires optical components of the highest quality throughout the system, including the windows of the observation section. The advent of holographic interferometry has provided a much more practical and equally effective alternative to this method.

Chapter 3

Holography

3.1 Introduction to the technique

Holography is an optical method that allows a wavefront of light to be stored on a photosensitive medium and subsequently reconstructed. The wavefront may be represented as a complex quantity, having at any point in space an amplitude and a phase. Photographic emulsions, being sensitive to irradiance, can only record the real amplitude of the light, whilst the phase information is irrevocably lost. The holographic process expands the capabilities of the photographic medium by combining the wavefront to be recorded with a plane wave from the same coherent source, and storing the resulting interference pattern in a high-resolution emulsion. The reference wave effectively encodes in the stored pattern the local phase information of the object wavefront as well as its amplitude. In the reconstruction process, a plane wave with the same orientation and wavelength as the original reference wave is used to illuminate the developed emulsion. The pattern stored in the emulsion spatially modulates the reconstruction wave so that the resulting light is a replica of the two waves originally interfering when the hologram was recorded. The object wave is therefore restituted in its entirety when the hologram is reconstructed.

The first holograms (Gabor, 1949) were recorded with collinear beams using

monochromatic light of very short coherence length, and had the disadvantage of having to be viewed by staring directly into the reconstructing beam. The holographic technique truly came of age with the discovery of the laser and the invention of off-axis holography (Leith and Upatnieks, 1962, 1963, 1964), in which the reference beam impinges on the film from a different direction than the object wave. The reconstructed wavefront is then angularly separated from the reconstructing beam and can be observed without difficulty. This is by far the most commonly used kind of holography, and the basis for numerous variations.

3.2 Hologram formation equations

In later parts of this dissertation some aspects of the recording technique used in the present work will be analysed theoretically. It is therefore useful to lay the groundwork by briefly describing the hologram formation process from a mathematical standpoint. The notation that will be followed here is the one used in the classical book on holographic interferometry by Vest (1979).

In the recording of an off-axis hologram, as previously mentioned, the reference wave propagates in a direction different from that of the object wave. Postulate a plane reference wave whose propagation vector is parallel to the y-z plane and forms an angle θ_R with the normal to the film plane $z = 0$. The complex amplitude (representing real amplitude and phase) of this wave at $z = 0$ is

$$\mathbf{U}_R(x, y) = a_R \exp(i2\pi f_y y), \tag{3.1}$$

where $f_y = \sin\theta_R/\lambda$ is the *spatial frequency* of the reference wave. An object wave $\mathbf{U}_o(x, y)$ coherent with the reference wave also impinges on the film. When the two waves interfere at the film plane, the reference wave may be regarded as producing a set of "carrier" fringes of spatial frequency f_y that is modulated by the object wave to yield the interference pattern constituting the hologram. This interpretation (Leith and Upatnieks, 1962) is an exact analogy to ordinary communication theory,

in which a signal is encoded by modulating a *temporal* carrier wave. The irradiance at the film plane from the two waves combined is

$$\begin{aligned} I(x,y) &= |\mathbf{U}_o + \mathbf{U}_R|^2 \\ &= |\mathbf{U}_o + a_R \exp(i2\pi f_y y)|^2 \\ &= |\mathbf{U}_o|^2 + a_R^2 + a_R \mathbf{U}_o \exp(-i2\pi f_y y) + a_R \mathbf{U}_o^* \exp(i2\pi f_y y). \end{aligned} \quad (3.2)$$

After having been exposed to the irradiance pattern and developed the film has an amplitude transmittance $\mathbf{t}(x,y)$ that is proportional to $I(x,y)$:

$$\mathbf{t}(x,y) = \mathbf{t}_b + \beta \left[|\mathbf{U}_o|^2 + a_R \mathbf{U}_o \exp(-i2\pi f_y y) + a_R \mathbf{U}_o^* \exp(i2\pi f_y y) \right], \quad (3.3)$$

where the constant term βa_R^2 has been absorbed inside $\mathbf{t}_b$. It is instructive to express $\mathbf{U}_o(x,y)$ as a function of real amplitude and phase:

$$\mathbf{U}_o(x,y) = a_o(x,y) \exp\left[-i\phi_o(x,y)\right], \quad (3.4)$$

and substitute the above into equation 3.3 to obtain, after combining the exponentials,

$$\mathbf{t}(x,y) = \mathbf{t}_b + \beta a_o^2(x,y) + 2\beta a_R a_o(x,y) \cos\left[2\pi f_y y + \phi_o(x,y)\right]. \quad (3.5)$$

Equation 3.5 clearly shows that the holographic recording in the emulsion consists of a set of fringes of spatial frequency f_y modulated in amplitude by $a_o(x,y)$ and in phase by $\phi_o(x,y)$.

For reconstruction, the hologram is illuminated by a plane wave having the same spatial frequency as the reference wave used in the recording:

$$\mathbf{U}_c(x,y) = a_c \exp(i2\pi f_y y). \quad (3.6)$$

The resulting complex amplitude of the light emerging through the film, in the vicinity of the hologram plane, is given by $\mathbf{t}(x,y)\mathbf{U}_c(x,y)$:

$$\mathbf{U}_I(x,y) = \left(\mathbf{t}_b + \beta |\mathbf{U}_o|^2\right) a_c \exp(i2\pi f_y y) + \beta a_c a_R \mathbf{U}_o + \beta a_c a_R \mathbf{U}_o^* \exp(i4\pi f_y y). \quad (3.7)$$

The second term in the above expression is the only one of relevance for most applications, since it represents a diffracted wave which is a replica of the original object wave. The irradiance of this reconstructed object wave is

$$I_{oI}(x,y) = \beta^2 a_c^2 a_R^2 \left|\mathbf{U}_o\right|^2 . \tag{3.8}$$

The other two terms in equation 3.7 describe additional reconstructed waves. The first term represents a portion of the reconstruction wave which is transmitted by the hologram with some irradiance modulation, whilst the third term represents a wave which is the conjugate of the original object wave. All the reconstructed waves are angularly separated, and the conjugate wave is generally suppressed by diffraction effects in the emulsion unless the angle θ_R is small.

3.3 Holographic interferometry

3.3.1 Principles and application

Through the use of off-axis holography, it is possible to produce images overlaid by a pattern of interference fringes that reveal changes in the state of the object being holographed. These changes may consist of deformation, displacement or rotation in the case of an opaque, diffusely reflecting object, or variations in thickness or refractive index in the case of a transparent object. This type of interferometry is achieved by recording holographically the wavefront of light from the object at a given time and comparing it interferometrically with either the direct wavefront from the object at a later time or a holographic recording of it. The interferometric comparison simply consists of reconstructing the hologram or holograms in such a way that the two wavefronts are in perfect spatial registration and observing or photographing the combined wave. A major advantage of holographic interferometry over conventional (Mach-Zehnder) interferometry is that the reference arm and the test arm are spatially coincident but temporally separated, so that path length

differences are only introduced by the time-varying phenomenon under study and not by characteristics of the optical equipment.

There are many variations in the technique of holographic interferometry which are extensively described in the aforementioned book by Vest. Here the attention is limited to the specific method used in the present work, that is, two-exposure holographic interferometry. Moreover, the only case considered is where the object beam is formed by a plane wave propagating through a refractionless transparent medium (also known as a phase object). This situation closely corresponds to the actual experimental conditions in our optical system: the collimated object beam is normal to the window surfaces in the test section, and except at the shock fronts the refraction of the beam traversing the test volume of gas can be shown to be negligible (van Netten, 1988).

In two-exposure holographic interferometry, two successive recordings of the same object are made on the same film or plate, so that upon reconstruction the wavefronts corresponding to the two exposures interfere with each other and reveal changes in optical path length as a pattern of fringes. The two exposures usually record a reference condition and an altered state due to some physical phenomenon. For some studies it may be useful to record two different phases of an evolving phenomenon, in which case the interferogram shows the change between them (differential holographic interferometry). In the present application, one hologram was recorded when no shock was present in the test section and the other during shock passage. For an object beam propagating in the z direction and traversing a phase object having refractive index distribution $n(x, y, z)$, the optical path length Φ through the medium is

$$\Phi(x, y) = \int n(x, y, z) dz. \tag{3.9}$$

If the refractive index distribution is $n_1(x, y, z)$ during the first holographic exposure and $n_2(x, y, z)$ during the second, the object waves recorded on the film and

then jointly reconstructed are

$$\mathbf{U}_{o1} = a_1(x,y)\exp\left[i\frac{2\pi}{\lambda}\Phi_1(x,y)\right] \tag{3.10}$$

and

$$\mathbf{U}_{o2} = a_2(x,y)\exp\left[i\frac{2\pi}{\lambda}\Phi_2(x,y)\right], \tag{3.11}$$

where Φ_1 and Φ_2 are given by equation 3.9. Assuming for simplicity that a_1 and a_2 in the reconstructed object waves are uniform, unit amplitudes, the irradiance $I(x,y) = |\mathbf{U}_{o1} + \mathbf{U}_{o2}|^2$ of the combined reconstructed waveforms in the image plane may be expressed as

$$\begin{aligned} I(x,y) &= 2\left\{1 + \cos\frac{2\pi}{\lambda}\left[\Phi_2(x,y) - \Phi_1(x,y)\right]\right\} \\ &= 2\left\{1 + \cos\left[\frac{2\pi}{\lambda}\Delta\Phi(x,y)\right]\right\}. \end{aligned} \tag{3.12}$$

In most applications the refractive index during one of the exposures, say the first, is uniform and can be denoted by n_0. Then the optical path length difference between exposures is

$$\Delta\Phi(x,y) = \int \left[n(x,y,z) - n_0\right] dz. \tag{3.13}$$

In the experimental configuration used in this work, the reflection of a plane shock wave may be treated as a strictly two-dimensional phenomenon in the plane normal to beam direction. The refractive index distribution induced by the shock is therefore a function of x and y only, and the expression for the optical path length difference is reduced to

$$\Delta\Phi(x,y) = \left[n(x,y) - n_0\right] L, \tag{3.14}$$

where L is the distance that the light must travel in the test section.

An important parameter in the recording of holograms is the ratio of reference beam to object beam brightness, which affects the diffraction efficiency for reconstruction. The nonlinear response characteristics of the emulsion make it virtually

impossible to establish a clear cut value that will give best results under all circumstances. Reference-to-object-beam ratios of 3:1 to 10:1 are often suggested in order to keep the modulation within the linear part of the response curve. For holographic interferometry, in which the ultimate motive is to produce interference fringes of high visibility in the reconstructed image, a reference-to-object-beam ratio of 1:1 is recommended (Vest, 1979) on the basis of experimental evidence, though the ratio can be higher if other conditions dictate it.

3.3.2 Fringe interpretation

According to equation 3.12, bright fringes will form at those positions where $\Delta\Phi = N\lambda$, or substituting 3.14,

$$[n(x,y) - n_0]\, L = N\lambda. \tag{3.15}$$

These *infinite fringes* describe contours of constant refractive index. Applying equation 3.15 at any two points on the reconstructed image which lie on bright fringes, we obtain by subtraction a formula relating the difference in refractive index to the fringe count N_{1-2} between the two points:

$$\Delta nL = N_{1-2}\lambda. \tag{3.16}$$

The refractive index throughout the field is mapped by giving order numbers to the fringes, assigning the number $N = 0$ to a bright fringe in an area where the refractive index n_0' is known. The centers of all subsequent bright fringes are assigned numbers $N = 1, 2, 3, \ldots$ consecutively, and the centres of the interspacing dark fringes are assigned numbers $N = 0.5, 1.5, 2.5$, etc. At any location the refractive index is then given by

$$n = n_0' + \frac{N\lambda}{L}. \tag{3.17}$$

Because changes in optical path length of $-\Delta\Phi$ and $\Delta\Phi$ yield identical fringe patterns, there is a sign ambiguity in fringe order numbers. Generally the experimenter

has sufficient knowledge of the flow field to infer the appropriate sign. If this is not the case, it is possible to resolve the ambiguity by introducing *finite fringes* in the interferogram through a small tilt of the reference beam angle between the two exposures (see Vest, 1979). Finite fringes reveal changes in refractive index by their local displacement from a regular straight line pattern, and allow quantitative measurements to be made with no doubt about the sign of the change. On the other hand, they yield a much less readily understandable map of the refractive index distribution than infinite fringes. Only infinite fringe interferometry was involved in the work presented here.

From the refractive index, the density of a gas may be obtained using the *Gladstone-Dale equation*:

$$n - 1 = K\rho, \tag{3.18}$$

where K, the Gladstone-Dale constant, is a property of the gas. It is a weak function of the recording wavelength and is nearly independent of temperature and pressure under moderate physical conditions. Combining the above with equation 3.17 gives the following expression for the density along a fringe of order N:

$$\rho = \rho_0' + \frac{N\lambda}{KL}, \tag{3.19}$$

where ρ_0' is the density at the zeroth order fringe.

3.4 The existing holographic interferometer

The original optical system that was used as foundation for the present work is shown in Figure 3.1. A thorough description of the equipment is given by van Netten (1988), and only an overview will be presented here.

The source of light for the holographic system was a ruby laser. The laser cavity was bounded by two plane dichroic mirrors, having reflectances of 100% (back mirror) and 60% (front mirror) at the ruby emission wavelength of 694.3 nm. The lasing element was a ruby rod surrounded by a helical flashtube that

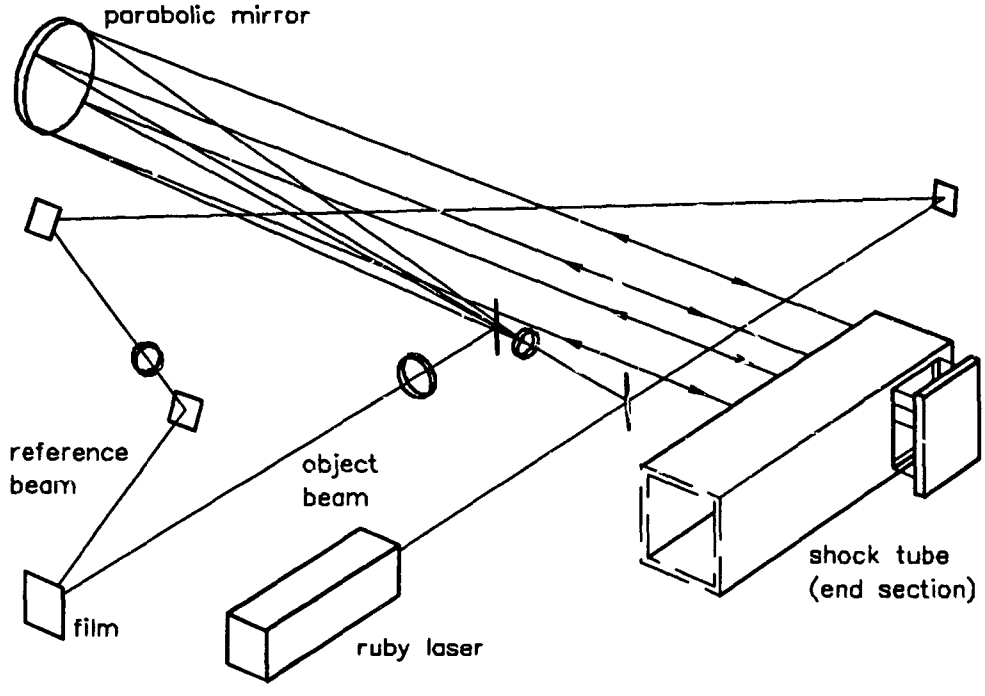

Figure 3.1: Original layout of the holographic interferometer used for producing infinite fringe interferograms of shock waves.

provided the optical pumping for approximately 1 ms. The cavity also contained a Q-spoiling system composed of an air-spaced polarizer and a transverse Pockels cell configured as a switchable quarter-wave plate. The lasing action within the pumping period could be enabled or inhibited by modulation of the Q-switch, generating trains of light pulses. To obtain a pure Gaussian beam suitable for holographic applications, a 2 mm aperture coaxial with the ruby rod was placed in the cavity. By introducing large diffraction losses, this aperture purified the fundamental TEM_{00} mode of oscillation from higher transverse modes that could be sustained in the 10 mm diameter ruby rod (Barnes, 1970).

The light from the laser was divided into two equal portions by a 50% primary beam splitter. The reflected portion was expanded by a diverging lens so that it filled a parabolic mirror 30.5 cm in diameter, in a slightly off-axis configuration.

The focal lengths and spacing of lens and mirror were such that the wide beam leaving the latter was parallel. The light then traversed the test section of the shock tube (see Section 2.4) at normal incidence to the windows, and was folded back onto itself by a plane stainless steel mirror located behind the back window. The fact that the light travelled twice through the test volume classifies this as a *double-pass* design. The reflected light retraced its path to the parabolic mirror and thence converged toward the expanding lens. A secondary beam splitter deflected 50% of this return beam into a lens system that imaged it onto a segment of 35-mm holographic film held in a stretch mount. Note that this beam splitter unavoidably wasted half of the outgoing beam on its way to the parabolic mirror by deflecting it out of the apparatus. Assuming negligible losses in the other parts of the object beam path, therefore, 25% of the light reflected by the primary beam splitter reached the film.

The portion of laser light transmitted through the primary beam splitter formed the reference beam of the holographic system. It was routed via three mirrors along a path whose length matched that of the object beam to within the coherence length of the laser (several centimetres), a necessary condition for the formation of holograms. Between the second and the third mirror, which directed the light onto the film from an angle of about 30° to the normal, was placed a diverging lens that expanded the beam so that it covered the whole image area. Because of the 4:1 power imbalance between the two beams due to the presence of the secondary beam splitter on the object beam path, the local brightness ratio at the film was reduced to the desired value of about 1:1 by making the size of the reference beam projection proportionately larger (van Netten, 1989).

Holographic interferograms were recorded with two light pulses created by Q-switching the laser cavity twice during a single firing of the flashtube. Laser firing was triggered by the passage of the shock wave over a pressure transducer in the wall of the shock tube, through an adjustable electronic delay. The triggering delay and

pulse spacing were set so that the first hologram would record the undisturbed field just before shock wave arrival in the test section, and the second would capture the shock in the desired position. Typical intervals between the two exposures were in the order of 100 to 500 μs. The double-pass design of this interferometric system effectively doubled its sensitivity with respect to a single-pass system, since the density gradient per fringe is inversely proportional to the distance that the light must travel in the test section (equation 3.19).

Because the object beam projected a focused image on the film, each point of the imaged object corresponded uniquely to a point on the emulsion, and the reconstructed holographic image also appeared at the film plane. Under such conditions, a hologram can be reconstructed with a light source of wavelength different from that of the recording laser without introducing any distortions in the reconstructed image or the interferometric fringes. The expanded beam from a low-power Helium-Neon laser, having a wavelength of 632.8 nm, was generally used for the reconstruction and photographing of the holograms, but the white light from a slide projector was also a convenient and equally effective reconstruction source. Details of the optical set-up for photographing the reconstructed images are given by van Netten (1988).

Chapter 4

Time-resolved holography

4.1 Objectives

Holographic interferometry has assumed a position of importance as a tool for the study of compressible flows, but it still widely lacks one feature that most other methods can offer: the ability to record sequences of images in order to follow the evolution of a phenomenon in time. One way to achieve time-resolved recordings is a hybrid method based on real-time holographic interferometry. A single hologram of the undisturbed field is exposed, developed and replaced in the exact position where it was recorded (or even developed *in situ*). The original reference beam then works as a reconstruction beam and creates a replica of the object wave under no-flow conditions. During the phenomenon, the direct beam from the optical system and the reconstructed object beam from the hologram interact with each other to give a real-time interferogram. The interference pattern may be recorded by conventional high-speed cinematography. This technique, aside from its technical complexity, requires that the reference exposure be taken several minutes before the phenomenon. Extraneous changes to the field may easily occur during such a long gap.

The goal of the project described in this dissertation was to develop a time-resolved holographic interferometric apparatus that would be as simple to use as

the existing system and yield a series of individually reconstructible two-exposure holograms through a process of multiplexing. An additional requirement was that the changes to the original optical layout be kept to a minimum, especially with regards to the object beam path. The optical equipment in the Shock Studies Laboratory had undergone an evolutionary process from a schlieren system to a holographic interferometric system that had preserved all the original characteristics, allowing the former mode of operation to be easily restored if desired. It was hoped that this trend could be maintained in the upgrade to time-resolved operation.

4.2 Hologram multiplexing techniques

4.2.1 Spatial multiplexing

The majority of existing implementations of time-resolved holographic systems adopt in one form or another the technique of *spatial multiplexing*, whereby each hologram is recorded on a separate area of film by successive laser pulses. Spatial multiplexing does not rely on optical properties unique to the holographic recording process: ordinary cinematography is nothing but a non-holographic form of this technique. The recording of each hologram on a fresh area of photographic emulsion may be achieved by deflecting the light, by moving the film, or by a combination of the two methods.

The major challenge of the first approach is to make the object beam and the reference beam coincide at the film plane. However, if the object is diffusely illuminated the object wave may be allowed to fall on the entire surface of the film whilst the reference beam illuminates different areas at different times. Gates et al. (1968, 1970) demonstrated a method in which a scatter plate was used to diffusely transilluminate the scene whilst a portion of the light was transmitted without scattering through the plate and formed the reference beam. Time-resolved

sequences were obtained by illuminating different areas of the scatter plate through a rotating prism or nutating mirror so that the reference beam projection on the film moved with time. A modified version of their original scanning method (Hall et al., 1970) selected the illuminated area on the scatter plate by means of an aperture in a rotating disc placed in front of a wide beam. The second method relaxed the need for extremely short exposure times by effectively eliminating the motion of the beam during exposure. By synchronizing the laser pulsing with the angular position of the scanning device, those authors were able to obtain time-resolved sequences of interferograms by exposing each image twice over two separate sweeps. More complex rotating masks have been used by workers such as Dubovik et al. (1977) to generate differential interferograms. Feldman (1970) presented a spatial multiplexing system using a solid-state acousto-optical deflector (see Chapter 7) to redirect the light to different areas of film. For the holography of transparent subjects, he used an arrangement that concurrently displaced both object and reference beams to the same spot on the emulsion to minimize dispersion of object light. Thomas et al. (1972) used three separate lasers to implement a high-speed multiplexing system. The light from each laser was divided into a reference beam that reached a photographic plate and an object beam that traversed the phenomenon along a path common to all the lasers. The common object beam path was then split into three branches that illuminated all the plates, the two additional object beams giving incoherent exposures that did not significantly affect the hologram.

Systems achieving spatial multiplexing by displacing the film have the potential for recording very long sequences of frames. A reel of film in a conventional movie camera transport may be used in applications requiring an extended run length at moderate framing rates (Decker, 1982, Smigielski et al., 1985). For high-speed holographic cinematography, a rapidly rotating holographic plate or a film mounted on the circumference of a spinning drum have been used. Hentschel and Lauterborn

(1985) combined this technique with an acousto-optical beam deflection system to further increase the multiplexing rate by recording quadruplets of frames in a direction perpendicular to the film motion. This composite system achieved framing rates up to 300 kHz and series lengths up to about 4000 images. For holographic interferometric applications, however, a method relying on film displacement would not be suitable because of the great difficulty of exactly repositioning the moving medium over successive sweeps in order to overlay the two required exposures.

4.2.2 Spatial frequency multiplexing

There is a second method of recording sequences of individually reconstructible holograms, taking advantage of a unique property of the hologram formation process. In Chapter 3 it was described how a hologram is recorded by modulation of a set of "carrier" fringes having a specific spatial frequency. The analogy with communications theory may be carried further. In the same way as communications signals having different carrier frequencies can be freely mixed and still remain separable, so can holograms with different "carrier" spatial frequencies be superimposed without losing individuality. This is the underlying principle of *spatial frequency multiplexing.* By having the reference beam fall on the film from a different direction for each exposure, recordings of the object beam may be overlaid on the same area of emulsion and subsequently reconstructed individually. The selection is achieved by shining the reconstruction beam at the same angle as the reference beam used in the desired exposure. This hologram multiplexing technique offers several advantages. The object beam, whether diffused or not, does not need to be repositioned in any way for different exposures. The size of the holograms is not restricted by the need to crowd spatially separated recordings in a given area of emulsion as with most spatial multiplexing schemes. Observation and photography of the reconstructed holograms is simple because the film and the eye or camera may be placed in a fixed position and only the reconstruction

beam reoriented to select a given image. There are, however, limitations to the spatial frequency multiplexing technique, particularly linked to the fact that images are superimposed on a photographic emulsion of finite dynamic range. These limitations, which restrict the number of images that can be multiplexed and also the angle of viewing of each image, will be discussed as part of a separate section analysing the technique in more detail.

Spatial frequency multiplexing has been used by several workers as a method for recording fast holographic sequences of a small number of images. It is interesting to note the use in some early work of a somewhat different but related technique in which the reference beam was stationary and the object beam was imaged from different directions onto the same area of film (Gates et al., 1968) or both beams were stationary and the film was spun about the reference beam axis (Paques and Smigielski, 1965, Smigielski and Hirth, 1970). A single reconstruction beam would then generate angularly separated images propagating from a common pupil.

Lowe (1970) designed a hologram camera based on spatial frequency multiplexing as defined earlier in this section. A rapidly rotating mirror shone the reference beam sequentially onto a series of fixed mirrors that reflected it onto a single area of film, on which the object beam also impinged. The pulses of the laser system were synchronized with the angular position of the spinning mirror by means of a continuous tracer light beam reflected off the latter and a system of photomultipliers positioned in correspondence with the fixed mirrors.

A spatial frequency multiplexing configuration involving multiple laser sources has been presented by Yamamoto (1989), who described different designs for merging the laser outputs into a single object beam with high efficiency. This approach, though capable of high framing rates, is clearly impractical for recording more than a very small number of images. Solid-state spatial frequency multiplexing systems using a single, multiply pulsed laser and selectable reference beam paths have been used by various workers (Hinsch and Bader, 1974, Lauterborn and Ebeling, 1977,

Yamamoto, 1989). The beam switching devices used in these configurations will be examined in Chapter 7. Optical delay lines that generated sets of spatially and temporally separated light pulses have also been used to record spatial frequency multiplexed sequences of interferograms at extremely short intervals (Bush and Charatis, 1982).

For the present work, spatial frequency multiplexing appeared preferable to spatial multiplexing because its implementation exclusively involved the reference beam path. The focused object beam and its optical system could be left unchanged from the previous system, an important factor in assuring easy backward compatibility. The other advantages previously mentioned were also relevant to this application. The limitations of the method in terms of number of frames and viewing angle did not weigh against the choice, because the targeted run length for the recordings was only about five or six images and the focused object beam offered no lateral parallax. Royer and Smigielski (1970) indicate a practical limit of about ten images for spatial frequency multiplexing on standard holographic film.

4.3 Spatial frequency multiplexing—an in-depth look

To clarify the principles and limits of spatial frequency multiplexing, the recording and reconstructions of superimposed holograms with different reference beam angles will be considered mathematically. The geometrical configuration postulated in Section 3.2 will be assumed. For the k-th exposure in a sequence of n, the complex amplitudes of the two waves at $z = 0$ are:

$$\text{object wave:} \qquad \mathbf{U}_{o_k}(x, y) \tag{4.1}$$

$$\text{reference wave:} \qquad \mathbf{U}_{R_k}(x, y) = a_R \exp\left(i2\pi f_{y_k} y\right), \tag{4.2}$$

where $f_{y_k} = \sin\theta_k/\lambda$ is the spatial frequency of the reference wave meeting the film at the angle of incidence θ_k. Each pair of waves in the series records a hologram on the film at successive times. Assuming an ideal response, the overall amplitude

transmittance of the multiply exposed film after developing is obtained by linear superposition of terms having the form of equation 3.3:

$$\mathbf{t}(x,y) = \mathbf{t}'_b + \beta \sum_{k=1}^{n} \left[|\mathbf{U}_{o_k}|^2 + a_R \mathbf{U}_{o_k} \exp\left(-i2\pi f_{y_k} y\right) + a_R \mathbf{U}^*_{o_k} \exp\left(i2\pi f_{y_k} y\right) \right], \quad (4.3)$$

where the constant term $n\beta a_R^2$ has been absorbed inside $\mathbf{t}'_b$.

To reconstruct an individual image in the series, say the j-th, the multiple hologram is illuminated with a plane wave propagating in the same direction as the reference wave used in the recording of that image:

$$\mathbf{U}_{c_j}(x,y) = a_c \exp\left(i2\pi f_{y_j} y\right). \quad (4.4)$$

The resulting complex amplitude of the light emerging through the film, in close proximity to the hologra ı plane, is

$$\begin{aligned} \mathbf{U}_{I_j}(x,y) \;=\; & \left(\mathbf{t}'_b + \beta \sum_{k=1}^{n} |\mathbf{U}_{o_k}|^2 \right) a_c \exp\left(i2\pi f_{y_j} y\right) \\ & + \beta a_c a_R \mathbf{U}_{o_j} \\ & + \beta a_c a_R \sum_{\substack{k=1 \\ k \neq j}}^{n} \mathbf{U}_{o_k} \exp\left[i2\pi \left(f_{y_j} - f_{y_k}\right) y\right] \\ & + \beta a_c a_R \sum_{k=1}^{n} \mathbf{U}^*_{o_k} \exp\left[i2\pi \left(f_{y_j} + f_{y_k}\right) y\right]. \end{aligned} \quad (4.5)$$

Equation 4.5 reveals several important facts about spatial frequency multiplexing and deserves close attention. The first term is simply the transmitted reconstruction beam variously modulated by the recorded pattern. The second term is a reconstruction of the selected object beam, exactly as one would obtain from a non-multiplexed hologram. Therefore, every image stored in a spatial frequency multiplexed hologram can theoretically be reconstructed without degradation or interference from the others, subject to the assumption that the multiple exposures are recorded linearly by the emulsion. As indicated by the third term, all the remaining object beams are simultaneously reconstructed as well, but they are angularly separated from the desired beam and can therefore be excluded from

view. This, however, places a limit on the lateral viewing angle and the divergence of the reconstructed object beam, since crosstalk will occur if rays from an adjacent image fall within the viewing angle for the chosen image. The separation between the selected reconstruction and one angularly adjacent to it is given by the difference in their carrier spatial frequencies, and is equal to the angle $\Delta\theta$ formed by their respective reference beams. Unless the natural divergence of the object beam is less than $\Delta\theta$, a suitable restricting aperture must be placed between the subject and the film when the hologram is recorded. The last term in 4.5 describes the conjugate reconstructions of all the object beams, which also are angularly separated from the main reconstructed beam. However, if the carrier spatial frequencies of two of the recordings are identical but of opposite signs, the conjugate of one of the object waves will be overlaid on the reconstruction of the other. It is important in designing a spatial frequency multiplexing system to avoid the possibility of this condition, which occurs if the angles of incidence of the reference beam in the two exposures are symmetric with respect to the film plane normal. In the configurations presented in this work the reference beam had an additional, constant slant with respect to the y-z plane which eliminated the possibility of conjugate image overlap by introducing an extra component of spatial frequency in the x direction.

The fact that all the object beams are reconstructed simultaneously, albeit at different angles, also results in a reduction of the brightness of the selected image compared to a single-recording hologram of comparable efficiency, since the amplitude of the reconstruction wave must be subdivided among all the images. In the hypothesis that all exposures are equal, the irradiance of each reconstructed image diminishes according to $1/n^2$ (Royer and Smigielski, 1970) where n is the number of images. This intrinsic property of spatial frequency multiplexing does not constitute a serious a limitation on the number of images that can be recorded, since it may be compensated by making the reconstruction beam brighter.

The true limitation in the recording potential of spatial frequency multiplexing

arises from the fact that photographic emulsions have a finite dynamic range and a nonlinear response to light. The intensity transmittance t of the exposed and developed film is a function of the exposure E, which is the product of irradiance and exposure time. The t-E function is a monotonically decreasing S-shaped curve with a nearly linear central portion straddling the inflection point. Since the hologram formation equations assume a linear response of the emulsion, an ideal hologram should be exposed so that its transmittance range lies entirely on the linear portion of the curve. Unfortunately, this criterion is not always compatible with exposure time requirements and optimal diffraction efficiency. In the case of spatial frequency multiplexed holograms, the need to overlay multiple exposures on the film often forces the transmittance range into the nonlinear portions of the t-E curve. The response characteristics of the emulsion for a given exposure are independent of its order in the sequence, and depend on the cumulative exposure level that the film has received before developing. This commutativity generally applies as long as the exposures are made within the latent image retention time of the film, which may vary from minutes to days depending on the type of emulsion.

The effects of the nonlinear film response on the multiplexed images may be analysed by expressing the amplitude transmittance function as a Taylor series (Royer and Smigielski, 1970). Assume that the cumulative mean exposure is close to the inflection point of the t-E curve, as is generally the case for a properly exposed hologram. The cumulative irradiance from all the exposures is

$$I(x,y) = \sum_{k=1}^{n} \left[|\mathbf{U}_{o_k}|^2 + a_R^2 + a_R \mathbf{U}_{o_k} \exp\left(-i2\pi f_{y_k} y\right) + a_R \mathbf{U}_{o_k}^* \exp\left(i2\pi f_{y_k} y\right) \right]. \quad (4.6)$$

Expressing the k-th object wave as

$$\mathbf{U}_{o_k}(x,y) = a_{o_k}(x,y) \exp\left[-i\phi_{o_k}(x,y)\right] \quad (4.7)$$

and substituting the above into 4.6 gives an expression in terms of real amplitude and phase that is easier to handle:

$$I(x,y) = \sum_{k=1}^{n} \left\{ a_{o_k}^2(x,y) + a_R^2 + 2a_R a_{o_k}(x,y) \cos\left[2\pi f_{y_k} y + \phi_{o_k}(x,y)\right] \right\}. \quad (4.8)$$

The intensity transmittance function of the film is expressed as a Taylor series about the working point given by the cumulative mean irradiance $\sum_{k=1}^{n}\left[a_{o_k}^2(x,y)+a_R^2\right]$:

$$t(x,y)=\sum_{m=0}^{\infty}t_m(x,y)\left\{\sum_{k=1}^{n}2a_Ra_{o_k}(x,y)\cos\left[2\pi f_{y_k}y+\phi_{o_k}(x,y)\right]\right\}^m. \tag{4.9}$$

When the hologram is reconstructed, the term $t_0(x,y)$ only modulates the undiffracted portion of the reconstruction beam. The first-order term

$$t_1(x,y)\sum_{k=1}^{n}2a_Ra_{o_k}(x,y)\cos\left[2\pi f_{y_k}y+\phi_{o_k}(x,y)\right] \tag{4.10}$$

is a linear superposition of single-hologram transmittance patterns and generates angularly distinct reconstructions of the original object waves and their conjugates, as previously described when analysing equation 4.5. The terms of even degree are composed of even powers of cosine functions and cross-products of cosine functions having different "carrier" frequencies. None of these have the same periodicity as the first-order hologram interference patterns, and therefore these terms cause diffraction along directions different from those of the reconstructed object waves. Furthermore, the Taylor series coefficient $t_2(x,y)$ is zero if the working point is at the inflection of the t-E curve.

This leaves the odd-power terms of higher degrees. Neglecting terms of degree 5 and above—a reasonable truncation point for the series expansion near the central part of the transmittance curve—only the third-order term is considered:

$$t_3(x,y)\left\{\sum_{k=1}^{n}2a_Ra_{o_k}(x,y)\cos\left[2\pi f_{y_k}y+\phi_{o_k}(x,y)\right]\right\}^3. \tag{4.11}$$

From here onwards, the (x,y) dependence of some parameters will no longer be shown explicitly. Expanding the cube of the summation and collecting terms, the above expression becomes

$$8t_3a_R^3\sum_{k=1}^{n}\left\{a_{o_k}^3\cos^3\left(2\pi f_{y_k}y+\phi_{o_k}\right)\right.$$

$$+ 3a_{o_k} \cos(2\pi f_{y_k} y + \phi_{o_k}) \sum_{\substack{l=1 \\ l \neq k}}^{n} \left[a_{o_l}^2 \cos^2(2\pi f_{y_l} y + \phi_{o_l}) \right.$$

$$\left. + 2\, a_{o_l} \cos(2\pi f_{y_l} y + \phi_{o_l}) \sum_{\substack{m=1 \\ m \neq k, m \neq l}}^{n} a_{o_m} \cos(2\pi f_{y_m} y + \phi_{o_m}) \right] \Bigg\}. \quad (4.12)$$

Using trigonometric identities for the square and the cube of a cosine gives

$$8t_3 a_R^3 \sum_{k=1}^{n} \left\{ \frac{1}{4} a_{o_k}^3 \left[3\cos(2\pi f_{y_k} y + \phi_{o_k}) + \cos(6\pi f_{y_k} y + 3\phi_{o_k}) \right] \right.$$

$$+ 3a_{o_k} \cos(2\pi f_{y_k} y + \phi_{o_k}) \sum_{\substack{l=1 \\ l \neq k}}^{n} \left\{ \frac{1}{2} a_{o_l}^2 \left[1 + \cos(4\pi f_{y_k} y + 2\phi_{o_k}) \right] \right.$$

$$\left. \left. + 2\, a_{o_l} \cos(2\pi f_{y_l} y + \phi_{o_l}) \sum_{\substack{m=1 \\ m \neq k, m \neq l}}^{n} a_{o_m} \cos(2\pi f_{y_m} y + \phi_{o_m}) \right\} \right\}. \quad (4.13)$$

The only terms in the above expression that may diffract the reconstruction beam along the same directions as the reconstructed object waves are those that contain no cross products of cosine functions nor higher harmonics of the fundamental "carrier" spatial frequencies used in recording the hologram. Disregarding all other terms leaves

$$6t_3 a_R^3 \sum_{k=1}^{n} a_{o_k} \cos(2\pi f_{y_k} + \phi_{o_k}) \left(a_{o_k}^2 + 2 \sum_{\substack{l=1 \\ l \neq k}}^{n} a_{o_l}^2 \right). \quad (4.14)$$

The effect of this component of the amplitude transmittance pattern is to generate a spurious set of reconstructed waves which are overlaid as noise on the reconstructed signals created by the first-order term (expression 4.10). For the reconstruction of the j-th exposure, the noise-generating term is

$$N_j = 6t_3 a_R^3 a_{o_j} \cos\left(2\pi f_{y_j} + \phi_{o_j}\right) \left(a_{o_j}^2 + 2 \sum_{\substack{l=1 \\ l \neq j}}^{n} a_{o_l}^2 \right) \quad (4.15)$$

and the signal-generating term is

$$S_j = 2t_1 a_R a_{o_j} \cos\left(2\pi f_{y_j} + \phi_{o_j}\right). \tag{4.16}$$

The signal-to-noise ratio for the j-th image is therefore

$$\frac{S_j}{N_j} = \frac{1}{3}\frac{t_1}{t_3}\left[a_R^2\left(a_{o_j}^2 + 2\sum_{\substack{l=1\\ l\neq j}}^{n} a_{o_l}^2\right)\right]^{-1}. \tag{4.17}$$

Since the noise term contains information from all the undesired images, its influence becomes more pronounced as the number of exposures increases. In addition, for larger numbers of recordings the overall exposure of the film is necessarily pushed farther outside the linear range if each hologram must be sufficiently exposed. Unlike a mere loss in brightness, the effect of emulsion nonlinearity is an actual corruption of the reconstructed image and constitutes therefore a severe limitation. It should be noted, however, that the extraneous content added to each image is limited to the real amplitude of the other images, without any information about their phase. It may therefore be argued that the influence of this noise is not as deleterious in applications involving exclusively phase objects.

Chapter 5

Mechanical scanning

5.1 Basic concept

As a first approach to the spatial frequency multiplexed recording of shock tube experiments, a mechanical system was designed that would angularly sweep the reference beam at high speed via a single, rotating plane mirror. The beam would then be folded by a continuous curved reflecting surface and aimed at a fixed area of film, upon which it would impinge at a rapidly changing angle while the laser was being pulsed. For holographic interferometry, two sweeps would have to be overlaid with accurate registration, one recording the empty field and the other the development of the phenomenon.

This configuration was known *a priori* to have a drawback: it would not allow the recording of holograms over the entire rotation of the mirror since the reference beam had to impinge on the film from the front. The dead time (at least 50%) when the beam was eclipsed would often lead to partially or entirely missed recordings unless the phenomenon being studied could be generated synchronously with the rotation of the mirror—a difficult option with the shock tube being used.

It was felt, nevertheless, that the prototype system would be a good test bench on which to develop the synchronization circuitry for interferometric recordings and generally assess the usefulness of the method. More elaborate mechanical scanners

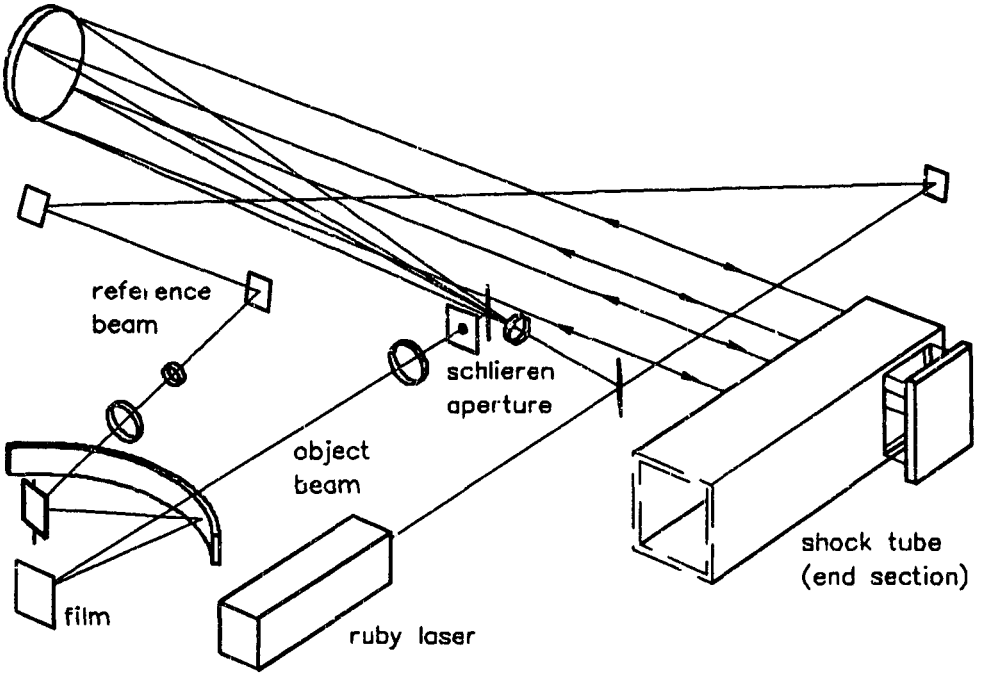

Figure 5.1: Layout of the multiframe holographic recording apparatus with a spinning-mirror reference beam sweeping system (shown enlarged in Fig. 5.2). The schlieren aperture is optional, and is not needed for interferometric recordings.

could have followed if the system proved its potential as a reliable tool for routine visualization work.

5.2 Implementation

5.2.1 Construction details

The layout of the interferometric system converted for time-resolved operation (Racca and Dewey, 1989a) is shown in Figure 5.1. No alterations were made to the original optical paths except for the introduction of the beam sweeping assembly in the reference beam path and the slight displacement of one mirror

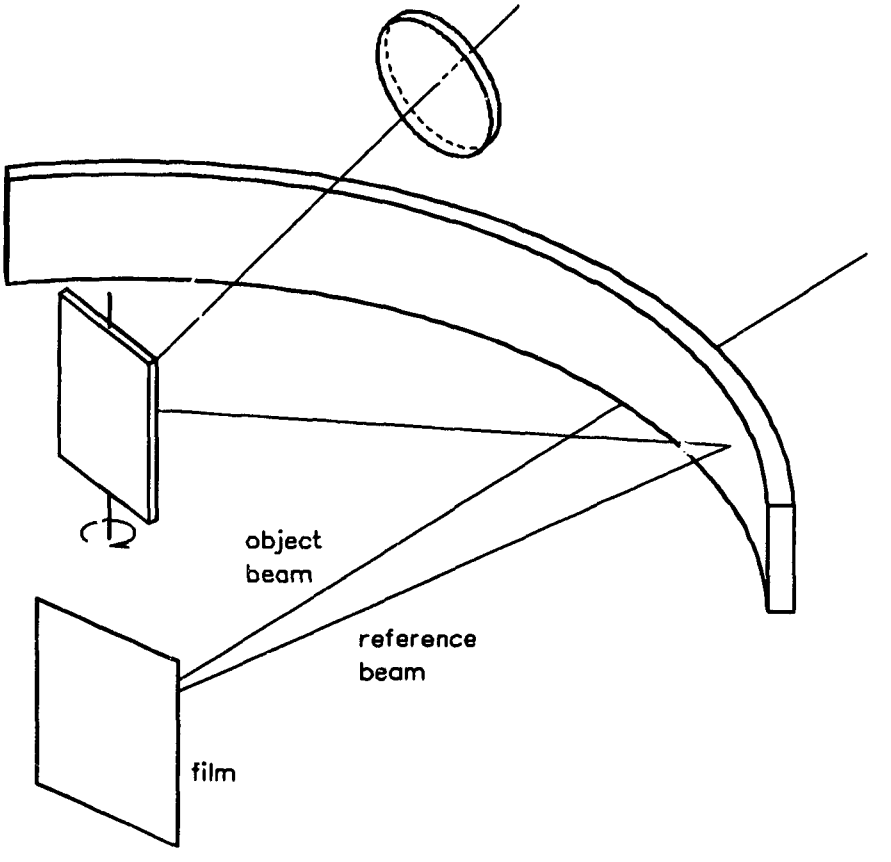

Figure 5.2: Detail drawing of the spinning-mirror beam sweeping assembly.

to compensate for the additional path length. The mechanical beam sweeping system was based on a spinning-mirror design (Fig. 5.2), similar in principle to the one devised by Lowe (1970) but different in construction. Lowe relied on a tracer light beam and photodetectors to establish the angular orientation of the mirror, whereas in the present work an optical pick-up on the mirror shaft was used to obtain a start-of-sweep signal. The reference beam was reflected off a flat, double-faced rotating mirror and was then redirected by a cylindrical mirror onto a fixed area of film where the object beam also impinged. The cylindrical

mirror was coaxial with the spindle of the rotating mirror. The expanded reference beam was made convergent by a positive lens placed before the spinning mirror, so that it reached a focal point about half-way between the latter and the cylindrical mirror surface. Under these conditions the cylindrical mirror virtually collimated the beam in the plane of the sweep, provided the width of the beam at the mirror surface was relatively small compared to the mirror diameter (paraxial condition). This gave the reference beam a uniform instantaneous spatial frequency in the sweep direction, which minimized crosstalk between successive images. No such requirement existed for the direction perpendicular to the sweep, and therefore no steps were taken to collimate the beam in that plane. A continuous, cylindrical reflecting surface was chosen for the prototype in order to give maximum flexibility in the choice of angular spacing between pulses. In a final set-up it would be possible to achieve full collimation of the reference beam by using individual mirrors at predetermined angular intervals. Such mirrors would be plane or parabolic depending on whether the swept beam was initially collimated or divergent.

The spinning mirror, made of polished stainless steel, rotated typically at 18,000 RPM, sweeping the reference beam at twice that rate. It was driven by a Makita power drill unit installed on a vibration-insulating mount and linked by a Mylar belt to the mirror spindle. The useful angular range of approximately 110^o (determined by the cylindrical mirror) was covered by the beam in about 500 μs.

The ruby laser was capable of producing sequences of about ten pulses at at repetition rates up to 10 kHz in the configuration used in the original holographic interferometric system. The only change that had to be made was to increase the size of the intra-cavity aperture from 2 mm to 4 mm since the laser was not able to sustain repeated, closely spaced pulses with the smaller restriction. Hologram quality was not severely affected by the increase in aperture size.

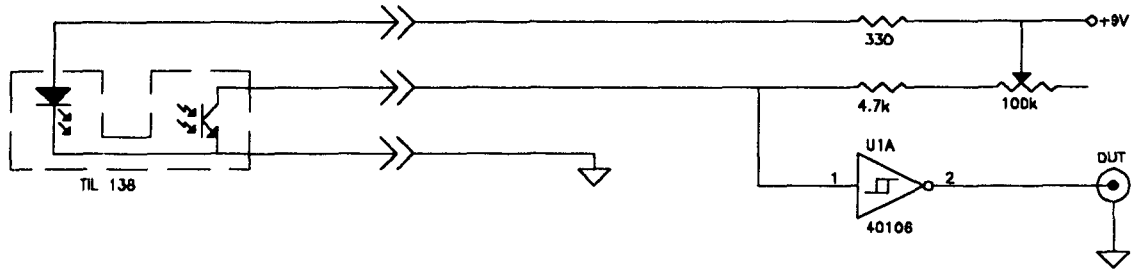

Figure 5.3: Schematic diagram of the mirror position optical pick-up circuit.

5.2.2 Electronics

The firing of the laser was synchronized with the rotation of the spinning mirror by an optical pick-up that indicated when the mirror was at the start of the useful sweeping angle. Figure 5.3 shows the circuit used to drive the transmissive-type optical switch (Texas Instruments emitter-detector TIL 138) which detected a diametrical hole through the mirror axle and therefore generated a pulse every half revolution. The 40106 CMOS Schmitt Trigger prevented trigger jittering and produced an output signal level compatible with the rest of the circuitry. The 100 KΩ variable resistor allowed the pick-up sensitivity to be adjusted for use with various types of emitter-detector assemblies.

The pulses from the optical pick-up circuitry went through a gating circuit (mirror face discriminator, Fig. 5.4) that prevented them from propagating until a signal from a pressure transducer indicating shock wave arrival was received at the ENABLE IN line. This signal triggered one of the two D-type flip-flops in the 4013 chip, which in turn enabled the other flip-flop, wired in toggle mode. The latter was clocked by the pulses from the mirror pick-up via the IN line and acted as a divide-by-two counter, generating a positive transition on the OUT line for every two such transitions on the input. The multivibrator in the 4047 chip provided a time-out signal that reset the trigger flip-flop to its armed state when the mirror

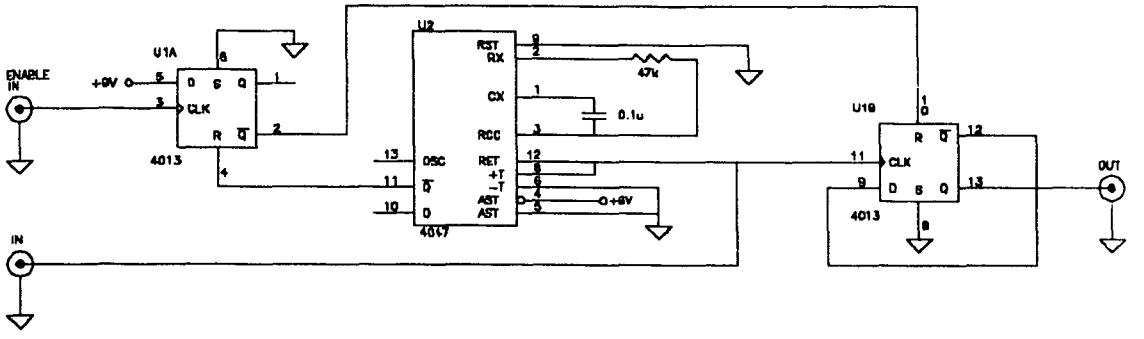

Figure 5.4: Schematic diagram of the mirror face discriminator circuit. This circuit generated one pulse per revolution of the mirror following an initial triggering.

was stopped between recordings, viz. whenever a mirror pulse was not detected within about 10 ms from the previous one. The overall effect of this circuit was to block the pulses from the mirror pick-up until a signal was received from the pressure transducer, and afterward allow through every other pulse, i.e. one pulse per revolution of the mirror.

The circuit shown in Figure 5.5 (reference exposure delay unit) was used to assure that the reference exposure would always be properly recorded. Its purpose was to initiate the firing of the laser pumping flashtube at such a time that it would attain peak intensity just as the spinning mirror reached the start of its useful sweep angle. The firing sequence was enabled by a pushbutton. This signal was debounced by one of the J-K flip-flops in the 74LS73 and enabled the second flip-flop, which was triggered by a signal from the spinning mirror electronics on the TRIG IN line. This initiated a delay interval on a multivibrator in the 74C221 (adjustable via the 100 kΩ trimmer) at the end of which a short positive pulse was generated on OUT1 and OUT2 by the second multivibrator in the 74C221. The OUT2 output could be independently driven by a signal on the AUX IN line, which was used in the recording of the phenomenon exposure.

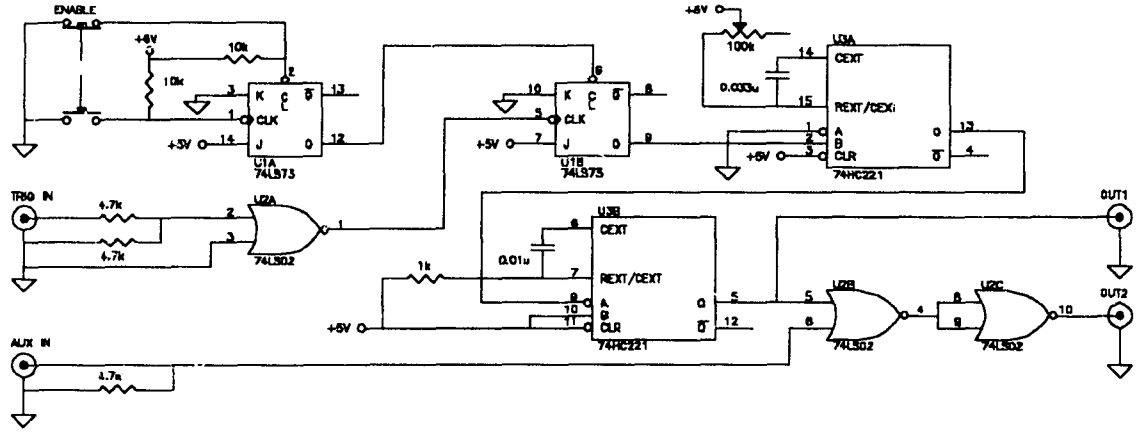

Figure 5.5: Circuit diagram of the reference exposure delay unit. This device was used to synchronize the laser flashtube firing with the position of the spinning mirror for the reference exposure.

These new circuits were combined with the existing electronics to provide the necessary synchronizations for phenomenon and reference exposures. The interplay of the various components is described below.

5.2.3 Exposure synchronization

Figure 5.6 shows in 'black box' form the interconnections of the various electronic units involved in exposure synchronization. The sequence of events and responses that made up a full interferometric recording will now be outlined in detail.

1. The compression chamber of the shock tube was pressurized.

2. The spinning mirror was started.

3. The laser capacitor banks were charged, a process that took a few seconds.

4. A signal indicating the achievement of full charge automatically triggered the pin which burst the pressure-retaining diaphragm in the shock tube. A shock wave started traveling down the tube.

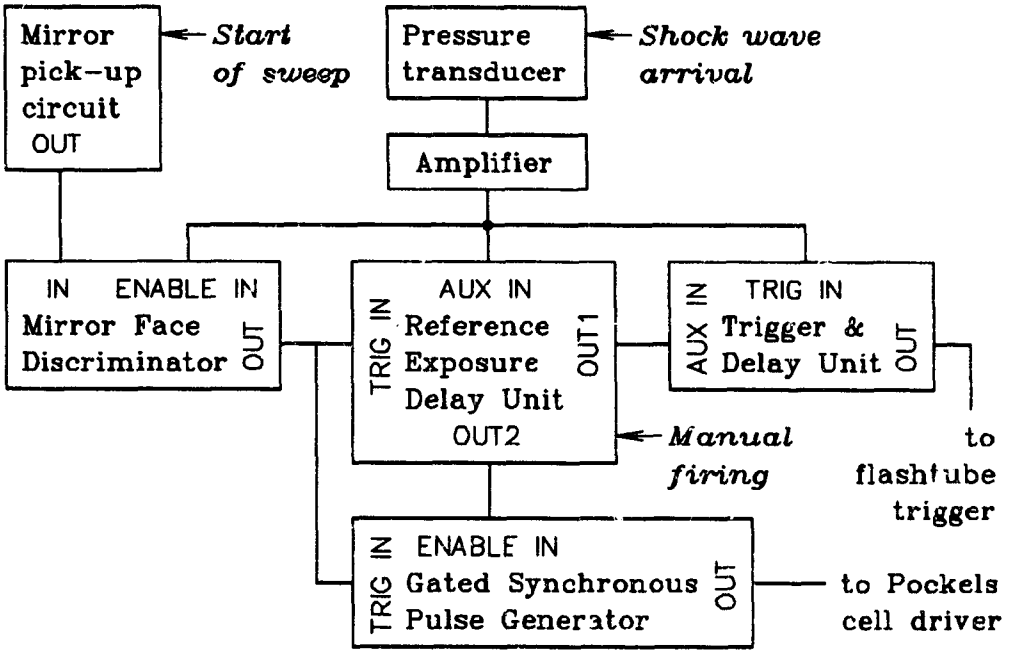

Figure 5.6: Block diagram of the exposure synchronization electronics for the mechanical scanning system.

5. As the shock wave reached a pressure transducer located some centimetres upstream of the window section, it generated a signal (through an amplifier) at the ENABLE IN line of the mirror face discriminator, at the TRIG IN line of the trigger & delay unit, and at the AUX IN line of the reference exposure delay unit—from which it propagated instantly to the OUT2 line connected to the ENABLE IN of the gated synchronous pulse generator. The mirror face discriminator was then enabled to transmit to the OUT line the next pulse reaching its IN line, and every second pulse thereafter. Simultaneously, the gated synchronous pulse generator was enabled to be triggered by a signal reaching its TRIG IN line.

6. After a preset delay to allow the shock wave to travel closer to the window section, the trigger & delay unit generated a signal on its OUT line that fired

the flashtube. The delay was such that the flashtube would reach full intensity by the time the shock entered the field of view.

7. Either face of the spinning mirror reached the angle θ_0 that would aim the reference beam at the beginning of the cylindrical mirror. A pulse from the optical pick-up then went through the mirror face discriminator and triggered the gated synchronous pulse generator via its TRIG IN line, causing it to emit a predetermined train of pulses that cycled the Pockels cell in the laser cavity. The resulting light pulses recorded the phenomenon exposure sweep on the holographic film, subject to conditions to be discussed later.

8. The capacitor banks of the laser were charged again.

9. The reference exposure delay unit was manually enabled by pushbutton when the capacitors reached full charge.

10. The same face of the mirror that was involved in the phenomenon exposure reached θ_0, causing a pulse to be output by the mirror face discriminator. This pulse triggered the reference exposure delay unit, now enabled.

11. After a delay equal to the revolution period of the spinning mirror minus the rise time of the flashtube, the reference exposure delay unit generated a pulse on its OUT1 and OUT2 lines. The former went to the AUX IN of the trigger & delay unit, causing immediate firing of the flash tube, whereas the latter enabled once again the gated synchronous pulse generator through its ENABLE IN line.

12. After a whole revolution, the spinning mirror reached θ_0 again and generated a pulse at the TRIG IN line of the gated synchronous pulse generator. This triggered the emission of a train of pulses that controlled the Pockels cell, generating a sequence of laser pulses which recorded the reference exposure sweep.

Steps 6 and 7 did not necessarily happen in the order listed above, since they were both determined by unrelated events. As a consequence, there was no guarantee that the shock wave arrival in the window section would find the mirror at or near the beginning of the useful sweep angle. It frequently happened that only a partial sequence or no sequence at all would be captured. This and other problems inherent to the mechanical sweeping system will be discussed later.

5.3 Results

The spinning-mirror equipment was used to record holographic sequences both in single-sweep operation and in the full double-sweep mode. In the former, the reference exposure was not impressed on film, that is, the recording sequence outlined in the previous section was only carried out to step 7. To visualize the shock fronts in this case, the optical path of the object beam was configured as a schlieren system (Section 2.5.1) by introducing a small aperture at a focal point. The holographic recording was used in this instance as a convenient substitute for conventional cinematography. Figure 5.7 shows three frames, spaced 200 μs from each other, from a sequence taken at 10,000 pictures per second on Kodak SO-173 film—the photographic material which was used in all experiments. The subject is a plane shock wave travelling from left to right in the image and reflecting off a double-surface wedge. The images clearly show the transition from regular reflection on the first surface to Mach reflection on the second. In frames a) and c), a faint negative 'ghost' of the shock image from frame b), which left a marked impression on the holographic film, can be seen. This happens because a schlieren image is an amplitude phenomenon, and as such it macroscopically affects the local density of the developed film. When dealing with pure phase objects, as in the interferometric recording of transparent phenomena, this type of crosstalk cannot occur.

Of much more interest is the double-sweep mode of operation, which yields a sequence of time-evolving interferograms, or maps of the fluid density distribution

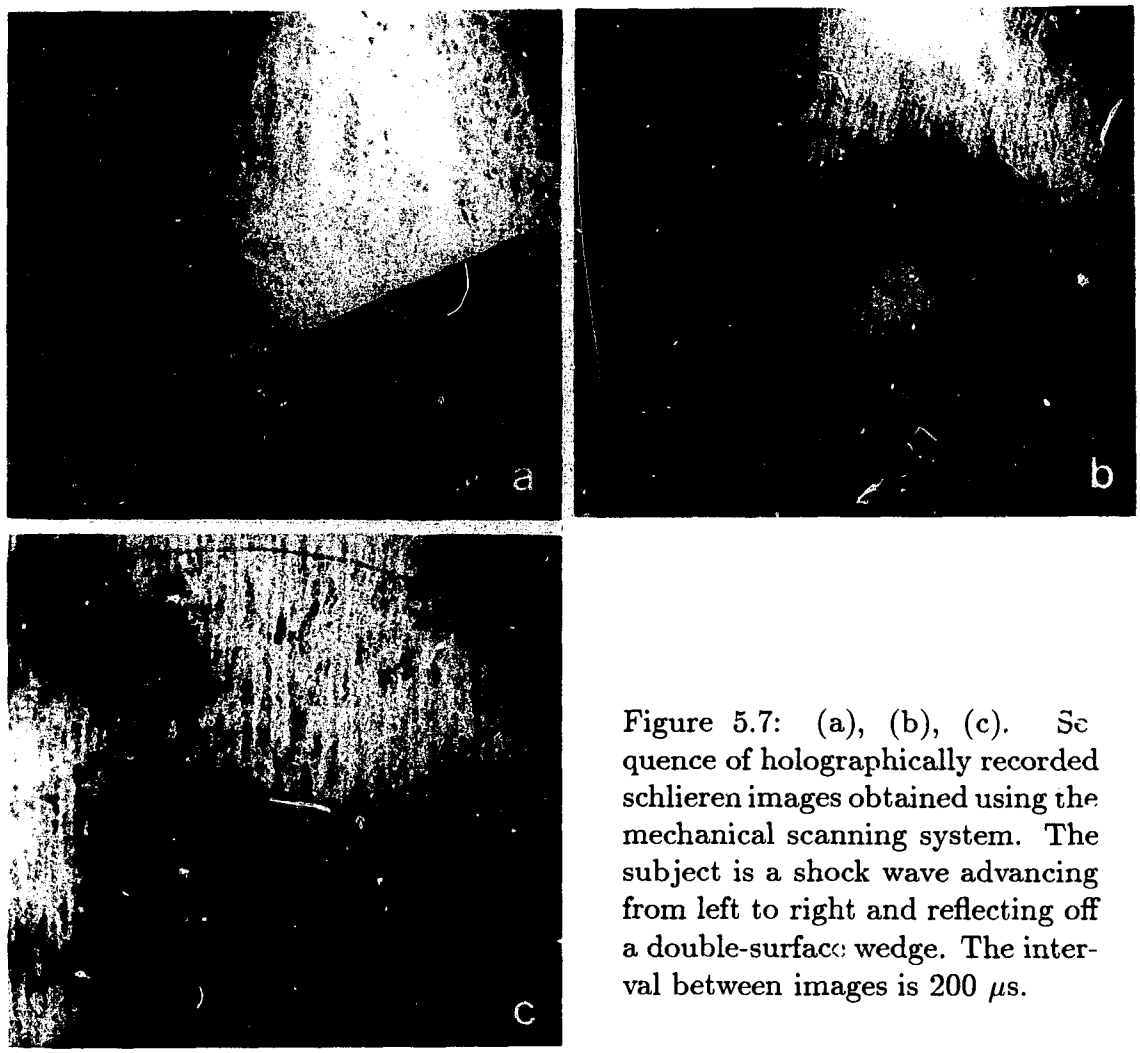

Figure 5.7: (a), (b), (c). Sequence of holographically recorded schlieren images obtained using the mechanical scanning system. The subject is a shock wave advancing from left to right and reflecting off a double-surface wedge. The interval between images is 200 μs.

in the field of view. Unfortunately the spinning mirror system never afforded a level of sweep-to-sweep registration sufficient to produce more than one satisfactory interferogram per run. Figure 5.8 shows such a frame from a double-sweep sequence taken at a rate of 10,000 pictures per second. The quality of this interferogram is comparable to that of recordings obtained with conventional single-frame holographic systems.

Satisfactory reconstruction of the recorded sequences was obtained both with the expanded beam of a He-Ne laser and with white light from a slide projector, shone in progression from the various directions of the recording reference beam.

Figure 5.8: Holographic interferogram from a double-sweep sequence obtained using the mechanical scanning system. The other images in this sequence did not reconstruct good interferograms due to insufficient registration between sweeps.

With either illumination source, crosstalk between adjacent images due to simultaneous reconstruction was found to be unnoticeable, which indicated that the angular density of recordings could be increased. All the reconstructed images presented in this dissertation were photographed on Kodak T-MAX 100 film under laser light illumination, using a 35-mm camera with a 50-mm Zeiss Planar lens and interposing an additional 85-mm Zeiss Planar lens between the hologram and the camera. Stray light scattered by dust and scratches on the holographic film was largely eliminated by stopping down the camera lens to f:16.

The spinning-mirror approach, to an extent, exhibited the potential to generate the desired time-resolved holographic recordings. However, several technical difficulties to be discussed shortly made it appear unlikely that whole sequences of images could ever be obtained with any degree of consistency.

5.4 Shortcomings

5.4.1 Non-continuous coverage

The reference beam was reflected onto the film for only a portion of the spinning mirror rotation, namely the angular range subtended by the cylindrical mirror.

Since the spinning mirror was free-running and not linked with the event to be recorded, proper timing of the useful beam sweep with respect to shock wave arrival could not be ensured. No mechanical device generally available, such as a stepping motor, synchronous motor, or galvanometer-type deflector, would allow the sweep to be initiated synchronously with an external event whilst achieving the required speed, range and linearity in the short time involved of a few hundred microseconds. Conversely, it was not possible to synchronize the generation of the shock wave with the rotation of the already-spinning mirror because of the substantial variability in the burst characteristics of the plastic diaphragm used to retain the compressed gas. Given that the firing of the optical pump flashtube was linked to shock wave arrival, whereas the Q-switching of the laser cavity was linked to the mirror reaching the start of the useful sweep, it was clearly up to chance whether the two events would occur in sufficient coincidence to capture a reasonable portion of the phenomenon. The reference exposure, as it was seen in a previous section, could always be reliably synchronized because it only depended on the mirror position.

In view of the practical impossibility of linking the start of the mirror sweep to the arrival of the shock wave, the most crucial requirement for a workable mechanical system appeared to be the capability of continuous recording with no dead time. Several mechanical-sweep designs capable of continuous coverage were considered.

One possibility was to replace the flat mirror in the original design with a polygonal mirror that would pick up the beam on a new face as soon as it left the previous one, effectively scanning it several times, always in the same direction, in the course of a full rotation. This approach is widely used in commercial devices such as laser printers and supermarket check-out code scanners, where it is used to sweep a very fine beam. Its use with a beam a few centimetres in diameter would have posed serious problems related to the size of the polygonal mirror to be spun at very high speeds. A scan angle of 120°—a convenient value for practical use—

would have required a hexagonal-based parallelepipedal mirror with faces as tall as the beam diameter and as wide as several beam diameters. Because each face of a polygonal mirror describes an orbital motion about a central axis, its width would need to be large enough to intercept the whole beam for the duration of the sweep, with the exception of a short transition period when one face is replaced by the next.

Another approach, operating on a principle similar to that of the polygonal mirror, but posing fewer structural problems, was to use a stack of n plane, double-faced mirrors similar to the single one used in the original design. All mirrors would rotate on a common axis, and each would be advanced $180/n$ degrees with respect to the one underneath it. This structure would be easier to spin than a large polygonal mirror and would pose fewer balancing problems. On the negative side, each mirror would require its own beam shaping lenses and secondary curved mirror or array of mirrors to aim the swept beam onto the film. The reference beam would be directed onto all mirrors in the stack in equal portions by a system of beam splitters. For a 120° sweep angle, a stack of three mirrors would have been required, along with a triplicate optical system.

A simpler scanning concept, assuring continuous coverage and not involving multi-faceted mirrors or multiple paths, was based on a nutating-mirror design (Fig. 5.9) which swept the incident beam along the surface of an imaginary cone. The flat mirror surface would be spun about an axis slanted with respect to its normal. A crown of fixed secondary mirrors, placed at regularly spaced angular positions, would redirect the beam onto the film. This configuration was considered superior to the other continuous-coverage options, because it used a rotating element of smaller size and mass, required a relatively simple optical system, and spread the sweep over an entire rotation of the mirror instead of retracing it several times per revolution. The change in reference beam angle between consecutive images would also be increased because the scan did not occur in a single plane. The latter fact

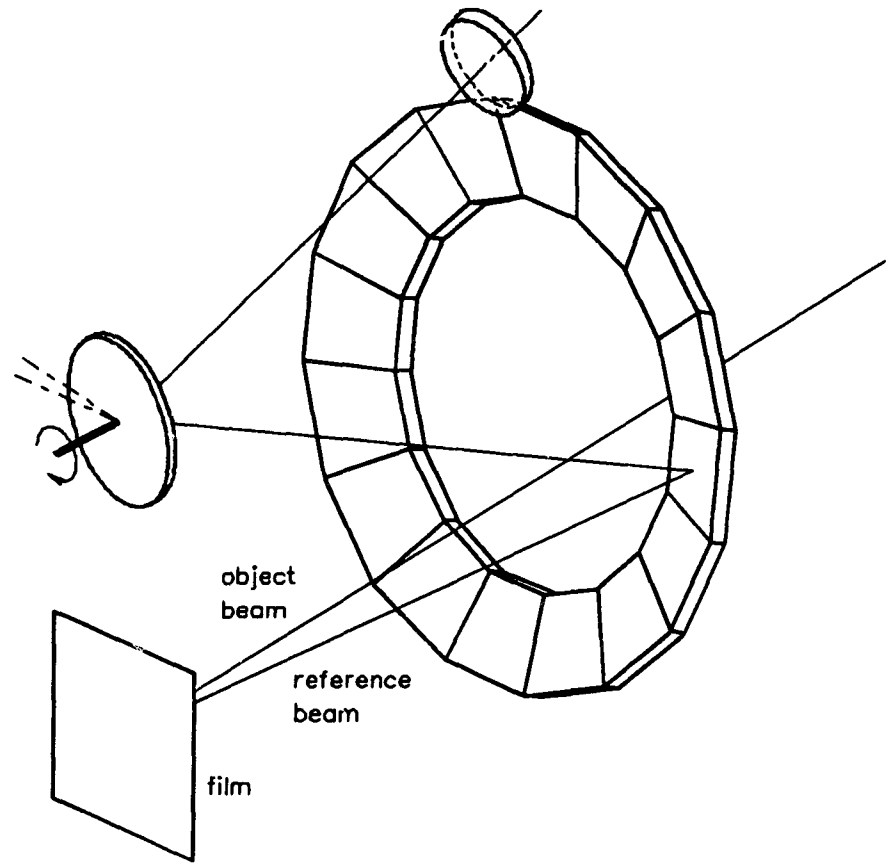

Figure 5.9: Possible design of a nutating-mirror reference beam sweeping assembly for multiframe holographic recording.

would help reduce crosstalk, albeit at the cost of somewhat complicating proper beam positioning for reconstruction. Had it been decided to further pursue the mechanical scan approach, this would have been the preferred option. Some design work for this configuration, such as structural stability studies and the development of synchronization electronics, was carried out and gave satisfactory results.

With any of the methods proposed above the sequence could begin at any point of the scan, depending on the time of arrival of the shock wave. For the multifaceted mirror designs, the recording could start at the middle of the sweep angle range,

proceed to the end and then restart from the beginning of the range toward the centre. For the nutating mirror system, any segment of the conical scan could be involved in a given recording. In either case, the subsequent reference exposure sweep would have to exactly match the phenomenon exposure, i.e. begin at the same angle of rotation of the mirror. Even for a regular polygonal mirror it would be almost essential for good registration that the same face be involved in both sweeps. A precise angular encoder and related control logic, to be further discussed in the next section, would therefore form an integral part of these systems.

5.4.2 Angular registration inaccuracy

The recording of holographic interferograms requires excellent registration of the phenomenon and reference exposures. Any variation in reference beam angle between the two would result in the formation of a finite fringe interferogram (see Chapter 3) if the difference were small, or no interferogram at all if it exceeded a small fraction of a degree. Whilst finite fringe interferometry has its merits in enhancing certain characteristics of the density field, its usefulness depends on the control that can be exercised over fringe orientation and spacing. As a by-product of inaccurate registration, finite fringes are merely detrimental. It is generally not difficult to maintain registration within the necessary limits in ordinary double-pulse holographic interferometry, where the optical path of the reference beam can be rigidly fixed. The difficulty increases substantially when registration must be achieved between two sequences of exposures in which the reference beam is being swept over a wide angle by a continuously rotating mirror system.

In the spinning mirror system used in the initial part of this research, angular registration of the two sweeps was based on a single start-of-sweep signal produced by an optical pick-up. The first laser pulse triggering was produced synchronously with this signal, and subsequent pulses were triggered at constant time intervals. This approach was based on the initial assumption that the mirror speed would

remain nearly constant over the duration of a recording, namely the approximately ten seconds that were required for firing the laser, recharging the capacitor banks and firing it again. It was found that the angular accuracy of the start pulse was adequate for interferometric purposes, in that the first image in double-exposed sequences usually yielded a good infinite-fringe interferogram. Subsequent images, however, most often showed either a pronounced finite fringe pattern or no interferogram at all. It was easily established from observation of the recordings that the registration of the holograms steadily worsened as the scan progressed, clearly due to a change in rotational speed over the several seconds elapsed between the two sweeps. The discrepancy was small, but sufficient to prevent the interferometric effect. As an alternative to making the mirror speed absolutely uniform, which is not a simple task unless a specialized synchronous motor was used, it would be possible to have the pulse triggering signals generated by the mirror rotation itself so that the angular separation between pulses was constant. To this end, a high resolution angular encoder such as the Hewlett-Packard HEDS-5500, which produces a signal for each 1° rotation of its shaft, could be used to control the pulse circuitry. The time interval between laser pulses would in this case vary with mirror speed, and monitoring of the pulse spacing for a given recording would be required to obtain a time base for the phenomenon. With any of the continuous-coverage schemes suggested, the use of such an angular encoder would be mandatory.

5.4.3 Time smear

The problems mentioned above were due to technical shortcomings and could, at least in principle, be eliminated by the improvements that have been outlined. A further serious difficulty, however, was due to the fact that the reference beam angle was being continuously altered. In spite of the short duration of each laser pulse, the angular change occurring during the exposure time was found to have very detrimental effects on the quality of the holograms. It was noticed that, with

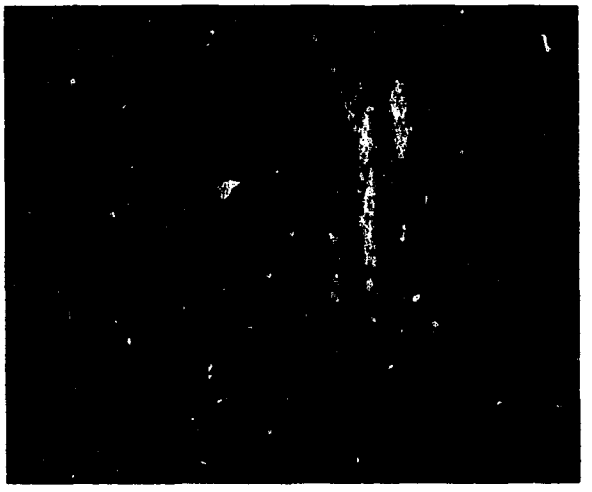

Figure 5.10: Example of a reconstructed image showing vertical fringes and lateral brightness loss due to time smear.

rare exceptions, single sweep holographic sequences recorded with the mirror at full working speed generated images characterized by a pattern of straight vertical fringes and a pronounced lateral drop in brightness (Fig. 5.10). An analysis of this phenomenon, generally known as time smear, revealed that only a reduction in pulse width to values that the available laser could not consistently achieve would have alleviated this problem. Eisfeld (1982) described a spinning mirror camera design in which a rapidly oscillating mirror counteracted the angular motion of the beam during exposure, thus reducing time smear. A similar arrangement could have been used here, but the complexity of achieving the required oscillation rate and synchronization whilst retaining the tight registration needed for holographic interferometry made the prospect appear impractical. Time smear was one of the crucial factors that steered this research away from mechanical scanning and toward solid state methods. A detailed analysis of the effects of time smear in the original swept-beam recording configuration is given in the next chapter.

Chapter 6

Time smear

6.1 General equations

The hologram formation equations presented in Chapter 3 apply to the case where the spatial frequency of the reference beam is constant. If the spatial frequency is time dependent, the equations must take this variation into account. Aleksoff (1971) has given a thorough general development of the theory and practice of temporal modulation techniques. Here will be analysed in detail the case of a spatial frequency variation due to angular sweeping of the reference beam (Racca and Dewey, 1989b).

When the reference beam is angularly swept, the shape of the laser pulse (its time-amplitude profile) becomes relevant to the analysis of the hologram formation process, since the light intensity at any given time corresponds to a different spatial frequency of the reference wave. In general terms, let $A(t)$ be the amplitude modulation function defining the profile of a laser pulse. Assume a plane reference wave whose propagation vector is parallel to the y-z plane and forms an angle θ_R with the normal to the film plane $z = 0$. If the reference beam is angularly swept with speed ω, it reaches the film at an angle $\theta_R(t) = \theta_0 + \omega t$, giving a time-dependent spatial frequency $f_y(t)$ $\sin(\theta_0 + \omega t)/\lambda$. The instantaneous complex amplitudes

of the waves reaching the film plane are then:

$$\text{object wave:} \qquad A(t)\mathbf{U}_o(x,y) \tag{6.1}$$

$$\text{reference wave:} \qquad A(t)a_R \exp(i2\pi \frac{\sin(\theta_0+\omega t)}{\lambda} y). \tag{6.2}$$

The instantaneous irradiance at the film plane is

$$\begin{aligned} I(x,y,t) &= \left| A(t)\mathbf{U}_o + A(t)a_R \exp\left(i2\pi \frac{\sin(\theta_0+\omega t)}{\lambda} y\right)\right|^2 \\ &= A^2(t)\left|\mathbf{U}_o\right|^2 + A^2(t)a_R^2 + A^2(t)a_R\mathbf{U}_o \exp\left(-i2\pi \frac{\sin(\theta_0+\omega t)}{\lambda} y\right) \\ &\quad + A^2(t)a_R\mathbf{U}_o^* \exp\left(i2\pi \frac{\sin(\theta_0+\omega t)}{\lambda} y\right). \end{aligned} \tag{6.3}$$

Assume that the laser pulse is confined to the time interval $-\Delta/2 \le t \le \Delta/2$. The film is therefore exposed to the irradiance pattern for that period, and its amplitude transmittance $\mathbf{t}(x,y)$ after developing is then proportional to $\Delta^{-1}\int_{-\Delta/2}^{\Delta/2} I(x,y,t)dt$:

$$\begin{aligned} \mathbf{t}(x,y) &= \mathbf{t}_b + \frac{\beta}{\Delta}\left[\left|\mathbf{U}_o\right|^2 \int_{-\Delta/2}^{\Delta/2} A^2(t)dt + a_R^2 \int_{-\Delta/2}^{\Delta/2} A^2(t)dt\right. \\ &\quad + a_R\mathbf{U}_o \int_{-\Delta/2}^{\Delta/2} A^2(t)\exp\left(-i2\pi \frac{\sin(\theta_0+\omega t)}{\lambda} y\right)dt \\ &\quad \left. + a_R\mathbf{U}_o^* \int_{-\Delta/2}^{\Delta/2} A^2(t)\exp\left(i2\pi \frac{\sin(\theta_0+\omega t)}{\lambda} y\right)dt\right]. \end{aligned} \tag{6.4}$$

The second term inside the square brackets in the above expression can be absorbed inside $\mathbf{t}_b$. For typical recording conditions, $\omega t \ll 1$ over the integration interval, so that the small angle approximation applies:

$$\sin(\theta_0+\omega t) = \sin\theta_0\cos\omega t + \cos\theta_0\sin\omega t \approx \sin\theta_0 + \omega t\cos\theta_0. \tag{6.5}$$

This gives:

$$\begin{aligned} \mathbf{t}(x,y) = \mathbf{t}_b &+ \frac{\beta}{\Delta}\left[\left|\mathbf{U}_o\right|^2 \int_{-\Delta/2}^{\Delta/2} A^2(t)dt\right. \\ &+ a_R\mathbf{U}_o \exp\left(-i2\pi \frac{\sin\theta_0}{\lambda} y\right)\int_{-\Delta/2}^{\Delta/2} A^2(t)\exp\left(-i2\pi \frac{\omega t\cos\theta_0}{\lambda} y\right)dt \\ &\left. + a_R\mathbf{U}_o^* \exp\left(i2\pi \frac{\sin\theta_0}{\lambda} y\right)\int_{-\Delta/2}^{\Delta/2} A^2(t)\exp\left(i2\pi \frac{\omega t\cos\theta_0}{\lambda} y\right)dt\right]. \end{aligned} \tag{6.6}$$

Reconstruction of the hologram is achieved with a plane wave incident at angle θ_0, that is, coincident with the original reference beam at $t = 0$:

$$\mathbf{U}_c(x,y) = a_c \exp\left(i2\pi \frac{\sin\theta_0}{\lambda} y\right). \tag{6.7}$$

The resulting complex amplitude of the light emerging through the film, in close proximity of the hologram plane, is

$$\begin{aligned}
&\mathbf{U}_I(x,y) = \\
&\quad \left(\mathbf{t}_b + \frac{\beta}{\Delta}|\mathbf{U}_o|^2 \int_{-\Delta/2}^{\Delta/2} A^2(t)dt\right) a_c \exp\left(i2\pi \frac{\sin\theta_0}{\lambda} y\right) \\
&\quad + \frac{\beta a_c a_R}{\Delta}\mathbf{U}_o \int_{-\Delta/2}^{\Delta/2} A^2(t) \exp\left(-i2\pi \frac{\omega t \cos\theta_0}{\lambda} y\right) dt \\
&\quad + \frac{\beta a_c a_R}{\Delta}\mathbf{U}_o^* \exp\left(i4\pi \frac{\sin\theta_0}{\lambda} y\right) \int_{-\Delta/2}^{\Delta/2} A^2(t) \exp\left(i2\pi \frac{\omega t \cos\theta_0}{\lambda} y\right) dt.
\end{aligned} \tag{6.8}$$

The second term in the above expression describes a reconstructed replica of the object wave, i.e. of the original image, modified by a function that depends on the laser pulse characteristics and the reference beam angle and sweep rate. The irradiance of this reconstructed wave is

$$\begin{aligned}
I_{oI}(x,y) &= \left|\frac{\beta a_c a_R}{\Delta}\mathbf{U}_o \int_{-\Delta/2}^{\Delta/2} A^2(t) \exp\left(-i2\pi \frac{\omega t \cos\theta_0}{\lambda} y\right) dt\right|^2 \\
&= \beta^2 a_c^2 a_R^2 |\mathbf{U}_o|^2 \left|\frac{1}{\Delta}\int_{-\Delta/2}^{\Delta/2} A^2(t) \exp\left(-i2\pi \frac{\omega t \cos\theta_0}{\lambda} y\right) dt\right|^2.
\end{aligned} \tag{6.9}$$

The above consists of the product of the standard irradiance of the reconstructed object beam, $\beta^2 a_c^2 a_R^2 |\mathbf{U}_o|^2$, and a modulation factor. This factor, which describes the effect of time smear on the reconstructed image, can be identified as the Fourier transform of the pulse irradiance profile clipped at $t = -\Delta/2$ and $t = \Delta/2$. For a given set of parameters Δ, ω and θ_0, and a specific pulse amplitude function $A(t)$, the modulation function describes the ratio of the local brightness of the reconstructed image to the value it would have in the absence of time smear. The dependence on y alone indicates that the brightness ratio only varies with horizontal displacement across the image field and is uniform across the vertical (x) dimension.

6.2 Numerical model

The light emission from the laser could be monitored through a photodetector, thus giving a realistic description of the pulse amplitude profile over time. Assuming a linear response of the detector, the output signal could be considered proportional to the instantaneous irradiance of the laser beam, that is, to $A^2(t)$. Numerical values of A(t) at discrete points t_i were obtained by taking the square root of the digitally sampled output. The effect of time smear could then be modeled by evaluating the hologram irradiance modulation function by numerical integration for this amplitude function $A(t_i)$.

The solid curve in Figure 6.1 shows the irradiance profile of a typical Q-switched pulse from the laser used in these experiments. This profile was recorded at an actual rate of 100 megasamples per second on a Tektronix 2430A digital oscilloscope, but data density was increased to 1 gigasample per second by the built-in interpolation feature of the instrument at a time base setting of 50 ns/division. A GPIB (IEEE-488) interface linked the oscilloscope to a computer. 101 points were recorded over the 100-ns duration of the pulse (Δ), and the square root of these values was used to describe $A(t_i)$ in a numerical algorithm that evaluated the irradiance modulation function of the reconstructed hologram. Figure 6.2 shows the resulting plot of modulation factor versus horizontal displacement for typical recording conditions, $\omega = 1200\pi$ rad/s and $\theta_0 = 20°$. The range of y corresponds to the width of a focused holographic image in the experimental set-up, some 2 cm. The position $y = 0$ corresponds to the intersection of the reference beam with the film plane, which ideally coincides with the vertical centreline of the image. The irradiance factor is plotted on a logarithmic axis because the human eye judges brightness differences on an approximately logarithmic scale. The model does indeed describe the experimentally observed pattern of periodic modulation with horizontal displacement (vertical fringes) and overall decrease of image brightness at the sides of the centreline.

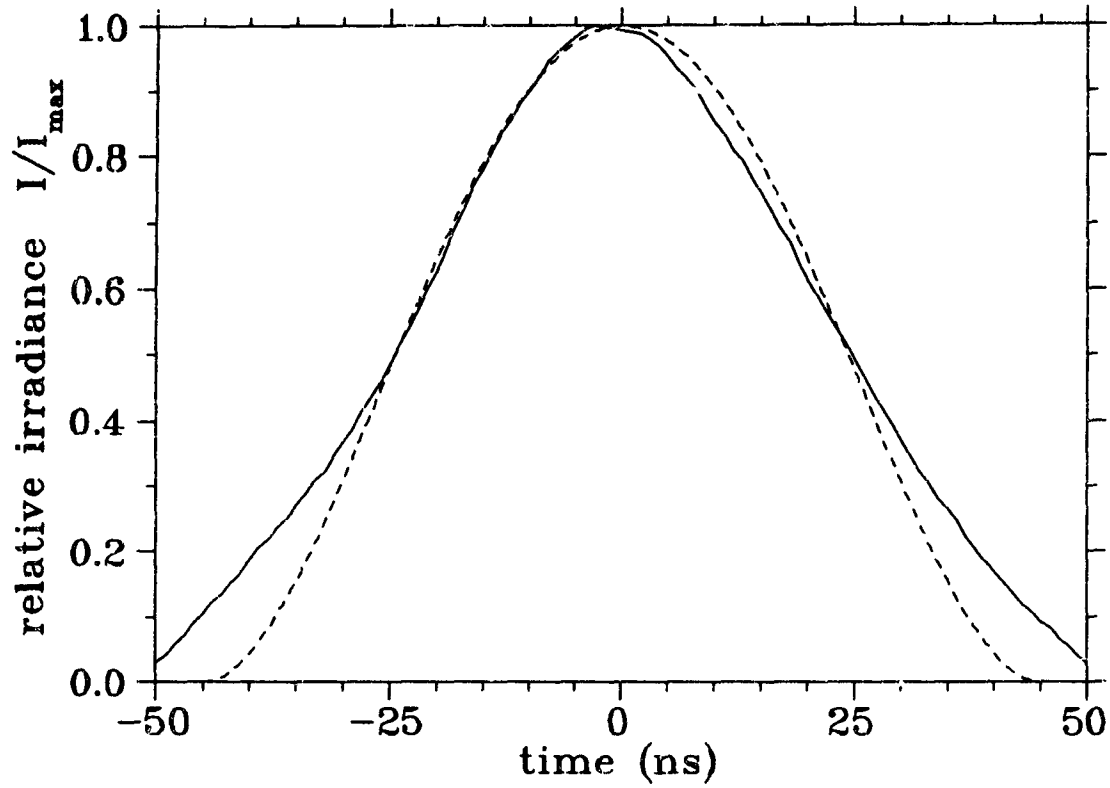

Figure 6.1: Profiles of laser pulse irradiance vs. time used to demonstrate the time smear models. The solid curve shows the digitized irradiance as recorded through a photodetector. The dashed curve shows the analytical function (the square of a parabola) used to approximate the measured irradiance profile.

6.3 Analytical model

A full analytical development of the time smear equations requires that $A(t)$ be described by a suitably integrable function. Then the formula for the modulated irradiance of the reconstructed object wave derived in Section 6.1 may be reduced to algebraic form to give a mathematical description of the effect of reference beam deflection on the holographic image.

It was observed that a downward-opening parabola, truncated where it crossed the abscissa axis, reasonably modeled the square root of the typical intensity profile

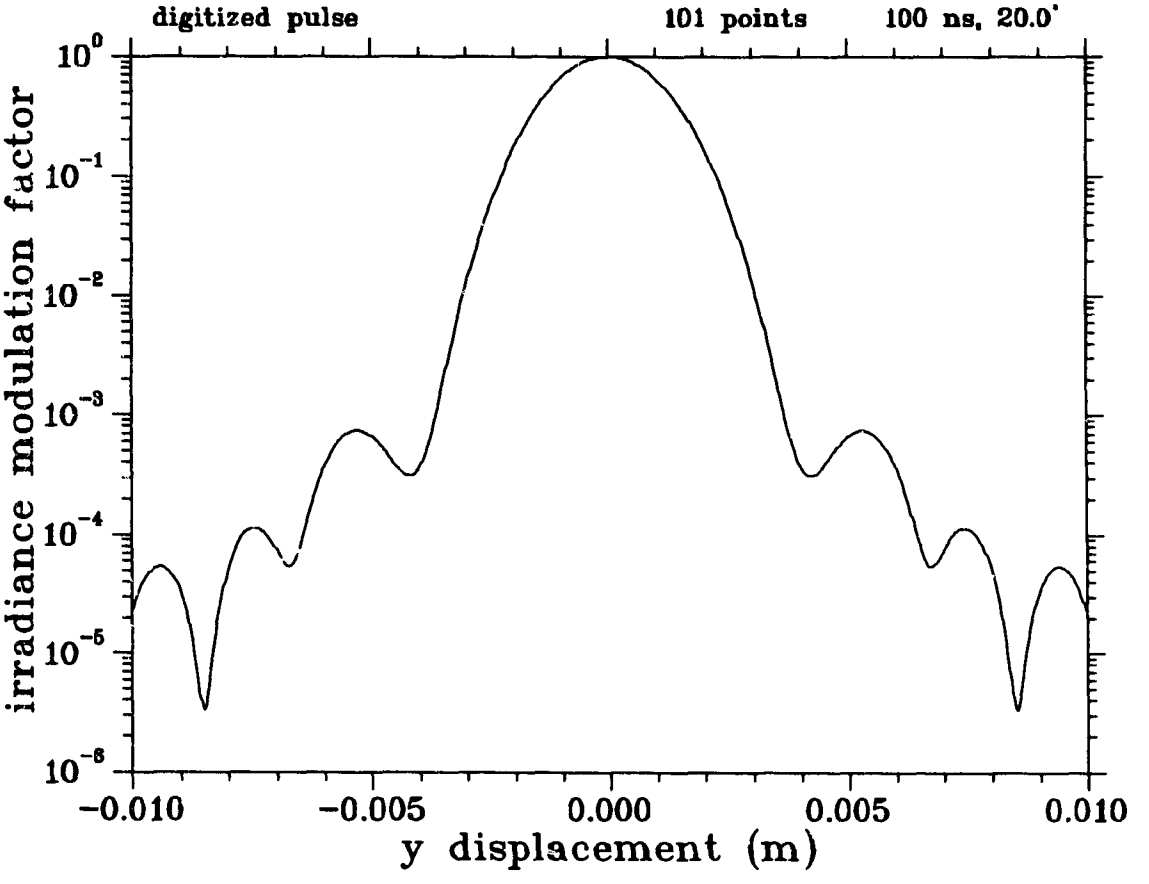

Figure 6.2: Graph of hologram irradiance modulation vs. lateral displacement given by the numerical model using the digitized laser pulse irradiance profile of Fig. 6.1.

of laser pulses. The following analytical model of the laser pulse amplitude function was therefore used:

$$A(t) = \begin{cases} \sqrt{30}\left(\frac{1}{4} - \frac{t^2}{\Delta^2}\right) & \text{for } -\frac{\Delta}{2} \leq t \leq \frac{\Delta}{2} \\ 0 & \text{elsewhere} \end{cases}, \tag{6.10}$$

which is normalized so that $\Delta^{-1} \int_{-\Delta/2}^{\Delta/2} A^2(t)dt = 1$. Introducing the above into the expression for the reconstructed object beam irradiance yields, after evaluating the

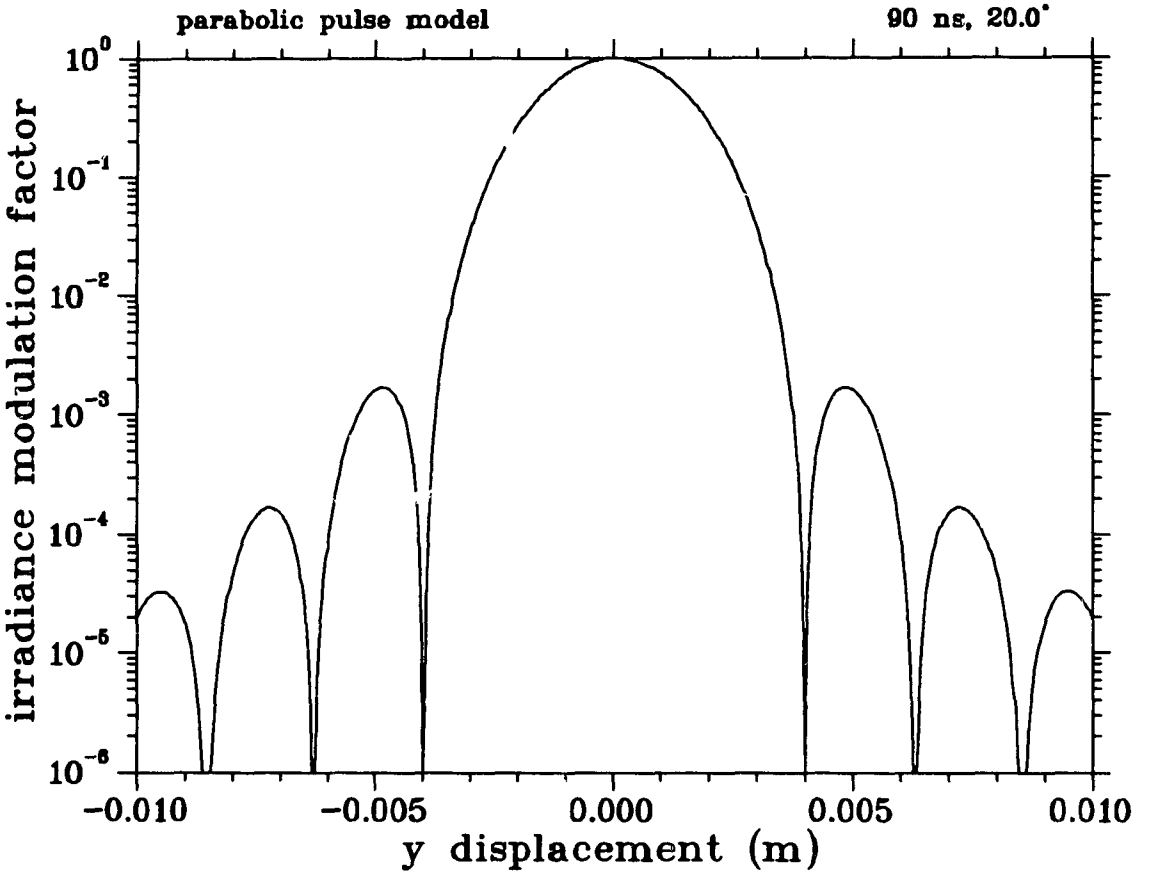

Figure 6.3: Graph of hologram irradiance modulation vs. lateral displacement given by the analytical model based on a parabolic laser pulse amplitude profile (square root of the dashed curve in Fig. 6.1).

integral,

$$I_{oI}(x,y) = \beta^2 a_c^2 a_R^2 \left|\mathrm{U}_o\right|^2 \frac{225}{(\delta y)^6}\left[\frac{3}{\delta y}\cos\delta y + \left(1 - \frac{3}{(\delta y)^2}\right)\sin\delta y\right]^2, \qquad (6.11)$$

where

$$\delta = \frac{\pi\omega\Delta\cos\theta_0}{\lambda}. \qquad (6.12)$$

A plot of the irradiance modulation function versus horizontal displacement for the following set of recording parameters: $\Delta = 90$ ns, $\omega = 1200\pi$ rad/s and $\theta_0 = 20^o$ is shown in Figure 6.3. The value of Δ was chosen so that the width

at half maximum of the squared analytical amplitude function (dashed curve in Figure 6.1) would be equal to that of the real pulse used in the numerical model example. Once again, the irradiance modulation pattern describes the formation of periodic fringes and lateral drop in image brightness.

6.4 Discussion of the models

The numerical and analytical models give similar results in terms of fringe spacing and rate of lateral decrease in brightness, as a comparison of Figures 6.2 and 6.3 shows. The two models behave similarly in response to changes in any of the recording parameters. The most notable difference in the modulation patterns is that the model based on the parabolic pulse shape describes the formation of totally black fringes whereas the model using a real pulse shape shows a brightness modulation that does not reach complete nulls. This discrepancy, although worthy of mention, was not crucial to the main scope of this analysis, which was to theoretically describe the behavior of the fringe pattern as recording parameters were altered in order to determine tolerable operating limits without the need for extensive experiments. In that regard either model can be used.

Reducing either ω or Δ has the effect of broadening the fringe spacing and reducing the lateral drop in brightness, so that the central bright fringe may be brought to cover the entire useful width. This defines the condition of negligible time smear effect. The influence of time smear is more pronounced at small values of the reference beam angle θ_0, and therefore setting $\theta_0 = 0$ in the equations gives the worst-case scenario to contend with. For the analytical model presented in Section 6.3, postulating for example that the angular speed of the reference beam sweep must be kept at 1200π rad/s, the base width of the laser pulse should be in the order of 20 ns in order to generate a fringe-free field with a drop in irradiance of less than a factor of 10 from centre to sides at any reference beam angle (Fig. 6.4). The numerical model yields similar results when the digitized pulse shapes

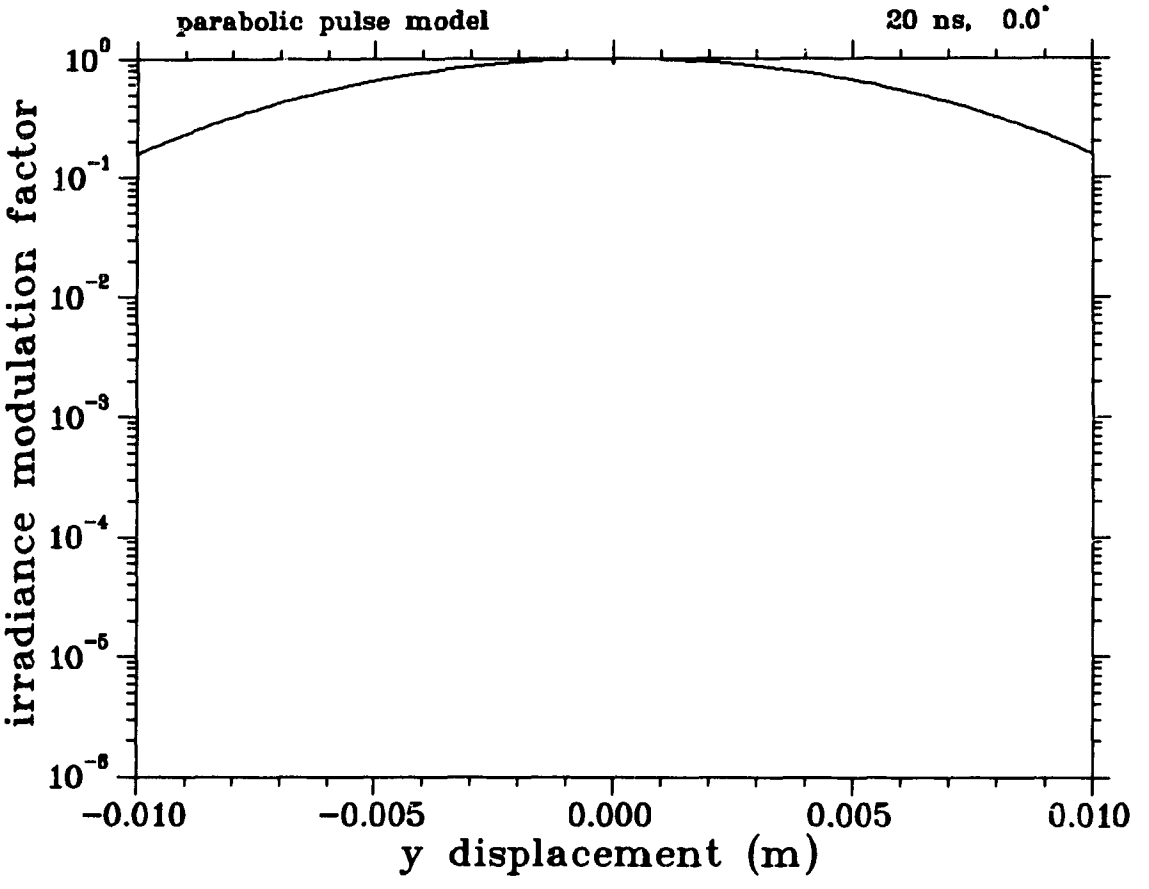

Figure 6.4: Graph of hologram irradian e modulation vs. lateral displacement given by the analytical model for a parabolic laser pulse amplitude profile of narrow width. The effects of time smear are almost negligible in this case.

are compressed to narrower widths.

The actual experimental configuration differs from the mathematical treatment presented here in that the reference beam impinges on the film at a constant, nonzero angle ψ with respect to the y-z plane, and so does the reconstruction beam. The spatial frequency in the y direction contains therefore an extra factor of $\cos\psi$. This factor is carried through in all the exponentials in the equations, which results in a widening of the fringe spacing in the reconstructed image by a factor of $1/\cos\psi$ for any pulse shape. In practical terms, this indicates that time

smear effects are reduced when the swept reference beam is angled with respect to the plane of the sweep.

A further factor that may affect hologram recording with an angularly swept reference beam is the possibility of lateral drift of the latter on the film as a result of the axis of rotation of the mirror not being exactly imaged onto the film plane. This would introduce a displacement with time of the reference position $y = 0$ used in the modeling, with consequent blurring of the described fringe pattern. Considering that careful design of the optical system should in any case minimize beam wandering, it was felt that the mathematical treatment did not need to take its influence into account, especially in view of the fact that the time smear fringes observed did not exhibit significant blurring.

Chapter 7

Solid-state scanning

7.1 General advantages

All the shortcomings of the original spatial frequency multiplexing system described in Chapter 5 were directly related to the mechanical nature of the beam sweeping device. Even the suggested improvements might not have entirely eliminated the registration inaccuracies, and would not have alleviated at all the problem of time smear. It clearly appeared that a scanning system with no moving parts would be the only solution to all the difficulties encountered.

A solid-state beam positioning system, however implemented, would allow the beam to be reoriented in a very short time and with great accuracy. The synchronization of the sweep with an external event would therefore pose no problem, and the registration from scan to scan would be virtually assured. Moreover, the orientation of the reference beam could be left stationary during exposures and altered only in the intervals between pulses, eliminating time smear.

7.2 Available beam routing technologies

A variety of non-mechanical devices may be used to select a prescribed path for a beam of light. These devices fall into one of two technological categories: acousto-optical or electro-optical. Before examining the different ways in which such units

can be applied to spatial frequency multiplexing, the two types will be briefly discussed.

Acousto-optical (AO) devices partially deflect a light beam by an angle proportional to a driving signal applied to them. They consist of a block of optical transmission medium (glass, a TeO_2 crystal, etc.) to which is bonded an ultrasonic transducer. A control circuit drives the transducer with a carrier frequency (several tens of MHz) which is frequency-modulated by the input signal, and the resulting compressional or shear wave travels through the optical medium. The operation of these devices is based on the interaction between a light beam and an ultrasonic plane wave, which acts as a sinusoidal phase grating moving with the speed of sound. The interaction produces a zeroth-order beam traveling in the original direction and a set of higher diffraction orders whose angles of deflection are directly proportional to the sound frequency. By appropriate choice of parameters such as the intensity of the sound, the material in which sound and light interact, and the width and relative directions of the light and sound beams in the medium, it is possible to achieve selective diffraction into one direction (Bragg diffraction). The device then splits the light mainly into the undeflected zeroth-order beam and one first-order beam whose direction depends on the sound frequency. The acousto-optically deflected light experiences a frequency shift equal to the frequency of the diffracting sound wave.

Electro-optical (EO) devices generally work by rotating the plane of polarized light under the effect of a switchable electric field, so that the output beam interacts differently with polarization-sensitive optical components. A variety of materials exhibit electro-optical properties, and EO devices based on liquids such as nitrobenzene or carbon disulfide (Kerr cells) or crystals such as KD*P (Pockels cells) have been in use for decades. These units can provide switching rates as high as 10^{10} Hz, but require high driving voltages—typically several kilovolts. More recently, EO devices using liquid crystals have been increasingly employed in applications

not requiring ultra-fast switching. They are particularly convenient because they require very low voltages and minimal amounts of current to operate. EO devices are most often configured as light shutters or modulators by placing the active cell between crossed polarizers, so that the light is either stopped or transmitted by the output polarizer (analyser) depending on the electrical state of the cell. If a polarizing beam splitter (which transmits one polarization and deflects the other) rather than a simple analyser is placed on the output side, the device works as a binary path selector.

7.3 Choice of spatial frequency multiplexing strategy

7.3.1 Deflection of beam into one of several paths

The intuitive approach to implementing a solid-state spatial frequency multiplexing system is to use one of the switching technologies discussed in the previous section to route the entire reference beam along one path at a time. A few systems designed along this principle have appeared in the literature. Feldman (1970) introduced the method of acousto-optically deflecting the reference beam between exposures, though not in a spatial frequency multiplexing configuration, as each projection of the beam fell on a different area of film. Hinsch and Bader (1974) used two AO deflectors working as switchable beam splitters to direct the reference beam along one of two paths, an arrangement easily adaptable to more channels. Lauterborn and Ebeling (1977) employed a single AO deflector to proportionally steer the reference beam along different paths. Their approach makes more efficient use of the AO deflector, but requires a more complex frequency-modulated power driver than the previous method. The number of separate channels that may be selected by this method is limited in practice by the relatively small beam steering range (usually a few degrees).

The quality of holograms obtained from an acousto-optically deflected reference

beam and a non-deflected object beam may be affected by the frequency shift due to the ultrasonic wave, which introduces a temporal periodicity (beat frequency) in the interference pattern. Hinsch and Bader (1974) studied this phenomenon and concluded that to minimize its effect the time of exposure (laser pulse length) should be less than half the sound period, and the shorter the better.

The use of EO units in beam deflection applications is less widespread. Yamamoto (1989) presented a system using a linear stack of three high-voltage EO devices to route the reference beam to one of four paths in sequence. Each EO unit was configured as a binary path selector, with a polarized beam splitter that either deflected the beam into a perpendicular output channel or allowed it to reach the next element in the system. The last unit performed the selection between two output paths.

7.3.2 Shuttering of multiple coexisting beams

The approach that was followed in the present work departs substantially from the ones presented above. Instead of being sequentially routed along one of several mutually exclusive paths, the reference beam was fanned into a set of coexisting branches, each branch passing through a solid-state shutter and illuminating the film from a unique angle. This requires that a greater portion of the laser energy be given to the reference beam compared to other methods, in order for each branch to have the correct intensity ratio to the object beam. Because the individual beams do not undergo any deflection that depends on the stability of an external signal, this system can assure absolute registration between repeated exposures involving a given path. The type of shutter technology used is irrelevant to the principle of operation: any kind of modulator would be suitable, the choice being dictated by convenience and required performance criteria. For this project, a recently developed type of EO shutters based on ferroelectric liquid crystals (FLCs) was adopted.

By opening a single shutter at a time in a regular sequence as the laser was pulsed, the reference beam was effectively stepped from angle to angle, yielding a spatial frequency multiplexed series of holographic images. It was, however, in holographic interferometric applications that this configuration offered a unique advantage, in that it was possible to open all shutters at once and record the reference, or empty field, exposure on all images with a single pulse of the laser. Successive pulses were then allowed through one path at a time as the phenomenon developed in the field of view, thereby recording holographic interferograms with perfect registration. This novel approach to time-resolved holographic interferometry has many desirable qualities that will be discussed in detail later in the chapter.

7.4 Implementation

7.4.1 Optical system

The layout of the solid-state time-resolved interferometric system (Racca and Dewey, 1990) appears in Figure 7.1. It was identical to the previously described optomechanical implementation (Fig. 5.1) save for the beam multiplexing assembly. A line drawing of the prototype three-channel multiplexing system is shown in Figure 7.2, and a photograph of the beam splitting and shuttering optics is presented as Figure 7.3. The reference beam was subdivided into three branches of equal intensity by a combination of two beam splitters, the first deflecting 30% of the beam and the second deflecting 50% of the light transmitted through the first. Before entering the stack of beam splitters, the beam passed through a negative lens that made it sufficiently divergent to cover the whole image area when it reached the film. Since the object beam only had one-fourth the light intensity of the undivided reference beam (see Section 3.4), and the latter was split three ways, the beam ratio at the film was considered sufficiently close to the optimal

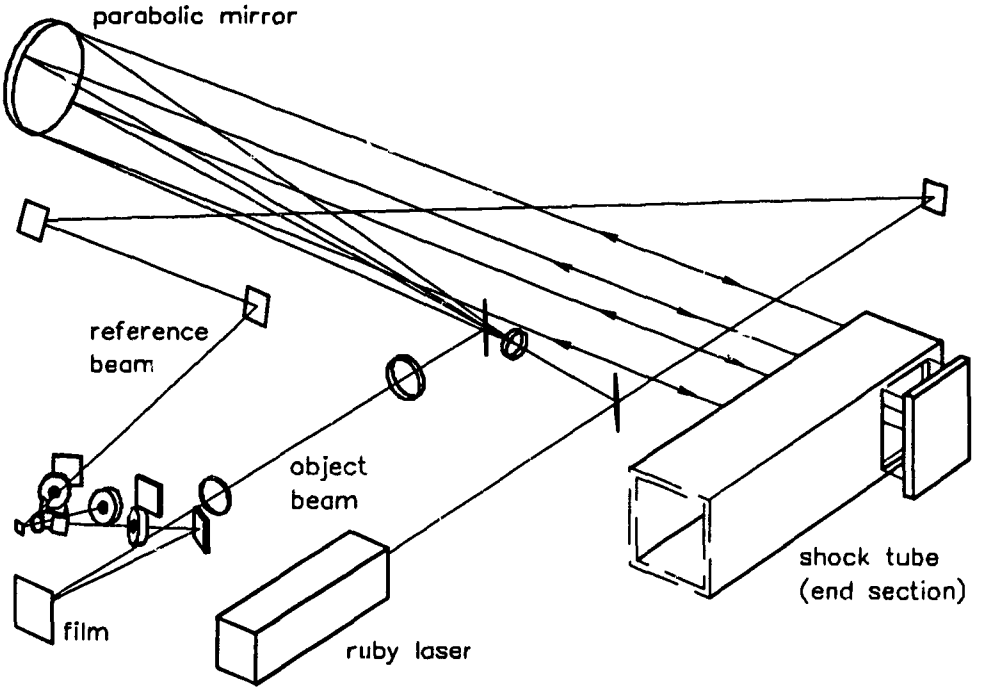

Figure 7.1: Layout of the multiframe holographic interferometer with a solid-state reference beam multiplexing system (shown in detail in Fig. 7.2).

1:1 proportion. Each of the branches was routed through a FLC electro-optical shutter, to be described in detail in a later section, and was then folded by a plane front-surface mirror so that it would impinge on the film in correspondence with the object image. In this implementation it was not deemed necessary to introduce further optics in each channel to collimate the beam, since the angular separation between the three branches—a few tens of degrees at the film plane—was sufficient to prevent any crosstalk due to angular overlap of adjacent beams. If a greater number of channels were used, with closer angular spacing, it would become more important to collimate each beam in order to ensure good discrimination between the holographic images at the reconstruction stage. This could be achieved by placing a collimating lens in the path between each shutter and the film, or by

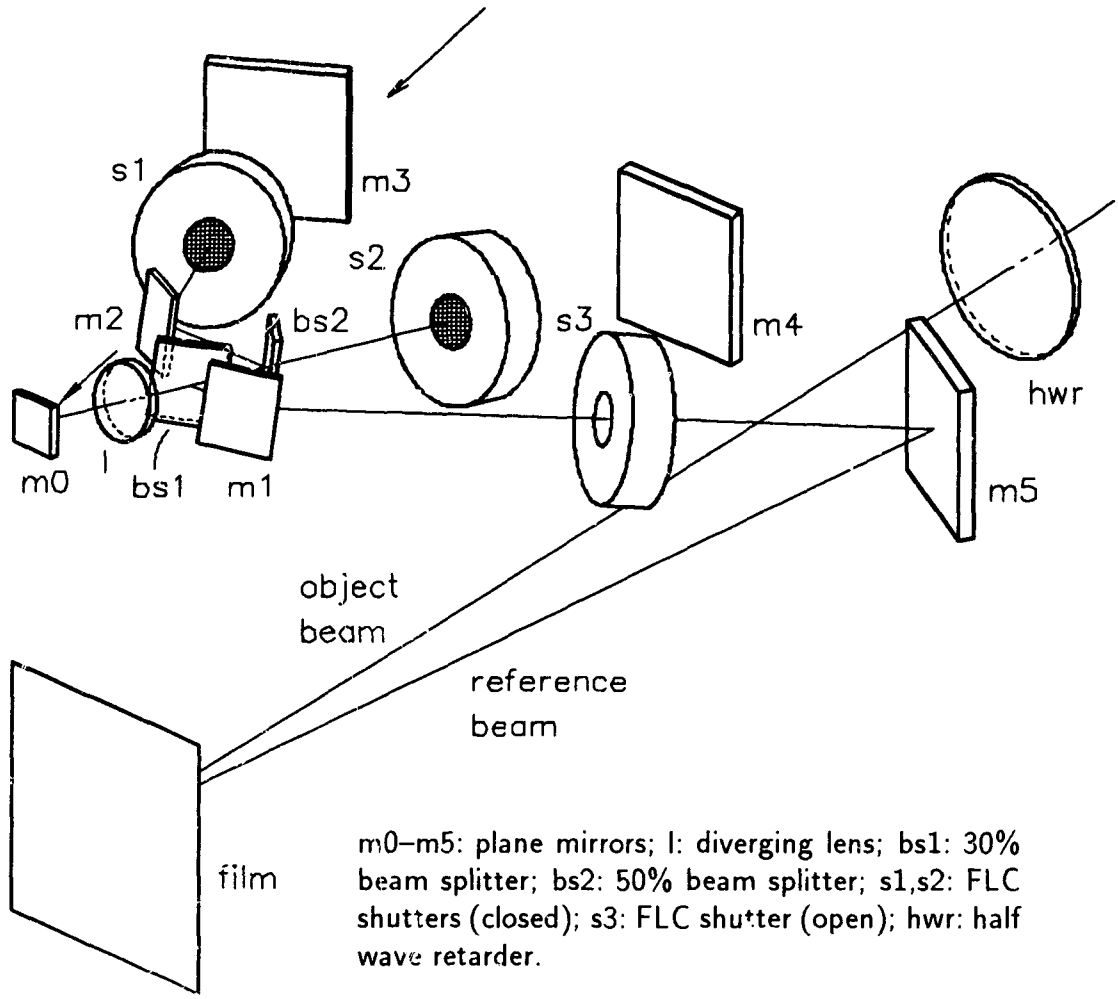

Figure 7.2: Detail drawing of the three-channel beam multiplexing assembly using liquid crystal shutters.

making the beam folding mirrors parabolic.

A mica half wave optical retardation plate was placed in the path of the object beam to rotate its plane of polarization by 90°. As it will be seen later, this was necessary in order to match its polarization to that of the shuttered reference beams.

Figure 7.3: Photograph of the reference beam splitting and shuttering optics. In the foreground are the two beam splitters (centre) and two mirrors (sides) used to subdivide and aim the reference beam. Behind them are the three electro-optical shutters.

7.4.2 Electro-optical shutters

Ferroelectric liquid crystal light valves are high speed, broadband optical shutters that may be used as choppers or modulators. In their basic design they consist of a thin cell of FLC material between crossed polarizers. Transparent electrode plates on both sides of the cell allow the application of the driving voltage. The FLC film functions as a switchable half wave optical retarder, and the polarizers provide the actual light blocking.

The principle of operation of the FLC cell is illustrated in Figure 7.4. The FLC material is composed of long, rod-shaped molecules arranged in layers, and is therefore classified as a smectic liquid crystal. The long axes of the molecules prefer to orient themselves parallel to each other, defining the so-called director $\hat{n}$, a unit

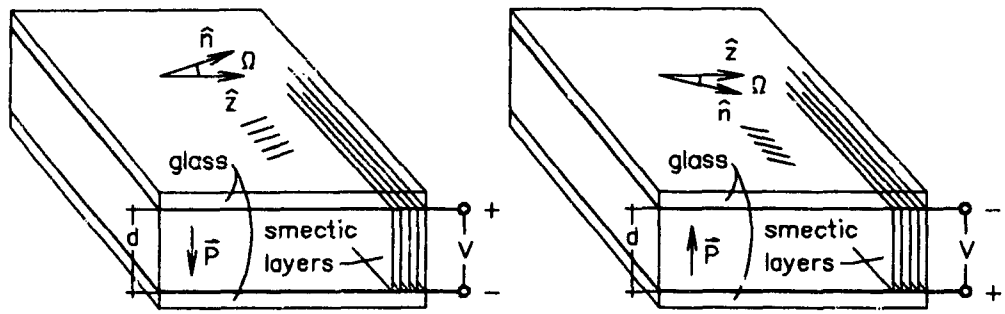

Figure 7.4: Structure of a FLC cell in its two voltage-selected states. A reversal of the driving voltage causes the optic axis of the cell to rotate by 2Ω ($45°$) in the plane of the glass plates. The thickness d of the FLC film is greatly enlarged in the figure so that the orientation of the molecular layers may be indicated.

vector parallel to the average molecular orientation. In smectic C* liquid crystals, the molecules are tilted at a characteristic angle Ω to the layer normal $\hat{z}$, inducing a permanent ferroelectric polarization $\vec{P}$ perpendicular to both the molecular axis and the layer normal $\left(\vec{P} = P_0\,\hat{n}\times\hat{z}\right)$. The glass face plates, which are coated on their inner surfaces with a transparent conductive layer, are oriented perpendicular to the smectic layers, so that the electric field $\vec{E}$ arising from voltages applied between the electrodes is in the plane of the ferroelectric polarization $\vec{P}$. An electric potential between the plates produces a torque on $\vec{P}$, causing molecular reorientation to bring $\vec{P}$ parallel to $\vec{E}$. Figure 7.4 shows the two molecular orientations (parallel line segments) selected by opposite applied voltages. The liquid crystal is nominally a uniaxial birefringent medium, with its optic axis parallel to $\hat{n}$. Thus, the two selected states both have their optic axis in the plane of the plates, but differing in orientation by an angle 2Ω. For the FLC material used in the light valves, this angle is 45 degrees. By controlling the thickness of the FLC film, the cell can be designed to work as a half wave plate for light of a chosen wavelength. Ferroelectric liquid crystals, like the more common nematic liquid crystals used

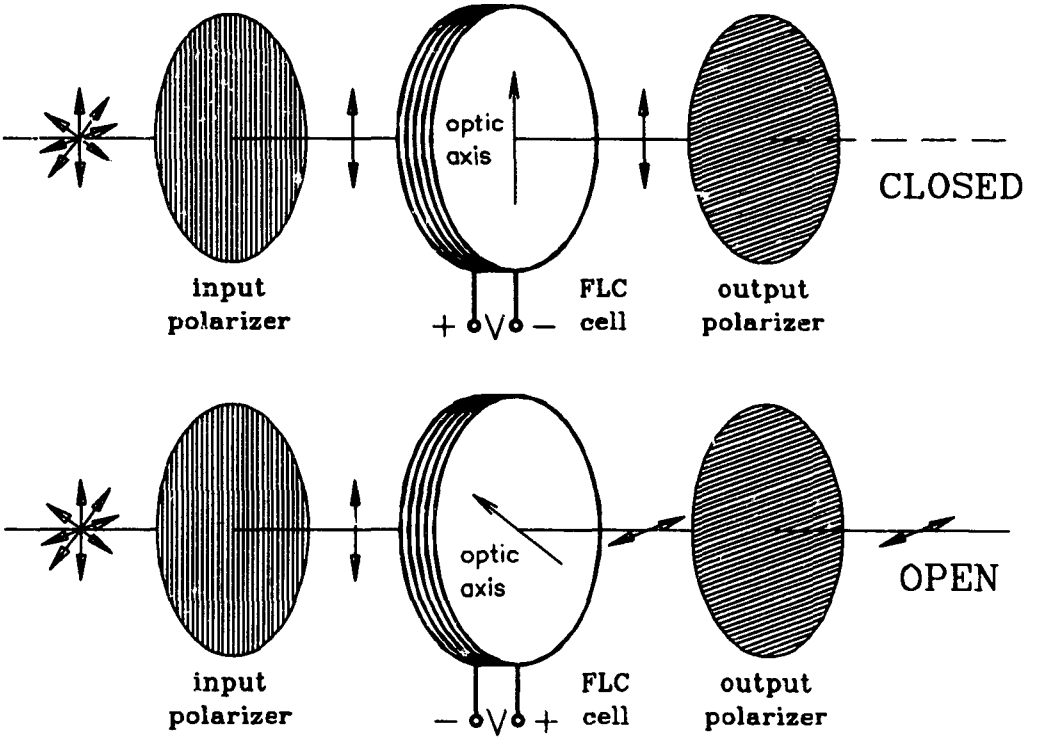

Figure 7.5: Diagram of a FLC shutter in its closed and open configurations.

in displays, require very little electrical power for operation. However, FLCs are several hundred times faster than the nematics, so they can be used in high speed applications.

The configuration of the electro-optical shutter in its two states is shown in Figure 7.5. The FLC cell is oriented with respect to the crossed polarizers so that the polarization of the light entering it will be parallel to one molecular state and 45° from the other. When the voltage across the liquid crystal cell has one polarity, say +V, the light traverses the cell unchanged because its polarization is parallel to the optic axis, and is then blocked by the output polarizer. When the voltage is switched to −V, thus turning the optic axis by 45°, the plane of polarization of the light is rotated by 90° as it goes through the cell; the light then passes

freely through the output polarizer. If the light to be shuttered is already linearly polarized—as is the case with the beam from the ruby laser used here—the device can be operated without the input polarizer, thus increasing its throughput by reducing absorption loss.

For applications such as the present work, in which the beam passing through the shutter must eventually interfere with an object beam to record a hologram, it is essential that the two beams have identical polarization when they reach the recording medium. Since by its principle of operation a FLC shutter rotates by 90° the plane of polarization of the light it allows through, a compensating half wave retarder must be placed on the path of either beam. This might in principle be avoided by configuring the shutter with the output polarizer parallel to the polarization of the beam, so that its behaviour is reversed. The problem with this approach is the poor performance of such a configuration at wavelengths different from the one for which the cell is designed.

The FLC cell can only be optimized to work as an exact half wave plate for a chosen wavelength of light. At other wavelengths the retardation given by the film when in its optically active state is not exactly one half wave, and the light emerging from it is elliptically polarized. As such, it will never be entirely blocked or entirely transmitted by the output polarizer, however the latter may be oriented. In the standard light valve configuration, where the output polarizer is crossed with respect to the original polarization of the beam, the result is that light will be only partially transmitted when the shutter is in its open (optically active) state, but virtually fully blocked in the closed (optically inactive) state. This gives a properly light-tight shutter whose transmittance decreases as one moves away from the center wavelength. Since the FLC film is a very thin first order retarder, the output polarization at wavelengths on either side of the centre wavelength is still nearly linear and rotated 90°. The device can therefore be used over a fairly broad range of wavelengths with only a modest lowering of the contrast from its

optimal value. Commercially available units feature a minimum open/closed ratio of 500:1 over the wavelength range from 400 to 700 nm.

In the reversed configuration mentioned earlier, where the output polarizer is parallel to the original polarization of the beam, the shutter would have virtually wavelength-independent transmittance in the open (optically inactive) state, but its opacity in the closed (optically active) state would deteriorate on either side of the center wavelength. Because the most important characteristic of a shutter is its ability to effectively block light when closed, the crossed-polarizer configuration is most often used.

The FLC light valves used in the present work were type LV050AC from Displaytech, Inc. (Boulder, Colorado). They feature a clear aperture of 0.5 inches diameter, a rise or fall time—from 10% to 90% of full transmittance or vice versa—of 50 μs or less, and a contrast of 500:1 or better. A parameter that is not listed in the specifications for these shutters, but must be taken into account when determining their minimum response time to a change in the driving signal, is the dead time that elapses between the electrical stimulus and the beginning of physical transition in the FLC cell. For the units that were used the dead time was of the order of a few tens of microseconds. As previously mentioned, the entrance polarizer was omitted from these devices since they were used with linearly polarized light. This modification produced a 15% increase in transmittance according to the specification sheets.

7.4.3 Control circuitry

The shutters require a driving potential of 15 V to 20 V across their leads, the open or closed state being determined by the polarity. Complementary Metal Oxide Semiconductor (CMOS) high-current buffers, which have an operating voltage limit of 15 V, are capable of driving the shutters directly, offering a seamless interface between the control logic and the power stage. CMOS circuitry is ideally suited

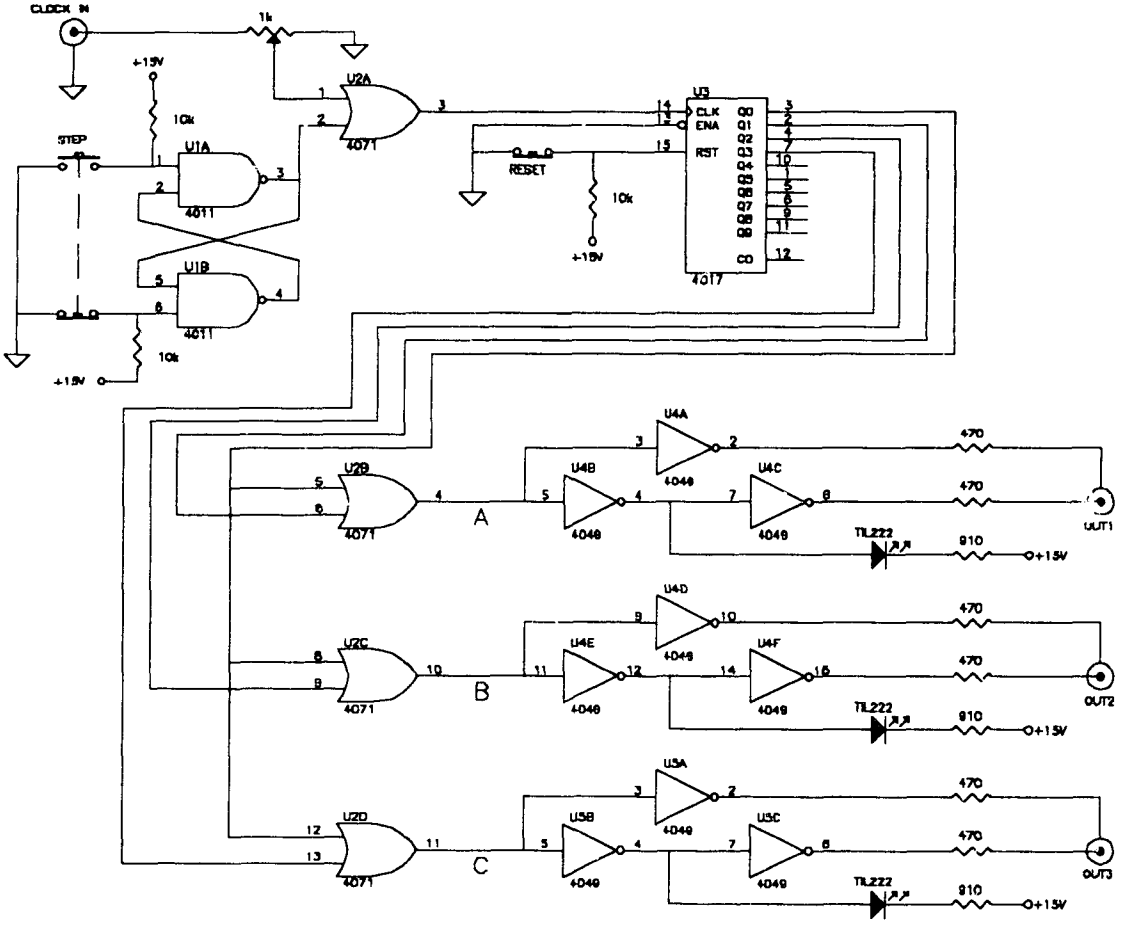

Figure 7.6: Circuit diagram of the shutter sequencing system for three FLC light valves. This unit provides the sequence for recording three interferograms with a four-pulse train from the laser.

for this application because of its low power consumption and immunity to signal noise.

The shutter sequencing system used to control the prototype three-shutter array is shown in Figure 7.6. The 4017-type integrated circuit is a CMOS divide-by-ten counter that at each cycle of the clock caused one and only one of the inputs, in sequence, to assume the logical 1 state. The simple OR-gate encoding network at the outputs of the 4017 brought the three lines A, B and C to the 1 state when the counter was reset. At each successive clock cycle these lines assumed

the following states in sequence: 1-0-0, 0-1-0, 0-0-1, 0-0-0. Subsequent steps were irrelevant because the unit was never advanced beyond this stage in the normal course of operation. Lines A, B and C controlled the shutters via three networks of inverting buffers that produced the appropriate +15 V or −15 V potential across the output leads, which were floating with respect to circuit ground. Each output was monitored by a light emitting diode on the control panel that visually indicated the state of the associated shutter. Adding more OR gates and buffer networks to the currently unused output lines of the 4017 would permit this design to be expanded to drive a series of up to 9 light valves.

The CLOCK IN line was driven by a low-voltage signal from the Pockels cell control circuit of the ruby laser, so that at each laser pulse the sequence was advanced one step. It was possible to step the sequence simultaneously with the triggering of a laser pulse because it would take a few tens of microseconds for the shutters to begin to react to the new driving condition. The sequence controller was manually reset before each recording and could also be stepped manually for testing and set-up of the shutters.

7.4.4 Exposure synchronization

The system of electronic units that controlled exposure synchronization is shown in block form in Figure 7.7. It was much less complex than the configuration required by the spinning-mirror approach (Fig. 5.6), and the sequence of events involved in a recording—listed below in point form—was correspondingly simpler.

1. The compression chamber of the shock tube was pressurized.

2. The shutter sequencing system was reset to its starting condition with all shutters open.

3. The laser capacitor banks were charged.

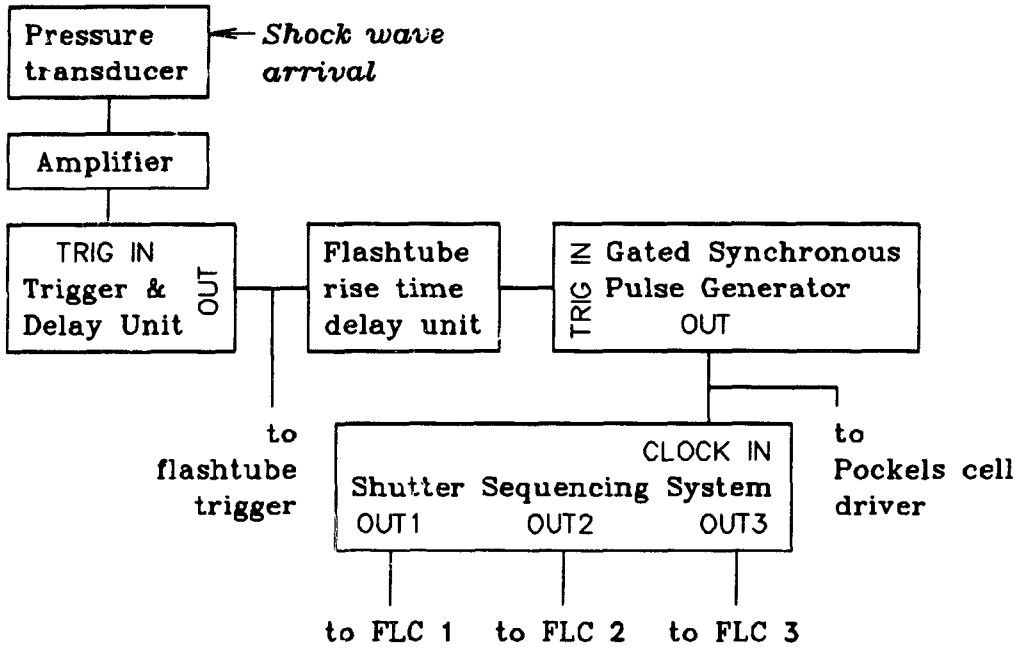

Figure 7.7: Block diagram of the exposure synchronization electronics for the solid-state scanning system.

4. A signal indicating the achievement of full charge automatically triggered the pin which burst the pressure-retaining diaphragm in the shock tube. A shock wave started traveling down the tube.

5. The shock wave reached a pressure transducer located some centimetres upstream of the window section, which sent a signal through an amplifier to the TRIG IN line of the trigger & delay unit.

6. After a preset delay to allow the shock wave to travel closer to the window section, the trigger & delay unit generated a signal on its OUT line that fired the flashtube. The delay was such that the flashtube would reach full intensity by the time the shock neared the entrance of the field of view. The signal from the trigger & delay unit also triggered a second delay circuit set for the

rise time of the flashtube.

7. The second delay circuit triggered the gated synchronous pulse generator which emitted a series of four pulses at predetermined spacing. Each of these pulses cycled the Pockels cell in the laser cavity, causing the laser to emit a flash of light, and simultaneously advanced the shutter sequencing system to reconfigure the optical paths for the next exposure. Thus the first light pulse propagated through all three channels, and the remaining three pulses through only one channel in sequence.

7.5 Results

The system was used to record holographic interferometric sequences of three images at intervals down to 100 μs, using trains of four Q-switched pulses at repetition rates up to 10 kHz. Figure 7.8 shows a sequence of interferograms, taken at 150 μs spacing, of a plane shock wave travelling from left to right in the image and reflecting off a double-surface wedge. The reference exposure was recorded simultaneously on all three images 150 μs before the start of the sequence, as the incident shock wave was at the left margin of the image area. The noisy background is mainly due to the optical quality of the available FLC shutters, which distorted the wavefront of the reference beams. Another noticeable shutter-related problem is some leakage of the first image of the sequence into the third hologram, due to incomplete closure of the third light valve by the time the first shock position was being recorded. Inter-image leakage was found to occur to a slight degree in many of the sequences recorded, and did not consistently involve the same shutter. The straight, parallel background fringes that appear in images (a) and (c) are caused by interference between the front surface and back surface reflections from the glass beam splitters that subdivided the reference beam. This image artifact, which does not affect the localization of the interferometric fringes, could be

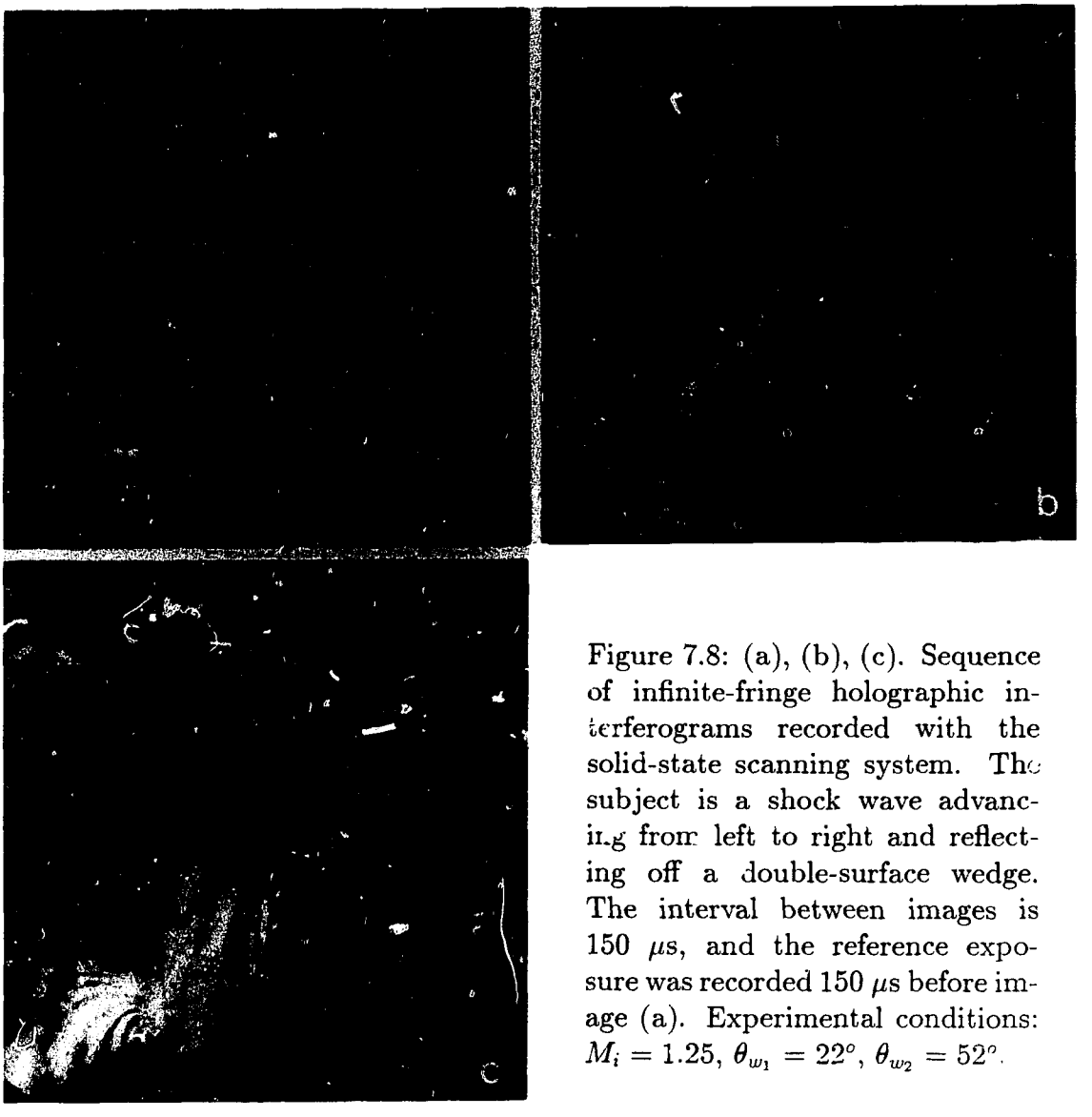

Figure 7.8: (a), (b), (c). Sequence of infinite-fringe holographic interferograms recorded with the solid-state scanning system. The subject is a shock wave advancing from left to right and reflecting off a double-surface wedge. The interval between images is 150 μs, and the reference exposure was recorded 150 μs before image (a). Experimental conditions: $M_i = 1.25$, $\theta_{w_1} = 22^o$, $\theta_{w_2} = 52^o$.

eliminated by using very thin pellicle-type beam splitters instead of coated glass slides.

Though technicall, ing, the sequence of interferograms gives a useful time-resolved depiction of the density field as the shock wave reflection evolves from Mach on the first surface to regular on the second. Figure 7.9 shows the same sequence after the first stage of the standard analysis process. The shock fronts and interferometric fringes were digitized from photographic prints using a crosshairs

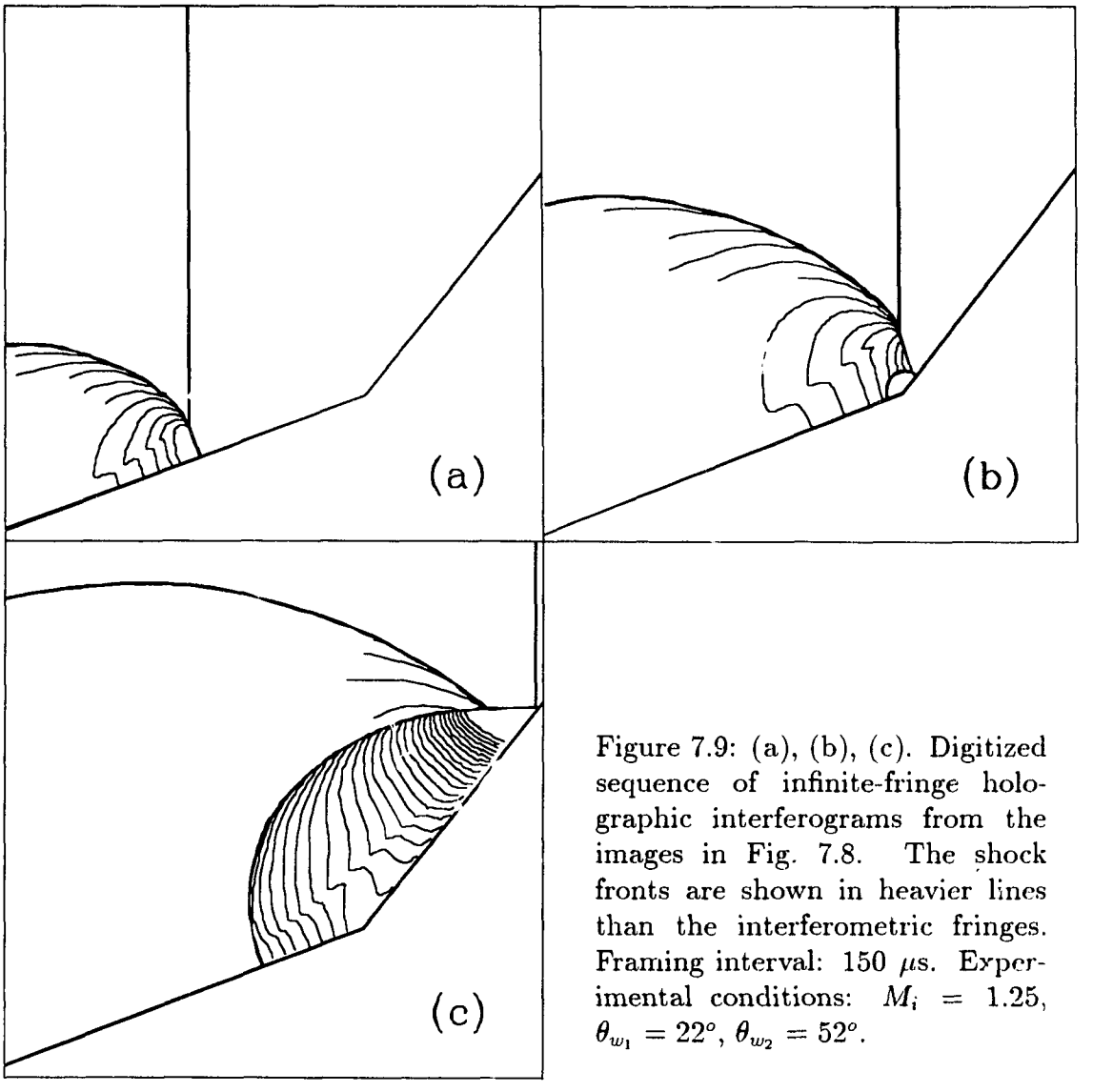

Figure 7.9: (a), (b), (c). Digitized sequence of infinite-fringe holographic interferograms from the images in Fig. 7.8. The shock fronts are shown in heavier lines than the interferometric fringes. Framing interval: 150 μs. Experimental conditions: $M_i = 1.25$, $\theta_{w_1} = 22^o$, $\theta_{w_2} = 52^o$.

digitizer. In certain areas the fringe system could not be distinguished in the reconsructed images, resulting in blank sections in the digitized set. For presentation purposes the three frames are grouped on a single page, but finer detail is visible on larger plots. For the interferometric system used here, the density difference between two points on adjacent infinite fringes is 2.018×10^{-2} kg/m^3 (van Netten, 1988).

The shock configuration in image (a) is a typical Mach reflection, which is con-

sistent with theory for the experimental parameters $M_i = 1.25$ and $\theta_{w_1} = 22^o$. The location of the slipstream is clearly shown by the S-shaped kink in the fringes, caused by the change in density across that boundary. If left to itself, this configuration would remain self-similar in an $(x/t, y/t)$ reference frame. The reflecting wedge, however, makes a transition to $\theta_{w_2} = 55^o$. The steeper second surface can sustain regular reflection at the given incident Mach number, and therefore the shock system will ultimately tend to that configuration. Since the change cannot happen instantaneously, during the transition period the shocks form a more complex system that is not self-similar in time. In image (b) the shock has just passed the inflection point of the wedge. The original triple point and upper part of the Mach stem have not yet been influenced by the change. To satisfy the new geometry a second triple point has formed near the surface of the wedge, with a small Mach stem joining it to the surface and a growing, curved reflected shock. As time progresses, the second Mach stem increases in size until the new and the old triple points coincide, and then progressively shrinks as the new triple point moves toward the wedge (Ben-Dor et al., 1987). In image (c) the triple point has almost reached the wedge surface to give regular reflection, although a very small Mach stem—clearly visible in Figure 7.8(c)—is still present. The reflected shock from the original configuration still exists, and its presence affects the density field under the new reflected shock. The S-shaped kinks in the fringes, some distance away from the wedge surface, indicate the presence of a slipstream which separates regions of gas that have traversed different reflected shocks. The fringes also bend in close proximity to the second wedge surface because of the slipstream associated with the nearly disappeared second Mach stem.

An additional phenomenon that may be observed in the interferometric sequence in Figure 7.8 is an advancing cross-shock, located near the top left corner of image (b) and diagonally across the centre of image (c). Cross-shocks, which arise from non-planar effects when the diaphragm of the shock tube is ruptured,

are an undesirable but unavoidable feature of shock tube flows. These cross-shocks are very weak and are of little significance to the phenomena being studied. Digitization of the interferograms for Figure 7.9 was limited to the region in which the density field was unaffected by the cross-shock.

The example presented here shows that the double-wedge shock reflection phenomenon, which has been surveyed and analysed extensively (Ben-Dor et al., 1987, 1988), could be conveniently studied in further detail using time-resolved holographic interferometry. The sensitivity of an existing single-frame interferometric system is not affected by the introduction of the reference beam multiplexing assembly, so that predetermined calibration parameters can be used without modification. The analysis of each interferometric image in a time-resolved sequence does not differ in any way from that of a single interferogram, for which well established techniques exist. Van Netten (1988) analysed several interferometric recordings of shock wave reflection obtained with the same optical arrangement used in this work, except for the absence of the multiplexing system. He developed a precise protocol which includes computerized correction of the image for geometric distortions arising at any stage of recording or reconstruction, on the basis of fiducial markers in the field of view. Once the fringes and shock fronts are digitized and geometrically corrected if necessary, a starting value for the gas density is determined in a region from which the fringes can be followed. This requires that the Rankine-Hugoniot equations be applied at some location along the shocks at which the shock Mach number is known. In the case of a pure Mach reflection such as in frame 7.9(a), the foot of the Mach stem at the wedge surface is an ideal computation point since it constitutes a normal shock travelling into a stationary gas at ambient conditions. The Mach number of this shock is directly related to that of the incident shock—independently monitored—by the ratio of the respective velocities, which can be determined by simple distance measurements on the digitized image record. Having computed the density behind the foot of the Mach stem, the

density in the entire region under the reflected shock can be mapped on the basis of the interferometric fringes, which can be followed across the slipstream.

A similar approach is used to map the density field under the initial reflected shock in frame (b). In this case, however, the original Mach stem does not extend all the way to the wedge surface, and it is therefore necessary to apply the Rankine-Hugoniot equations at some other location along the stem. Since the Mach stem is not a normal shock except near the wedge, its local velocity vector, which lies along a line joining the tip of the wedge to the stem, must now be resolved into its tangential and normal components to the shock front. The normal component alone is used in the Rankine-Hugoniot equations to find the conditions behind the Mach stem, as indicated in Chapter 2.

For the analysis of frame (c) a different approach is adopted. In principle it would be possible to use the technique given for frame (a), computing the Rankine-Hugoniot equations across the small Mach stem at the wedge surface. This method, however, may give uncertain results due to boundary effects occurring behind the reflection point near the transition from one type of reflection to the other, and at any rate would no longer apply when the reflection becomes regular. It is preferable to apply the Rankine-Hugoniot equations across the incident shock to find the uniform flow field conditions in the region behind it, and from there proceed across the reflected shock to obtain a starting value for the density. This applies both to the reflection from the second wedge surface and to the original reflection from the first surface, which must be treated independently. Only the section of the new reflected shock which lies ahead of the intersection with the original one can be used for this calculation. When applying the Rankine-Hugoniot equations across either reflected shock, the local shock velocity must again be resolved into its tangential and normal components, only the latter being relevant. Because the reflected shocks propagate in a gaseous field to which a uniform velocity has been imparted by the incident shock, the gas velocity vector must be subtracted from the

local reflected shock velocity before resolving the latter into its components. This method of computing the conditions behind the incident shock and then "crossing" the reflected shock at any suitable location may be used for any type of reflection including fully developed Mach reflection, if, for example, the fringes near the Mach stem cannot be resolved in sufficient detail.

7.6 Discussion of the recording method

This section focuses on the unique characteristics of the system described in the present chapter, since the general properties of spatial frequency multiplexing and of solid state scanning have been discussed elsewhere. The capability of recording the reference exposure simultaneously on all images gives to this method substantial advantages over other ways of implementing a time-resolved holographic interferometer. Some of these merits are intrinsically related to the holographic process, independently of the application. Others are more specific to the use of the method in shock tube research.

The first advantage is the reduction in overall film exposure, a factor of great importance in view of the limited dynamic range of the film. This technique avoids the repeated overlaying of identical object beam images that would be inevitable with any method requiring a separate reference exposure for each image. Spatial frequency multiplexing may place severe demands on the dynamic range of the recording medium, and this feature plays a significant part in lessening those demands. Assuming a 1:1 intensity ratio between object beam and each of the n reference beams, during the multiple reference exposure the film receives only $\frac{n+1}{2n}$ of the overall light energy to which it would be exposed if each image were recorded separately. A related advantage is the reduced darkening of the film, that results in greater hologram brightness. Unless the holograms are routinely bleached, a process whereby the emulsion is made transparent but still retains its phase modulation characteristics, this is an important factor in the achievement of

better recordings. The simultaneous reference exposure is also beneficial in that it establishes a common reference point for all the interferograms in the series. This is particularly relevant in applications where it may not be possible to ensure steady state conditions for the time necessary to record a sequence of individual reference exposures.

The fact that a single additional laser pulse is required to record interferograms, regardless of the number of exposures in the sequence, allows the entire recording to be performed using a single train of Q-switched pulses from the ruby laser. By contrast, a system involving a double set of exposures may easily exceed the maximum pumping time delivered by the flashtube and therefore require that the laser be fired twice, possibly with a relatively long recharging time between firings. The sequence in Figure 7.8, for example, could not have been recorded with a single firing had a separate reference exposure been necessary for each image, since the overall duration of the six-pulse train ($5 \times 150\ \mu s = 750\ \mu s$) would have exceeded the $\sim 500\ \mu s$ limit of the useful flashtube emission. In the specific case of shock tube studies, van Netten (1988) has reported that the recoiling of the tube may introduce spurious fringes unless the reference exposure is recorded no more than a few hundred microseconds before the shock wave reaches the test section. The system presented here easily meets that requirement regardless of the number of images in the sequence or their spacing. The single-pulse reference exposure can be recorded as close to the rest of the sequence as the shutter response and laser repetition rate allow.

A side effect of allowing all reference beams to reach the film simultaneously when recording the reference exposure is that they mutually record holograms of each other, so that they are then restituted as part of the reconstruction of each image. These extra beams, however, are angularly separated from the axis of the reconstructed object beam and can therefore be excluded from view when observing or photographing the interferograms, albeit introducing further restrictions to

the viewing angle. On the other hand, the presence of additional reconstructed beams requires careful consideration in terms of image brightness, since the amplitude of the reconstructing wave is subdivided among all the generated beams. The issues of interferometric fringe contrast and image brightness for this mode of recording will be examined in Section 7.7, where the hologram formation equations will be analysed for the general case of n reference waves. In the three-channel prototype, hologram brightness and fringe contrast were experimentally found to be satisfactory.

The system presented here requires that a greater proportion of the light from the laser be allocated to the reference beam than to the object beam, so that each individual branch of the former has the correct intensity relative to the latter. To give an ideal brightness ratio of 1:1, the object beam and each reference beam branch would be allocated only $1/(n+1)$ of the total beam energy, assuming no losses in the system. This requires that the pulsed laser be powerful enough to expose the film sufficiently even at this reduced level. The ruby laser used in these experiments, with a nominal light output of over one joule, could easily handle a system with several more channels than the prototype configuration.

The multiplexing system's ability to simultaneously record an exposure on more than one image can also be applied to time-resolved differential holographic interferometry, in which each image shows the optical changes relative to the previous one. A differential interferogram series would be recorded by keeping a given shutter open during two consecutive pulses of the laser, with a one-pulse overlap between successive shutters in the sequence. For a three-channel system, the shutters *a, b, c* would be opened according to the sequence *a, ab, bc, c* during a four-pulse train. The sequence can be generalized to any number of channels, always having two shutters open at once except for the first and the last pulse. In this mode of operation, as in the previously described one, only $n+1$ pulses are required for a series of n interferograms. The control circuitry could easily be designed to

record either absolute or differential interferograms at the throw of a switch, adding versatility to the system.

The time-resolved holographic interferometer presented here can be improved and modified in various ways to meet research requirements. The first demand is clearly for longer sequences of images, which entails the splitting of the reference beam into more channels. Instead of a stack of conventional beam splitters, a high-efficiency holographic optical element could be used to perform the subdivision of a single beam into several diverging branches. A desirable recording capability for a practical working device to be used in shock tube flow visualization would be six interferograms taken at periods down to 50 μs. It is estimated that FLC devices available at the time of this writing would allow full switching at a minimum pulse spacing of 75 μs, determined by the overall response of the shutters that includes dead time and rise/fall time. In applications that may justify the extra cost and driving complexity, it would be possible to increase the multiplexing speed by using two shutters in each branch, triggering one to open and the other to close so that the first would reach full transmittance and the second begin to darken just as a laser pulse was fired. This scheme would allow successive branches to be activated at rates only limited by the rise and fall times. The additional shutter would also restore the proper polarization relative to the object beam, eliminating the need for a compensating half wave retarder. Considering the performance improvement that commercial FLC light valves have undergone over a period of several months to this date, it may be expected that switching times will further drop in the near future. Faster closing, along with a higher open/closed contrast ratio, will eliminate the inter-image leakage encountered in some recordings. The superior optical quality of premium units that are now becoming available should also improve image purity. Although for this work FLC devices appear to have been a suitable choice in terms of cost and convenience, faster shuttering technologies mentioned earlier may be used in applications requiring substantially higher framing rates.

7.7 Multiple-beam reference exposure—a theoretical view

The simultaneous recording of the reference exposure on all the images is a useful characteristic of the system presented here, but its theory must be examined with care in order to establish the possible limitations of the method. The first consideration is whether the brightness of the reconstructed object beam from the common reference exposure is sufficiently close to that of the reconstructed beam from one of the sequential recordings to give a good interferogram, since differences in brightness between the two images can easily obliterate the fringe pattern (Royer and Smigielski, 1970).

In the analysis that follows, the ideal condition of linear response of the photographic emulsion to light is postulated. Consider the simultaneous recording of a hologram by the waves given below:

$$\text{object wave:} \qquad \mathbf{U}_o(x,y) \tag{7.1}$$

$$\text{reference waves:} \qquad \mathbf{U}_{R_k}(x,y) = a_R \exp\left(i2\pi f_{y_k} y\right) \quad \{k = 1, \cdots, n\}, \tag{7.2}$$

where $f_{y_k} = \sin\theta_k/\lambda$ is the spatial frequency of the reference wave meeting the film at the angle of incidence θ_k. The irradiance at the film plane from the $n+1$ waves combined is

$$\begin{aligned} I(x,y) &= \left|\mathbf{U}_o + \sum_{k=1}^{n} a_R \exp\left(i2\pi f_{y_k} y\right)\right|^2 \\ &= |\mathbf{U}_o|^2 + \left|\sum_{k=1}^{n} a_R \exp\left(i2\pi f_{y_k} y\right)\right|^2 \\ &\quad + a_R \mathbf{U}_o \sum_{k=1}^{n} \exp\left(-i2\pi f_{y_k} y\right) + a_R \mathbf{U}_o^* \sum_{k=1}^{n} \exp\left(i2\pi f_{y_k} y\right) \\ &= |\mathbf{U}_o|^2 + n a_R^2 \\ &\quad + a_R^2 \sum_{k=1}^{n-1} \sum_{l=k+1}^{n} \left\{\exp\left[i2\pi\left(f_{y_l} - f_{y_k}\right) y\right] + \exp\left[i2\pi\left(f_{y_k} - f_{y_l}\right) y\right]\right\} \\ &\quad + a_R \mathbf{U}_o \sum_{k=1}^{n} \exp\left(-i2\pi f_{y_k} y\right) + a_R \mathbf{U}_o^* \sum_{k=1}^{n} \exp\left(i2\pi f_{y_k} y\right). \end{aligned} \tag{7.3}$$

After being exposed to the irradiance pattern and developed, the film has the following amplitude transmittance:

$$\mathbf{t}(x,y) = \mathbf{t}'_b + \beta \left\{ |\mathbf{U}_o|^2 + a_R^2 \sum_{k=1}^{n-1} \sum_{l=k+1}^{n} \{ \exp\left[i2\pi \left(f_{y_l} - f_{y_k}\right) y\right] + \exp\left[i2\pi \left(f_{y_k} - f_{y_l}\right) y\right] \} \right.$$
$$\left. + a_R \mathbf{U}_o \sum_{k=1}^{n} \exp\left(-i2\pi f_{y_k} y\right) + a_R \mathbf{U}_o^* \sum_{k=1}^{n} \exp\left(i2\pi f_{y_k} y\right) \right\}, \tag{7.4}$$

where the constant term $n\beta a_R^2$ has been absorbed inside $\mathbf{t}'_b$.

To reconstruct the hologram corresponding to the j-th reference beam, a plane wave propagating in the same direction as that beam is used:

$$\mathbf{U}_{c_j}(x,y) = a_c \exp\left(i2\pi f_{y_j} y\right). \tag{7.5}$$

The complex amplitude of the light emerging through the film, in close proximity of the hologram plane, is given by $\mathbf{t}(x,y)\mathbf{U}_{c_j}(x,y)$. After extensive rearrangement, it may be expressed as follows:

$$\begin{aligned}
\mathbf{U}_{I_j}(x,y) \;=\; & \left(\mathbf{t}'_b + \beta |\mathbf{U}_o|^2\right) a_c \exp\left(i2\pi f_{y_j} y\right) \\
& + \beta a_c a_R \mathbf{U}_o \\
& + \beta a_c a_R \sum_{\substack{k=1 \\ k\neq j}}^{n} \mathbf{U}_o \exp\left[i2\pi \left(f_{y_j} - f_{y_k}\right) y\right] \\
& + \beta a_c a_R \sum_{k=1}^{n} \mathbf{U}_o^* \exp\left[i2\pi \left(f_{y_j} + f_{y_k}\right) y\right] \\
& + \beta a_c a_R \sum_{\substack{k=1 \\ k\neq j}}^{n} a_R \exp\left(i2\pi f_{y_k} y\right) \\
& + \beta a_c a_R \sum_{\substack{k=1 \\ k\neq j}}^{n} a_R \exp\left(-i2\pi f_{y_k} y\right) \exp\left(i4\pi f_{y_j} y\right) \\
& + \beta a_c a_R \sum_{\substack{k=1 \\ k\neq j}}^{n-1} \sum_{\substack{l=k+1 \\ l\neq j}}^{n} \left\{ \begin{array}{l} a_R \exp\left[i2\pi \left(f_{y_l} - f_{y_k} + f_{y_j}\right) y\right] + \\ a_R \exp\left[i2\pi \left(f_{y_k} - f_{y_l} + f_{y_j}\right) y\right] \end{array} \right\}.
\end{aligned} \tag{7.6}$$

The first four terms correspond quite closely to equation 4.5 which describes the reconstructed waves from a multiply exposed hologram, the only difference being

the presence of a single object wave in the coefficient of the first term and in the summations. The physical interpretation of each term was given in Section 4.3. This formally confirms that the reconstructions of the object beam are identical whether the hologram is recorded by multiple overlaid exposures or by a single exposure with all the reference beams present simultaneously.

The terms beyond the fourth are specific to the multibeam recording. The fifth term describes a set of $n-1$ reconstructed reference waves, namely the ones not corresponding to the reconstruction beam. The conjugates of these waves are also generated, as shown by the sixth term, and are angularly separated from the other reconstructions. The last term describes a set of $\binom{n-1}{2}$† additional reconstructed waves and their conjugates. These originate from hologram components recorded by the pairwise interaction of the $n-1$ reference waves not corresponding to the reconstruction beam. The last three terms of equation 7.6 are shown separately in order to illustrate their physical significance. They may be combined in an expression of the form

$$\beta a_c a_R \sum_{k=1}^{n-1} \sum_{l=k+1}^{n} \left\{ a_R \exp\left[i2\pi \left(f_{y_l} - f_{y_k} + f_{y_j} \right) y \right] + a_R \exp\left[i2\pi \left(f_{y_k} - f_{y_i} + f_{y_j} \right) y \right] \right\} \tag{7.7}$$

describing the $\binom{n}{2}$ reconstructed waves, and their conjugates, from hologram components recorded by the n reference waves interacting in pairs.

When an interferometric recording is made with the system described in this chapter, the film receives a reference exposure recorded with multiple reference beams and a sequence of spatial frequency multiplexed phenomenon exposures. Assuming an ideal response to light, the transmittance of the developed emulsion will be a linear superposition of the transmittance patterns for the individual exposures. When the hologram is reconstructed with a plane wave having the spatial frequency of the j-th reference beam, the combined output is then the algebraic

†The notation $\binom{m}{k}$ denotes the 'm choose k' integer function: $\binom{m}{k} \equiv \frac{m!}{k!(m-k)!}$

sum of expressions 4.5 and 7.6. Pairing up like terms gives

$$\begin{aligned}
\mathbf{U}_{I_j}(x,y) \;=\; & \left[\mathbf{t}_b'' + \beta\left(|\mathbf{U}_o|^2 + \sum_{k=1}^{n}|\mathbf{U}_{o_k}|^2\right)\right] a_c \exp\left(i2\pi f_{y_j} y\right) \\
& + \beta a_c a_R \left(\mathbf{U}_o + \mathbf{U}_{o_j}\right) \\
& + \beta a_c a_R \sum_{\substack{k=1 \\ k\neq j}}^{n} \left(\mathbf{U}_o + \mathbf{U}_{o_k}\right) \exp\left[i2\pi\left(f_{y_j} - f_{y_k}\right) y\right] \\
& + \beta a_c a_R \sum_{k=1}^{n} \left(\mathbf{U}_o^* + \mathbf{U}_{o_k}^*\right) \exp\left[i2\pi\left(f_{y_j} + f_{y_k}\right) y\right] \\
& + \beta a_c a_R \sum_{k=1}^{n-1} \sum_{l=k+1}^{n} \left\{ \begin{array}{l} a_R \exp\left[i2\pi\left(f_{y_l} - f_{y_k} + f_{y_j}\right) y\right] + \\ a_R \exp\left[i2\pi\left(f_{y_k} - f_{y_l} + f_{y_j}\right) y\right] \end{array} \right\}, \qquad (7.8)
\end{aligned}$$

where the last three terms of 7.6 have been combined. The second term in above expression reveals that the reference exposure $\mathbf{U}_o$ and the selected phenomenon exposure $\mathbf{U}_{o_j}$ are reconstructed with equal amplitude from the combined hologram, yielding the optimal condition for maximum fringe contrast in the interferograms. All the angularly separated reconstructions corresponding to the other exposures also contain interferograms of equally good contrast, as shown by the third term in the above.

The other issue to be considered is reconstructed image brightness. In addition to the $2n$ object beams (n from the reference exposure and n from the phenomenon exposures) and their conjugates, the combined hologram causes the reconstruction of $\binom{n}{2}$ extra waves plus their conjugates, as shown by the last term in 7.8. Postulating a 1:1 brightness ratio between the object and reference beams, it is assumed that the amplitude of the reconstruction wave is equally distributed among the $2n + \binom{n}{2}$ diffracted beams. It follows that each interferometric image is only $\{2n/[2n + \binom{n}{2}]\}^2 = [4/(n+3)]^2$ as bright as it would be if reconstructed from a similarly efficient hologram not containing the extra waves, such as one recorded using a separate reference exposure for each image (all other considerations aside). This indicates that the multiple-beam reference exposure scheme, though advantageous in various ways, is only suitable for a small number of multiplexed images,

as it is becomes rather wasteful of light as n increases. It should be noted that the assumption of equal diffraction into all the output beams represents an idealized situation, since the reconstruction efficiency of an actual hologram varies with the diffraction angle.

The presence of the extra reconstructed beams may also further restrict the viewing angle of the images, worsening the limitations intrinsic to spatial frequency multiplexing that were discussed in Section 4.3. The problem may be alleviated by ensuring that the extra beams are not coplanar with the set of reconstructed object beams, which may be achieved with a recording arrangement in which the reference beams are slanted with respect to the plane of the angular scan. This rule was observed in the design of the prototype system, and the additional beams could be easily excluded from view when observing or photographing the reconstructed images.

7.8 An alternative design

Although the research described here has led to the development of a system based on spatial frequency multiplexing, there may be situations where a configuration yielding spatially separated holograms would be preferable. Specifically, the restrictions in viewing angle or the loss of image brightness that are intrinsic to the spatial frequency multiplexing approach may be avoided, at the cost of having to introduce new optical components in the object beam path. A simple modification would convert the current system to spatial multiplexing operation whilst preserving the advantage of recording the reference exposure simultaneously on all images. The various branches of the reference beam would be aimed at different, non-overlapping areas of film rather than converging to a common spot, and the object beam would be similarly partitioned by a system of beam splitters into a set of branches aimed at the same areas. For convenience of hologram reconstruction, the beam angles with respect to the film could be made the same for all channels.

By operating the reference beam shutters in the same fashion as in the present system, each area of film would record a reference hologram and a single phenomenon hologram. There would be no absolute need to shutter the object beam branches as well, because the exposures in which no reference beam was present for a given area of film would only introduce an incoherent darkening of the emulsion. Such darkening, if kept within the dynamic range limits of the film, would merely lower the hologram transmittance and could be counteracted by bleaching the emulsion. If it were deemed necessary to avoid the extra exposures, each pair of corresponding reference beam and object beam could be shuttered by two light valves working in parallel or possibly by a single larger shutter intercepting both beams close to the film plane.

Chapter 8

Conclusions

A time-resolved holographic interferometer for the study of gas flow in a shock tube has been successfully conceptualized, designed and built. The present work constitutes the first practical application of time-resolved holographic interferometry to the study of shock tube flows. Spatial frequency multiplexing has been used to implement the multi-image capability, without the need to change the existing object beam path and film holder of the single image system. The multiplexing device, which directs the reference beam along different paths, can be installed or removed easily with only minor readjustments.

The initial implementation by mechanical means using a spinning-mirror beam sweeping system, which appeared attractive in terms of simplicity and cost, did not lead to good results because of several technical shortcomings. Such an approach was suitable for recording single-sweep, non interferometric sequences of holograms, but the registration accuracy required to record interferograms could not be achieved with a reasonably simple system. Another problem with the prototype was the lack of continuous coverage which often led to partially or totally missed recordings. Alternative systems which ensured continuous coverage were designed but not built. It was also shown that any design which swept the beam in a continuous motion during the exposure time--as any high-speed mechanical system is bound to do—would cause the formation of extraneous fringes in the

reconstructed holograms unless the exposure was very brief. A theoretical analysis of this time smear phenomenon correctly described the observed effects. The mathematical model developed was used to establish that time smear effects for the existing system could only be made negligible by using shorter light pulses than the available ruby laser could reliably generate.

A solid-state system was subsequently designed that overcame all the difficulties encountered with the mechanical device, as well as introducing some unique beneficial features resulting from the system's ability to produce a set of coexisting reference beams which can be selectively shuttered in any combination. A three-channel prototype was built using FLC light gates as shutters. This device demonstrated the feasibility of recording the reference exposure on all images with a single pulse of the laser, followed by a sequence of exposures that captured the evolution of the phenomenon on individual images. Advantages of this method are a reduction in the overall exposure of the film and in the number of pulses required to record a sequence. A theoretical analysis of the generation of a hologram with multiple, simultaneous reference beams revealed the only limitation to this approach to be the loss in brightness of the reconstructed image of interest due to the formation of several additional cross-recordings as the number of beams is increased. An alternative design was proposed that yields spatially separated holograms and consequently avoids the cross-recording problem and other restrictions associated with spatial frequency multiplexing. This design requires the object beam to be imaged simultaneously on separate areas of film and therefore involves a more complex optical system, but it retains the advantage of single-pulse reference exposure recording and may be useful in situations where loss of image brightness and limited viewing angle cannot be tolerated.

The use of FLC light valves as shutters allowed the multiplexing device to be realized with simple low-voltage electronics. The technology of these electro-optical shutters is in its early stages of development and the available units are still wanting

in terms of optical uniformity, switching speed and contrast ratio. It is expected that within a short time these light valves will reach the quality and performance required for clear holographic recordings at repetition rates in the tens of kilohertz.

The method described in this work makes the recording of short sequences of holographic interferograms as simple as that of single holograms. If the multiframe recording system is retrofitted to an existing holographic apparatus, the upgrade requires few modifications to the original optical layout, provided the available laser is capable of multipulse operation. Beside the intended use for shock tube studies, this system may find application in a variety of other experimental settings where the capability of high-speed multiframe holographic recording for short run lengths would be advantageous. In general, the system may be of benefit for the visualization of time varying phenomena in which the features are not exactly reproducible from one event to another with similar initial conditions. Examples include the analysis of the failure mode of structures under stress, the study of cavitation bubbles in liquids and the visualization of thermal and turbulent processes in gases.

Bibliography

Aleksoff, C. C., 1971, Temporally Modulated Holography, *Appl. Opt.*, **10**, 1329–1341.

Anderson, J. D., 1982, *Modern Compressible Flow. With Historical Perspective*, McGraw-Hill, New York.

Barnes, P. A., 1970, *Studies of Laser Induced Breakdown Phenomena in Liquid Water*, Ph. D. dissertation, Simon Fraser University.

Ben-Dor, G., Dewey, J. M., Takayama, K., 1987, The reflection of a plane shock wave over a double wedge, *J. Fluid Mech.*, **176**, 483–520.

Ben-Dor, G., Dewey, J. M., McMillin, D. J., Takayama, K., 1988, Experimental investigation of the asymptotically approached Mach reflection over the second surface in a double wedge reflection, *Exp Fluids*, **6**, 429–434.

Bush, G. E., Charatis, G., 1982, Multiframe holographic shadowgraphy and interferometry of laser target plasmas, in *15th International Congress on High Speed Photography and Photonics*, L. L. Endelman (Ed.), Proc. SPIE 348, pp. 650–657.

Decker, A. J., 1982, Holographic cinematography of time-varying reflecting and time-varying phase objects using a Nd:YAG laser, *Opt. Lett.*, **7**, 122–123.

Dewey, J. M., 1989, Explosive flows: shock tubes and blast waves, in *Handbook of Flow Visualization*, W.-J. Yang (Ed.), Hemisphere, Washington, D. C., pp. 481–497.

Dewey, J. M., Walker, D. K., 1975, A multiply pulsed double-pass laser schlieren system for recording the movement of shocks and particle tracers within a shock tube, *J. Appl. Phys.*, **46**, 3454–3458.

Dubovik, A. S., Filenko, Yu. I., Ginzburg, V. M., Ushakov, L. S., 1977, Cineholography investigation methods of high-speed events, in *12th International Congress on High Speed Photography (Photonics)*, M. C. Richardson (Ed.), Proc. SPIE 97, pp. 127–129.

Eisfeld, F., 1982, Rotating mirror camera for use in holographic high speed interferometry, in *15th International Congress on High Speed Photography and Photonics*, L. L. Endelman (Ed.), Proc. SPIE 348, pp. 621–625.

Feldman, M., 1970, High-Speed Photographic and Holographic Techniques Using Acoustic Light Deflection, in *Proceedings of the Ninth International Congress on High-Speed Photography*, W. G. Hyzer and W. G. Chace (Eds.), SMPTE, New York, pp. 16–20.

Gabor, D., 1949, Microscopy by reconstructed wavefronts, *Proc. Roy. Soc.*, **A 197**, 454–487.

Gates, J. W. C., Hall, R. G. N., Ross, I. N., 1968, Repetitive Q-switched laser light sources for interferometry and holography, in *High-Speed Photography—Proceedings of the 8th International Congress on High Speed Photography*, N. R. Nilsson and L. Högberg (Eds.), John Wilcy & Sons, New York, pp. 299–303.

Gates, J W. C., Hall, R. G. N., Ross, I. N., 1970, High-Speed Holographic Recording of Transilluminated Events, in *Proceedings of the Ninth International Congress on High-Speed Photography*, W. G. Hyzer and W. G. Chace (Eds.), SMPTE, New York, pp. 4–10.

Goldstein, R. J., 1970, Optical Measurement of Temperature, in *Measurement Techniques in Heat Transfer*, E. R. G. Eckert and R. J. Goldstein (Eds.), Technivision Services, Slough, England, pp. 177–228.

Hall, J. D., 1954, *The Design and Performance of a 9 Inch Plate Mach-Zehnder Interferometer*, UTIA Report no. 27, Toronto.

Hall, R. G. N., Gates, J. W. C., Ross, I. N., 1970, Recording rapid sequences of holograms, *J. Phys. E: Sci. Instr.*, **3**, 789–791.

Heflinger, L. O., Wuerker, R. F., Brooks, R. E., 1966, Holographic interferometry, *J. Appl. Phys.*, **37**, 642–649.

Hentschel, W., Lauterborn, W., 1985, High speed holographic movie camera, *Opt. Eng.*, **24**, 687–691.

Hinsch, K., Bader, F., 1974, Acoustooptic modulators as switchable beam-splitters in high-speed holography, *Opt. Commun.*, **12**, 51–55.

Hugoniot, H., 1887, Journal de l'Ecole Polytechnique, Paris, **57**, 1.

Jones, D. M., Martin, P. M. E., Thornhill, C. K., 1951, A note on the pseudo-stationary flow behind a strong shock diffracted or reflected at a corner, *Proc. Roy. Soc.*, **A 209**, 238–248.

Lauterborn, W., Ebeling, K.-J., 1977, High-speed holocinematography of cavitation bubbles, in *12th International Congress on High Speed Photography (Photonics)*, M. C. Richardson (Ed.), Proc. SPIE 97, pp. 96–103.

Leith, E. N., Upatnieks, J., 1962, Reconstructed Wavefronts and Communication Theory, *J. Opt. Soc. Am.*, **52**, 1123–1130.

Leith, E. N., Upatnieks, J., 1963, Wavefront Reconstruction with Continuous-Tone Objects, *J. Opt. Soc. Am.*, **53**, 1377–1381.

Leith, E. N., Upatnieks, J., 1964, Wavefront Reconstruction with Diffused Illumination and Three-Dimensional Objects, *J. Opt. Soc. Am.*, **54**, 1295–1301.

Lowe, M. A., 1970, A Rotating-Mirror Hologram Camera, in *Proceedings of the Ninth International Congress on High-Speed Photography*, W. G. Hyzer and W. G. Chace (Eds.), SMPTE, New York, pp. 25–29.

Paques, H, Smigielski, P., 1965, Cinéholographie, *C. R. Acad. Sc., Paris*, **260**, 6562

Racca, R. G., Dewey, J. M., 1989a, Time-resolved holography for the study of shock waves, in *18th International Congress on High Speed Photography and Photonics*, Wang Daheng (Ed.), Proc. SPIE 1032, pp. 578–586.

Racca, R. G., Dewey, J. M., 1989b, Time smear effects in spatial frequency multiplexed holography, *Appl. Opt.*, **28**, 3652–3656.

Racca, R. G., Dewey, J. M., 1990, High speed time-resolved holographic interferometer using solid state shutters, *Opt. Laser Technol.*, (accepted for publication).

Rankine, W. J. M., 1870, On the Thermodynamic Theory of Waves of Finite Longitudinal Disturbance, *Phil. Trans. Roy. Soc.*, **160**, 277–288.

Royer, H., Smigielski, P., 1970, Expositions multiples sur un hologramme. Qualité des images restituées. Applications, *Opt. Acta*, **17**, 97–105.

Smigielski, P., Fagot, H., Albe, F., 1985, Holographic Cinematography with the help of a pulse YAG laser, in *16th International Congress on High Speed Photography and Photonics*, M. André and M. Hugenschmidt (Eds.), Proc. SPIE 491, pp. 750–754.

Smigielski, P., Hirth, A., 1970, New Holographic Studies of High-Speed Phenomena, in *Proceedings of the Ninth International Congress on High-Speed Photography*, W. G. Hyzer and W. G. Chace (Eds.), SMPTE, New York, pp. 321–326.

Takayama, K., 1983, Application of holographic interferometry to shock wave research, in *Industrial Applications of Laser Technology*, W. F. Fagan (Ed.), Proc. SPIE 398, pp. 174–180.

Thomas, K. S., Harder, C. R., Quinn, W. E., Siemon, R. E., 1972, Helical field experiments on a three-meter theta pinch, *Phys. Fluids*, **15**, 1658–1666.

van Netten, A. A., 1988, *The Design of a Holographic Interferometer and Its Use for the Study of Curved Oblique Shocks Produced by Shock Wave Reflections*, M. Sc. thesis, University of Victoria.

van Netten, A. A., 1989, pers. commun.

Vest, C. M., 1979, *Holographic Interferometry*, John Wiley & Sons, New York.

von Neumann, J., 1943, *Oblique Reflection of Shocks*, Explosive Research Report no. 12, Navy Department Bureau of Ordnance, Washington, D. C.

Walker, D. K., Scotten, L. N., Dewey, J. M., 1982, Construction and evaluation of a simple and inexpensive rotating prism camera for recording the movement of shocks and particles within a shock tube, in *15th International Congress on High Speed Photography and Photonics*, L. L. Endelman (Ed.), Proc. SPIE 348, pp. 125–130.

Whitten, B. T., 1969, *Calibration of a Shock Tube by Analysis of the Particle Trajectories*, M. Sc. thesis, University of Victoria

Wortberg, G., 1973, A holographic interferometer for gas dynamic measurements, in *Recent Developments in Shock Tube Research*, D. Bershader and W. Griffith (Eds.), Stanford University Press, Stanford, pp. 267–276.

Yamamoto, Y., 1989, Multi-frame pulse holography system, in *18th International Congress on High Speed Photography and Photonics*, Wang Daheng (Ed.), Proc. SPIE 1032, pp. 587–594.